Wechselwirkung von Licht mit Metall-Nanopartikeln für die biomolekulare Manipulation

Kumulative Dissertation

zur Erlangung des akademischen Grades
doctor rerum naturalium (Dr. rer. nat.)

vorgelegt dem Rat der
Chemisch-Geowissenschaftlichen Fakultät
der Friedrich-Schiller-Universität Jena

von Diplom-Ingenieurin (FH) Janina Wirth

geboren am 20. Juni 1984 in Sömmerda

1. Gutachter: PD Dr. Wolfgang Fritzsche
Leibniz-Institut für Photonische Technologien Jena

2. Gutachter: Prof. Volker Deckert
Friedrich-Schiller-Universität Jena

3. Gutachter: Dr. J. Jussi Toppari
University of Jyväskylä, Finnland

Tag der öffentlichen Verteidigung: 11. Juli 2014

Kurzfassung / Abstract

Die dargelegte Arbeit beschäftigt sich mit der gezielten Einstellung der Wechselwirkung von Licht mit metallischen Nanopartikeln für die nanoskalige Manipulation von Biomolekülen. Neben der Vorstellung einer neuen Methode zur selektiven Veränderung der Streueigenschaften des Systems, liegt der Fokus dieser Arbeit insbesondere auf ihrer Verwendung zur Manipulation von DNA. In diesem Kontext beschäftigt sich die Arbeit zunächst mit der Optimierung der Wechselwirkung zwischen Laserpulsen und Nanopartikeln für eine effiziente Manipulation ihrer lokalen Umgebung. Die Anwendung der optimierten Laserintensität auf DNA zeigt erstmals einen Anregungstransfer entlang der Biomoleküle, welcher Distanzen von über 4 µm erreicht und in dieser Arbeit über die selektive Zerstörung eines Polymers entdeckt wurde. Mit Hilfe von Fluoreszenzexperimenten wurde dieser Effekt genauer untersucht und konnte über das Fluoreszenzbleichen entlang der DNA sowie eines Akzeptor-Nanopartikels bestätigt werden. Diese Kombination aus plasmonischen Nanostrukturen mit Biomolekülen könnte neue Wege in der Entwicklung molekular-basierter Technologien eröffnen.

Schlüsselwörter: Nanopartikel, Interferenz, PMMA, Polarisation, fs- Laserpuls, DNA, Energietransfer

The present work deals with a selective modulation of light-nanoparticle-interactions for the nanoscale manipulation of biomolecules. Apart from the demonstration of a novel method for the selective tuning of the scattering properties of the system, this work focuses on the application of nanoparticles for the manipulation of DNA. In this context, the work deals initially with the optimization of the interaction between laser pulses and nanoparticles for an efficient manipulation of their local surrounding. The application of the optimized laser intensity to DNA showed for the first time an excitation transfer within these molecules, achieving distances of about 4 µm. The excitation transfer was discovered in this work by the selective destruction of a polymer. This effect was studied more precisely by means of fluorescence experiments and could be confirmed by bleaching along the DNA as well as of an acceptor-nanoparticle. This combination of plasmonic nano-structures with biomolecules could offer new possibilities in the development of molecular-based technologies.

Keywords: nanoparticle, interference, PMMA, fs laser pulse, polarization, DNA, energy transfer

Inhaltsverzeichnis

1 Motivation

Die Entwicklung hochauflösender Detektionsmethoden, wie der Fluoreszenz- und Rastertunnelmikroskopie, ermöglicht die Visualisierung sowohl von nanoskaligen technischen Strukturen, als auch von molekularen Funktionseinheiten. Seitdem werden auch neue Ansätze zur Manipulation im Mikro- und Nanometerbereich entwickelt. Insbesondere für biologische Strukturen stellt die gezielte Manipulation im Mikro- und Nanometerbereich eine große Herausforderung dar. Die Idee, einen fokussierten Lichtstrahl für die gezielte Zerstörung biologischer Proben zu nutzen, reicht bereits 100 Jahre zurück. Im Jahr 1912 entwickelte der Mikrobiologe *Sergeï Tschachotin* einen einfachen Aufbau zur Fokussierung von ultraviolettem Licht, welches die selektive Zerstörung bestimmter Zelleinheiten im Mikrometerbereich ermöglichte[1]. Mit der Erfindung des Lasers wurde 50 Jahre später das Laser-Skalpell von *Marcel Bessis* entwickelt und erstmals die Abtragung zellulärer Organellen im Submikrometerbereich demonstriert[2]. Seitdem werden intensive Laserstrahlen sowohl zur Entfernung bestimmter biologischer Strukturelemente, als auch für die Herstellung optischer, mechanischer und elektronischer Komponenten für technische Systeme angewandt[3-5]. Jedoch sind für die Manipulation auf molekularer Ebene weitaus präzisere Verfahren notwendig, die eine bessere Lokalisierung ermöglichen. Dies ist einer der Problemstellungen der Nanobiophotonik, welche die Ideen, Werkzeuge und Materialien der Nanotechnologie mit denen der Biologie kombiniert. Für eine lokalisierte Manipulation im Nanometerbereich bedient sie sich metallischer Nanostrukturen, die sich im Größenbereich von biologischen Makromolekülen befinden. Dank ihrer resonant überhöhten Lichtabsorption erlauben sie die Konzentration der Energie auf Größenbereiche unterhalb der optischen Auflösungsgrenze. Dieser Nanoantennen-Effekt konnte bereits zur gezielten Manipulation verschiedener biologischer Strukturen eingesetzt werden, welche Zellen[6,7], Chromosomen[8] und Proteine[9] einschließt. Eine Anwendung dieser Methode auf molekularer Ebene wurde bisher noch nicht demonstriert. Aus diesem Grund beschäftigt sich diese Arbeit mit der experimentellen Untersuchung zur Manipulation von DNA-Molekülen. Im Rahmen dieser Untersuchungen wird ein neuer Ansatz vorgestellt, welcher es ermöglicht, DNA auf Einzelmolekülebene mit Hilfe von metallischen Nanopartikeln und Laserstrahlung

zu manipulieren. Das Ziel war es, über die Laserbelichtung der metallischen Nanopartikel gezielt Energie auf DNA-Moleküle zu übertragen und die dabei auftretenden Effekte zu charakterisieren. Hierbei konzentrieren sich die Forschungsarbeiten auf drei Bereiche (Schema 1).

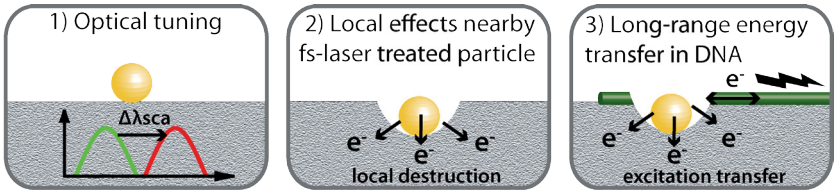

Schema 1. Aufgabenbereiche der durchgeführten Forschungsarbeiten.

Im ersten Teil wird zunächst eine neue Methode vorgestellt, mit der die Streueigenschaften von Metall-Nanopartikeln gezielt eingestellt werden können. In diesem Rahmen konzentrieren sich die Untersuchungen auf die spektrale Charakterisierung und mikroskopischen Abbildung von Nanopartikeln und dessen Verifizierung mit theoretischen Berechnungen.

Der zweite Teil beschäftigt sich mit der intensitätsabhängigen Laserbelichtung von metallischen Nanopartikeln, mit dem Ziel, eine optimale Wechselwirkung mit der Umgebung zu gewährleisten. Hierbei wird die hohe Lichtabsorption der Nanopartikel genutzt, um mittels Laserbestrahlung eine Elektronenemission aus der Partikeloberfläche herbeizuführen, welche über die lokale Zerstörung einer elektronensensitiven Polymer-Schicht unterhalb der Partikel detektiert wurde. Die dabei ermittelten Intensitäten wurden im dritten und wichtigsten Teil der Arbeit eingesetzt, um die Auswirkungen auf benachbarte DNA-Moleküle zu untersuchen. In diesem Zusammenhang wird erstmalig gezeigt, dass die plasmonisch unterstützte Elektronenemission nicht nur zu einer nanolokalen Zerstörung der DNA, sondern auch zu einem mikrometerweiten Anregungstransfer entlang der Moleküle führt.

The development of high spatial resolution detection techniques, such as fluorescence- and scanning probe microscopy, allows the visualization of miniaturized technical structures as well as molecular functional units. Since then, new approaches for the manipulation in the micro- and nanometer range has been developed. Especially for biological molecules the selective manipulation within this dimension represents a challenge. The idea to use a focused laser beam for

the selective destruction of biological samples goes back for 100 years. In 1912 the microbiologist *Sergeï Tschachotin* developed a simple setup for the focusing of UV-radiation, which enabled the selective destruction of certain cell units in the micrometre range[1]. In connection with the development of the laser the first laser scalpel was developed 50 years later by *Marcel Bessis* and the first ablation of cellular organelles in the sub-micrometre range was demonstrated[2]. Since then, intensive laser radiation is used for the ablation of selective biological structural units as well as for manufacturing of optical, mechanical and electronic components for technical systems[3-5]. However, for the manipulation on the molecular level much more precise techniques enabling a better localization are required. This is one of the problems in the field of nanobiophotonic, which combines the ideas, tools and materials of nanotechnology with that of biology. For the localized manipulation in the nanometer range it uses metal nanostructures with dimensions similar to biological macromolecules. Due to their resonant enhanced light absorption, they allow to concentrate the energy in a size range below the optical diffraction limit. This nanoantenna effect could already be demonstrated for the selective manipulation of biological structures, which include cells[6,7], chromosomes[8] and proteins[9]. An application of this method on the single molecular scale has not previously been demonstrated. For this reason, this work deals with the experimental investigation for the manipulation of DNA molecules. In this context a new approach is being presented, which allows to manipulate DNA on the single molecule level by using metal nanoparticles and laser light. The aim is to transfer energy selectively from the laser excited nanoparticle to DNA molecules and to characterize the occurring effects. In this connection the work focuses on three areas (Scheme 1).

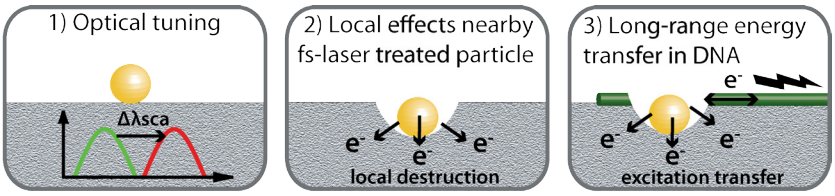

Scheme 1. Scope of the performed research.

In the first part a new method is presented, which allows the selective tuning of the scattering properties of metal nanoparticles. In this context, the research focuses on the spectral characterization of nanoparticles and their verification by theoretical calculations.

The second part deals with the intensity dependent laser irradiation of metal nanoparticles with the aim to ensure an optimal interaction with the surrounding. Here, the high light absorption of the nanoparticles is used to cause the emission of electrons out of the particle surface upon the laser irradiation, which was detected by the local destruction of an underlying electron sensitive polymer layer. The intensities thus obtained were used in the last and most important part to investigate the effects on neighboured DNA molecules. In this regard, the work presents for the first time that the plasmonic supported emission of electrons causes not only a nano local destruction of the DNA, but can also lead a micrometre wide excitation transfer along the molecules.

2 Stand der Technik

Im ersten Teil dieses Kapitels werden kurz die optischen Eigenschaften metallischer Nanopartikel beschrieben. In diesem Zusammenhang werden einige bestehende Methoden vorgestellt, die optischen Eigenschaften gezielt zu beeinflussen. Der zweite Teil gibt einen Überblick über die wichtigsten Wechselwirkungsmechanismen zwischen metallischen Nanopartikeln und Laserpulsen und erläutert die sich daraus ergebenden Anwendungsmöglichkeiten zur Manipulation biologischer Strukturen.

2.1 Optische Eigenschaften metallischer Nanopartikel

Die ausgeprägten optischen Eigenschaften metallischer Nanostrukturen werden durch die resonante Oszillation ihrer Leitungselektronen während der Wechselwirkung mit elektromagnetischer Strahlung verursacht. Sie tritt in einem bestimmten Frequenzbereich der elektromagnetischen Strahlung auf und wird als lokalisierte Oberflächenplasmonenresonanz (LSPR) bezeichnet. Die Wechselwirkung zwischen sphärischen Nanopartikeln und elektromagnetischer Strahlung wurde erstmals im Jahr 1908 von *Gustav Mie* unter Verwendung der *Maxwell*-Gleichungen analytisch beschrieben[10]. Die daraus ermittelten relevanten Größen ihrer optischen Eigenschaften sind der Streu- (C_{sca}) und Absorptionsquerschnitt (C_{abs}):

$$C_{sca} = \frac{k^4}{6\pi} \cdot (3V)^2 \cdot \frac{(\varepsilon_1(\omega)-\varepsilon_m)^2+\varepsilon_2(\omega)^2}{(\varepsilon_1(\omega)+2\varepsilon_m)^2+\varepsilon_2(\omega)^2} \quad (1)$$

$$C_{abs} = 3kV \cdot \frac{3\varepsilon_2(\omega)\cdot\varepsilon_m}{(\varepsilon_1(\omega)+2\varepsilon_m)^2+\varepsilon_2(\omega)^2} \quad (2)$$

Hierbei bezeichnet k die Wellenzahl der einfallenden Welle, V das Partikelvolumen, ε_m die dielektrische Konstante der Partikelumgebung und $\varepsilon(\omega) = \varepsilon_1(\omega) + i\varepsilon_2(\omega)$ die komplexe frequenzabhängige dielektrische Funktion des Partikelmetalls. Im sichtbaren Bereich der elektromagnetischen Strahlung ist die dielektrische Funktion von Metallen negativ. Im Resonanzfall wird der Nen-

ner in Gleichung (1) und (2) minimal, welches in einer stark erhöhten Lichtabsorption und -streuung resultiert. Im Fall von Silber- und Goldnanopartikeln befinden sich diese hauptsächlich im sichtbaren Wellenlängenbereich, weshalb sie einfach mit Halogen- und Laserlichtquellen angeregt werden können. Die spektrale Lage dieser lokalisierten Oberflächenplasmonenresonanz wird sowohl vom Brechungsindex des umgebenden Mediums, als auch von den intrinsischen Eigenschaften der Nanopartikel, wie Material, Form und Größe beeinflusst.

Die Brechungsindexänderung in der Partikelumgebung kann beispielsweise durch die Anbindung von Biomolekülen hervorgerufen werden. Dadurch ist es möglich, diese Moleküle über die spektrale Verschiebung der Plasmonenresonanz zu detektieren. Aus diesem Grund werden Nanopartikel intensiv für den Einsatz als chemische[11-14] und biologische Sensoren[15-19] erforscht und für die Detektion von Proteinen[20], Antikörpern[21,22] und DNA-Molekülen[23,24] eingesetzt. Die Selektivität wird hierbei durch die Funktionalisierung der Nanopartikeloberfläche mit einem Erkennungselement erreicht, welches spezifisch an das zu detektierende Molekül binden kann. Beispielsweise konnten somit Streptavidin-Molekülen mit einer Konzentration von 1 pM durch ihre Anbindung an einzelnen mit Biotin-Molekülen funktionalisierten Nanopartikeln erfolgreich über eine spektrale Verschiebung von 4 nm detektiert werden[25], sowie auch medizinisch relevante Proteine nachgewiesen werden[26].

Eine andere Möglichkeit ist die Verwendung von planaren Metallschichten in der Nähe des Nanopartikels. Zusätzlich zur vorher erwähnten Brechungsindexänderung kann die Plasmonenresonanz bzw. das Streuverhalten durch die Veränderung des Abstandes zwischen Nanopartikel und Metallschicht beeinflusst werden. Je nach Größe dieses Abstandes können verschiedene Wechselwirkungsmechanismen zwischen Partikel und Metallschicht auftreten. Befindet sich die Metallschicht in einem geringen Abstand (< 50 nm) zum Nanopartikel, findet eine Kopplung zwischen der Plasmonenresonanz des Partikels und den Oberflächenplasmonen der Metallschicht statt, die mit zunehmenden Abstand zu einer Verschiebung der Plasmonenresonanz zu kleineren Wellenlängen führt[27-29]. Bei einem größeren Abstand hingegen (> 50 nm) kommt es im Zwischenraum des Partikel und der Metallschicht zur Interferenz des gestreuten und reflektierten Lichts der Partikel. Dadurch wird lediglich das Streuverhalten der Partikel beeinflusst, welche gegenüber Änderungen der Interferenzweglän-

ge (Abstand zwischen Nanopartikeln und Goldschicht) sensitiv ist[30]. Eine erste sensorische Applikation konnte in Form eines pH-Sensors demonstriert werden. Über das An- und Abschwellen eines pH-sensitiven Polymers wurde der Abstand zwischen einer Goldschicht und einem Goldnanopartikel-Array verändert, welcher über die spektrale Charakterisierung des gesamten Partikelarrays detektiert werden konnte[31].

Im ersten Teil dieser Arbeit (Kapitel 3.1) erfolgten erstmals Untersuchungen zu diesem Effekt auf Basis einzelner Nanopartikel. Die Auswirkung von unterschiedlichen Interferenzweglängen wurde über die spektroskopische Charakterisierung und mikroskopischer Abbildungen einzelner Goldnanopartikel untersucht sowie mittels theoretischer Berechnungen verifiziert.

Des Weiteren werden die optischen Eigenschaften durch die intrinsischen Eigenschaften des Partikels bestimmt. Somit kann beispielsweise während der Partikelsynthese ihre Größe und Form so eingestellt werden, dass sie die Energie eines bestimmten Wellenlängenbereiches absorbieren und somit als Nanoantennen agieren. Durch die Konjugation der Nanopartikel an biologische Strukturen und anschließender Laserbestrahlung mit entsprechender Wellenlänge ist somit eine gezielte Manipulation dieser molekularen Strukturen möglich. Die Manipulation wird von den stattfindenden Prozessen an der Grenzfläche des Partikels zur Zielstruktur bestimmt. Die Art der Manipulation hängt von der Pulsdauer und Intensität der Laserstrahlung ab. Diese Prozesse werden im anschließenden Abschnitt kurz erläutert.

2.2 Wechselwirkung metallischer Nanopartikel mit Laserpulsen

Während der Laserbestrahlung wird die vom Partikel absorbierte Laserenergie zunächst über folgende Energie-Relaxationsprozesse an die Umgebung weitergeleitet[32-34]. Im ersten Schritt wird die Energie der Laserstrahlung von den Elektronen des Partikels absorbiert, welches zu einer Anregung dieser Elektronen auf ein höheres Energieniveau führt. Diese Energie wird anschließend auf mehrere Elektronen verteilt (Elektronen-Elektronen-Kopplung), sodass sich nach einer Zeitdauer von ca. 0,1 ps ein thermisches Gleichgewicht der Elektronen einstellt. Anschließend wird die Energie von den Elektronen in einem Zeit-

intervall von ca. 5 ps an das Atomgitter übertragen (Elektron-Phonon- Kopplung) und von dort aus schließlich über Gitterschwingungen (Phonon-Phonon-Kopplung) innerhalb von mehreren 100 ps an die Partikelumgebung weitergeleitet. Diese ist von der Wärmeleitfähigkeit der Umgebung abhängig. Innerhalb dieser charakteristischen Zeitenwird die absorbierte Energie eines Laserpulses an die Umgebung weitergeleitet. An der Grenzschicht können anschließend je nach eingesetzter Pulsdauer und der daraus resultierenden Intensität bei vergleichbarer Leistung unterschiedliche Prozesse stattfinden. Diese werden im Folgenden am Beispiel von langen Nanosekunden (ns)- und kurzen Femtosekunden (fs)-Laserpulsen beschrieben (Abb. 2.1).

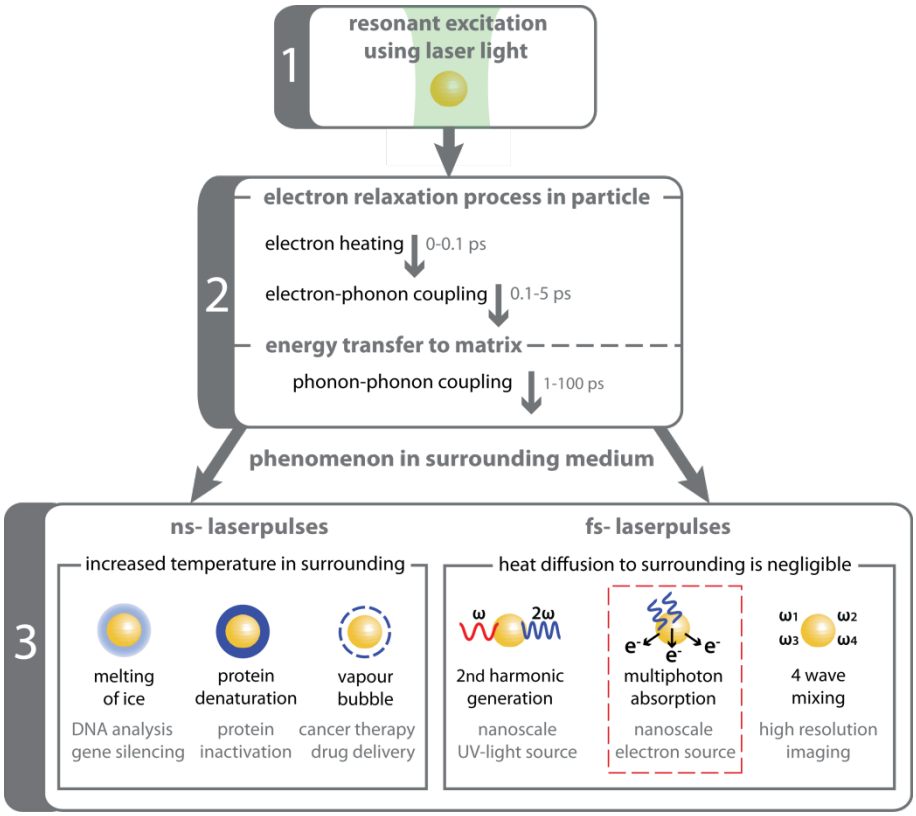

Abb. 2.1. Relaxationsmechanismus von Elektronen in Metall-Nanopartikeln nach ihrer plasmonischen Anregung und die möglichen Prozesse ihres Energietransfers in die Partikelumgebung mit Anwendungsbeispielen.

Während der Belichtung mit langen ns-Laserpulsen werden die Elektronen im Nanopartikel in einem Zeitraum von Pikosekunden nur schwach angeregt. Sie geben ihre Energie bereits während eines Laserpulses an die Gitteratome des Partikels ab. Über einen Zeitraum von mehreren hundert Pikosekunden erwär-

men sich die Nanopartikel sehr stark, bevor eine Wärmeleitung in die Umgebung einsetzt (Phonon-Phonon-Kopplung). Durch diese stark erwärmten Nanopartikel kommt es ebenfalls zu einer Temperaturerhöhung in der biologischen Umgebung (photothermischer Effekt), welche unterschiedliche Auswirkungen hervorrufen kann[35-40]. Eine der am häufigsten untersuchten Effekte stellt die Zerstörung einzelner Zellen *(in vitro)* durch die Bildung von Kavitationsblasen dar. Hierfür wurden Nanopartikel spezifisch an die Oberfläche der Zellmembran gebunden und mit ns-Laserpulsen belichtet. Dabei wird das Wasser nahe der Partikeloberfläche durch Überschreitung der Siedetemperatur verdampft, was zur Bildung von Dampfblasen führt, die zunächst schnell expandieren und anschließend schlagartig kollabieren. Dadurch entstehen Druckwellen, die die Zellmembran zerstören und zur Zelllyse führen[41-48]. Die Bildung der Kavitationsblasen kann durch die Reduktion der Laserintensität so kontrolliert werden, sodass die Zellmembran nur leicht geschädigt und dadurch dessen Permeabilität erhöht wird. Somit kann die Aufnahme bestimmter Stoffe in die Zelle begünstigt werden, welche beispielsweise zur Stilllegung ausgewählter Gene eingesetzt werden können[49-53].

Durch eine Belichtung des Partikels mit kurzen fs-Laserpulsen erhöht sich nur die kinetische Energie der Elektronen. Bevor die Elektronen-Phononen- Kopplung einsetzt, ist der fs-Laserpuls bereits vorbei. Demzufolge kann nur die in der kurzen Zeit deponierte Energie in die Elektronen an das Atomgitter des Nanopartikels weitergegeben werden. Dieser Energiebetrag ist sehr gering, weshalb der Nanopartikel kaum erwärmt wird. Somit wird auch die biologische Umgebung über die Wärmeleitungsprozesse unwesentlich erwärmt. Die starke Anregung der Elektronen führt zu nichtlinearen Prozessen, wie beispielsweise zur Frequenzverdopplung[54] und Vierwellenmischung[55,56], aber auch zum Elektronenaustritt aus der Partikeloberfläche, auf die hier näher eingegangen werden soll (rote Markierung in Abb. 2.1). In diesem Fall muss die Austrittsarbeit der Elektronen überwunden werden. Diese Größe ist materialabhängig und beträgt für Gold (Au) 4,8 bis 5,01 eV und für Silber (Ag) 4,1 bis 4,6 eV. Um diese Austrittsenergie zu erreichen, ist während der fs-Laserbestrahlung die gleichzeitige Absorption mehrerer Photonen erforderlich. Infolgedessen sind hohe Photonendichten nötig, die durch eine erhöhte Laserfluenz der Laserpulse gewährleistet werden. Die Laserfluenz (F) beschreibt hierbei die Energiedichte eines Laserpulses und wird durch folgende Gleichung beschrieben:

$$F = \frac{P}{A \cdot f} \tag{3}$$

Hierbei ist P die mittlere Leistung, A die Fläche des Laserfokus und f die Repetitionsrate der Laserpulse. Da in einem Experiment die Fokusfläche und Repetitionsrate oft konstant sind, kann die Laserfluenz über die mittlere Pulsleistung eingestellt werden.

In Abhängigkeit der Laserfluenz können bei konstanten Pulslängen (t_p) von ~ 100 fs die Auswirkungen auf die Partikelumgebung entweder stark auf den Bereich des Nanopartikels lokalisiert sein oder als Folge einer zu hohen Laserfluenz zu unspezifischen Zerstörungen führen. An einzelnen metallischen Nanopartikeln können demzufolge mit einer optimal gewählten Laserfluenz lokale Zerstörungen in einer unter den Partikeln befindlichen Oberfläche erzielt werden[57-61]. Eine zu hohe Laserfluenz hingegen führt zur Ionisation und Fragmentierung der Partikel (Coulomb-Explosion), welche unspezifische Zerstörungen in der Oberfläche auslösen[62-66]. Für eine effiziente Wechselwirkung mit der biomolekularen Umgebung ist deshalb die Einstellung der Laserfluenz notwendig.

Aus diesem Grund beschäftigt sich der zweite Teil dieser Arbeit (Kapitel 3.2) mit der Optimierung der Laserfluenz für die fs-Laserbelichtung von metallischen Nanostrukturen, mit dem Ziel, einen geeigneten Laserfluenzbereich für die anschließende Manipulation von DNA-Molekülen zu ermitteln. Die Detektion einer geeigneten Laserfluenz erfolgte über die lokale Zerstörung einer elektronensensitiven Polymerschicht unterhalb der belichteten Nanostrukturen.

Im Bereich der biomolekularen Manipulation ist es möglich, durch die fs-Laserbelichtung von metallischen Nanostrukturen DNA-Moleküle gezielt in die Richtung dieser Nanostrukturen zu bewegen, sie an diese zu fixieren und auch wieder freizusetzen[67,68]. Des Weiteren konnten an Chromosomen selektive Zerstörungen mit Dimensionen im Nanometerbereich erzielt werden[8]. In diesem Fall wurden einzelne Goldnanopartikel selektiv an das Centromer des Chromosoms gebunden. Durch eine anschließende Silberverstärkung der Partikel wurde dessen Plasmonenbande gezielt zu geringeren Wellenlängen von 400 nm verschoben. Dadurch gelang es die Partikel mit Wellenlängen von 800 nm über Zweiphotonen-Absorption plasmonisch anzuregen und so den Elektronenaustritt aus den Nanopartikeln plasmonisch zu unterstützen. Da sich die Laserwellenlänge im therapeutischen Fenster von biologischem Gewebe befindet, konnte

somit eine unspezifische Zerstörung des Chromosoms verhindert werden. Im Gegensatz zu einer rein laserinduzierten Zerstörung von Chromosomen[69], konnte diese durch den Einsatz metallischer Nanopartikel räumlich stark begrenzt werden.
Um diese Methode der Nanopartikel-vermittelten Zerstörung auf molekularer Ebene anzuwenden, wurden im dritten Teil dieser Arbeit (Kapitel 3.3) die Untersuchungen auf DNA-Moleküle übertragen. Für eine effiziente Wechselwirkung zwischen den belichteten Partikeln und der angelagerten DNA-Moleküle wurden die vorher optimierten Laserfluenzen eingesetzt.

3 Eigene Forschungsarbeiten

In diesem Kapitel werden die Forschungsergebnisse vorgestellt, die im Rahmen dieser Arbeit entstanden sind. Der erste Teil untersucht zunächst das Streuverhalten einzelner Nanopartikel über einer spiegelnden Metallschicht und stellt eine Methode vor, diese gezielt einzustellen. Der zweite und dritte Teil beschäftigt sich mit der intensitätsabhängigen fs-Laserbelichtung metallischer Nanostrukturen und beschreibt deren Auswirkungen auf DNA-Moleküle. Der dabei ausgelöste DNA-Energietransfer wurde über die lokale Zerstörung der DNA und eines Polymers detektiert, sowie mittels Fluoreszenzexperimenten genauer untersucht.

3.1 Einstellung der optischen Eigenschaften einzelner Metall-Nanopartikel [JW1]

In der Arbeit [JW1] wird erstmalig gezeigt, wie das Streuverhalten von einzelnen Goldnanopartikeln (AuNP) in einem Abstand von 100 bis 200 nm von der Partikeloberfläche beeinflusst werden kann. Hierfür dient eine interferometrische Anordnung, bestehend aus einem einzelnen Goldnanopartikel (ø = 80 nm) und einer 100 bis 200 nm entfernten Goldschicht. Der Abstand zwischen AuNP und Goldschicht und somit die optische Weglänge der Interferenz wird durch die Schichtdicke (Δd) einer transparenten Polymerschicht (Polymethylmethacrylat, Abk. PMMA) bestimmt. Hierbei wird in Abhängigkeit der optischen Weglänge des elektromagnetischen Feldes des vom AuNP gestreuten Lichtes in seiner Richtung wellenlängenabhängig verändert. Diese veränderte Feldrichtung hat einen starken Einfluss auf das optische Verhalten des AuNPs und resultiert sowohl in einer spektralen Verschiebung als auch in einem veränderten Streucharakter.

Der mikroskopische Aufbau zur Aufnahme der Partikelstreuspektren ist in Abb. 3.1 (links) dargestellt. Zunächst wird das polychromatische Licht einer Halogen-Lichtquelle in einer Durchlicht-Dunkelfeld-Anordnung über ein Objektiv (100x) auf ein einzelnes AuNP fokussiert. Das vom AuNP gestreute Licht

wird über das gleiche Objektiv gesammelt, durch eine eingebaute Lochblende (ø= 75 µm) in der Zwischenbildebene des Objektivs vom störenden Licht in der Partikelumgebung separiert und über eine Multimode-Faser zum Spektrometer geleitet.

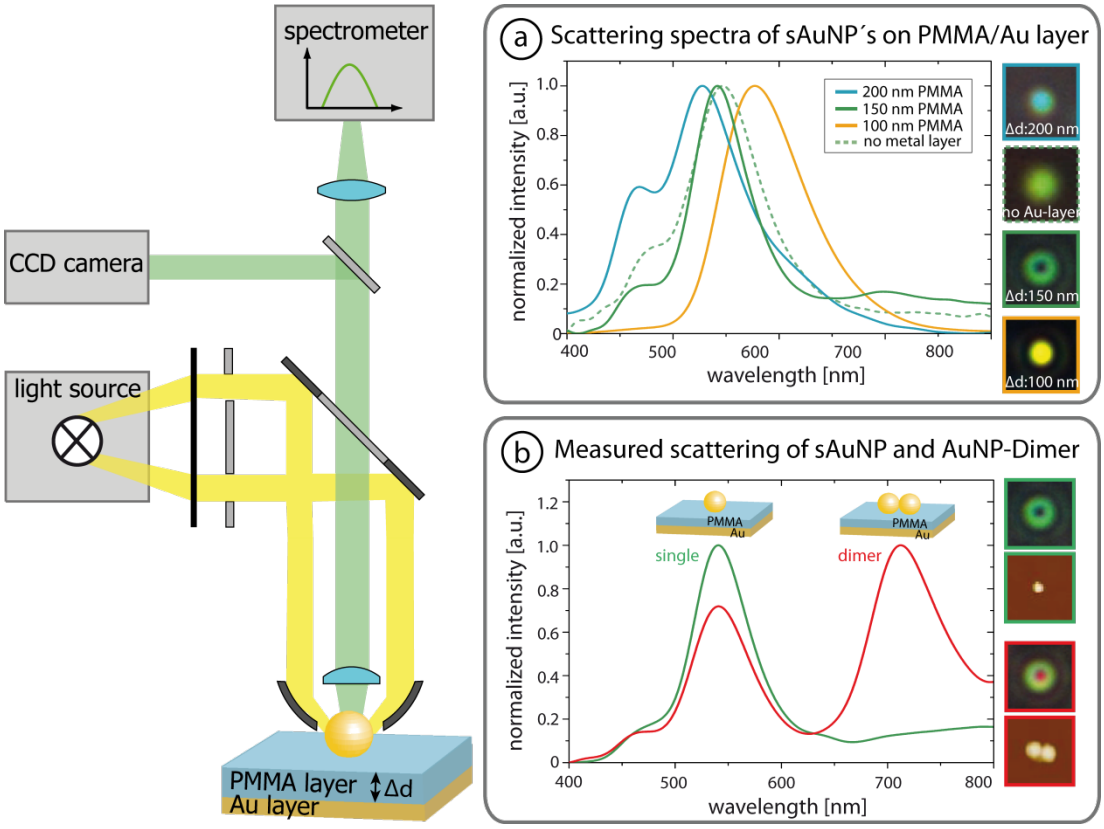

Abb. 3.1. (Links) Schematische Darstellung zur Aufnahme der Streuspektren einzelner AuNPs. (a) Gemessene Streuspektren einzelner AuNPs in Abhängigkeit vom Abstand (Δd) zur Goldschicht. Mit geringerem Δd verschiebt sich das Streuspektrum zu größeren Wellenlängen. Bei Δd= 150 nm ist das Streuverhalten der einzelnen AuNPs ringförmig (inset, rechts). (b) Vergleich der Streuspektren, Dunkelfeld- und AFM-Aufnahmen von einzelnen AuNPs (grün) und AuNP-Dimeren (rot) bei Δd= 150 nm. Das Streulicht des AuNP-Dimers zeigt die genannte grüne ringförmige Streuung mit einem roten Zentrum.

Die Streuspektren werden auch von der Partikelgröße beeinflusst. Der Durchmesser der verwendeten AuNPs variiert um ±7 nm. Für die Auswahl gleich großer AuNPs wurden vor der spektralen Charakterisierung die Durchmesser mit dem Rasterkraftmikroskop (AFM) bestimmt. Hierfür erfolgten zusätzliche Aufnahmen mit einer CCD-Farbkamera über Objektive geringerer Vergrößerung

(50x, 20x, 10x, 5x), welche das Auffinden der ausgewählten AuNPs während der AFM-Messung erleichtern.

Unter Berücksichtigung dieser Randbedingungen wurden zunächst einzelne AuNPs in Abhängigkeit von der PMMA-Schichtdicke (Δd= 100, 150, 200 nm) spektral charakterisiert. Im Vergleich zum ursprünglichen Streuspektrum eines AuNPs, welches die typische Plasmonenresonanz bei λ= 550 nm zeigt (gestrichelte Linie in Abb. 3.1a), konnte die Streuung einzelner AuNPs je nach PMMA-Schichtdicke spektral bis zu 40 nm verschoben werden. Befindet sich der AuNP stattdessen in einem Abstand von Δd= 150 nm zur Goldschicht, ändert sich die spektrale Lage zwar kaum im Vergleich zur typischen Plasmonenresonanz, jedoch aber der Streucharakter, die unter dem Dunkelfeldmikroskop als eine ringförmige Streuung wahrgenommen werden kann (Abb. 3.1a). Durch die Einstellung der optischen Weglänge zwischen einzelnen AuNPs und Goldschicht ist es somit möglich, das Streuverhalten der Partikel sowohl spektral, als auch in Richtung zu beeinflussen.

Um diesen Interferenzcharakter des Streulichtes auch für eine andere Partikelform zu testen wurden Desweiteren Paare bestehend aus zwei gleichgroßen AuNPs (AuNP-Dimere) untersucht. Hierfür wurden mittels AFM-Messungen AuNP-Dimere auf unterschiedlichen PMMA-Schichtdicken ausgewählt und ebenfalls spektroskopisch vermessen. Als Folge der Aufhebung der Formisotropie entsteht im Vergleich zum einzelnen AuNP neben der typischen Plasmonenbande bei λ= 550 nm eine weitere Resonanz im längerwelligen Bereich bei λ= 720 nm, welche auf die longitudinale Plasmonenmode zurückzuführen ist. Im Allgemeinen wird unter dem Dunkelfeldmikroskop mit einer unpolarisierten Lichtquelle das Streulicht von Partikelagglomeraten als gaußförmige Punktspreizfunktion emittiert, weshalb die beiden wesentlichen spektralen Streuanteile eines AuNP-Dimers ohne den Einsatz eines Spektrometers nicht wahrgenommen werden können. Mit dem interferometrischen Aufbau können jedoch beide Streuanteile der AuNP-Dimere beobachtet werden, ohne ein Spektrum aufnehmen zu müssen. Bei einer PMMA-Schichtdicke von 150 nm ist neben der grünen ringförmigen Streuung, wie sie auch beim einzelnen AuNP zu beobachten ist, ebenfalls der rote Streuanteil im Zentrum des Rings zu sehen (Abb. 3.1b).

Für ein besseres Verständnis dieser Messergebnisse wurden weiterhin theoretische Berechnungen durchgeführt und mit den Experimenten korreliert. Die Be-

rechnungen erfolgten auf Basis der *Maxwell*-Gleichungen zur Ermittlung des Streuverhaltens für sphärische Nanopartikel. Unter Berücksichtigung der PMMA-Schichtdicke und der Wellenlänge des einfallenden Lichtes konnte eine sehr gute Übereinstimmung mit den Messergebnissen erzielt, sowie die Ursachen für das spektrale Verhalten aufgeklärt werden. Damit könnten in Zukunft auch Einzelpartikel als sensorische Elemente dienen, bei der die optische Detektion über die Veränderung des Partikel-Streuverhaltens stattfindet.

3.2 Untersuchung der Wechselwirkungen zwischen fs-Laserpulsen und Metall-Nanopartikeln und ihre Auswirkungen auf die lokale Umgebung

Die hohe Lichtabsorption eines Nanopartikels ermöglicht es, während seiner Belichtung mit fs-Laserpulsen Energie gezielt und hochlokal in die Elektronen des Nanopartikels zu deponieren. Eine entsprechende Intensität der Laserpulse führt zum Elektronenaustritt und anschließender Manipulation der lokalen Umgebung. Für eine effiziente Manipulation ist es erforderlich, eine frühzeitige Zerstörung der Partikel zu vermeiden, die durch Coulomb-Explosion bei zu hohen Intensitäten ausgelöst werden können. Aus diesem Grund beschäftigt sich dieser Teil der Arbeit mit der intensitätsabhängigen Laserbelichtung von metallischen Nanopartikeln, um die Auswirkungen auf die Umgebung des belichteten Nanopartikels zu untersuchen und einen geeigneten Laserfluenzbereich für die DNA- Manipulation zu ermitteln. Die Detektion erfolgte über die lokale Zerstörung einer elektronensensitiven Polymerschicht unterhalb der belichteten Partikel. Mit den hier vorgestellten Ergebnisse aus den Publikationen [JW1, JW3, JW5] wird eine neue Methode demonstriert, mit der die Wechselwirkungen intensiver fs-Laserpulse mit Nanostrukturen untersucht werden können und über die lokale Zerstörung einer elektronensensitiven Polymerschicht (PMMA) im Bereich der belichteten Nanostruktur charakterisiert wird.

Für alle eingesetzten Lasersysteme betrug die Repetitionsrate 76 MHz. Der Fokusdurchmesser wurde für jede verwendete Laserwellenlänge experimentell bestimmt und betrug zwischen 5 und 7 μm^2. Die Laserfluenz wurde über die mittlere Pulsleistung eingestellt. Während der fs-Laserbelichtung der Nanopartikel wurde der Laserstrahl mäanderförmig über die Probe gescannt. Um si-

cherzustellen, dass jeder Bereich auf der Probe mit der gleichen Dosis belichtet wird, wurde eine Schrittweite von 1 µm gewählt. Auf jeder Probe wurden somit mehrere Flächen von 400 bis 1600 µm² mit bis zu mehreren hundert Partikeln belichtet. Eine optimale Laserfluenz ist dann erreicht, wenn die einzelnen Partikel in die PMMA-Schicht einsinken ohne dass diese dabei abladieren oder fragmentieren. Auf diese Weise konnten optimale Laserfluenzen sowohl für einzelne Goldnanopartikel (AuNP) bei einer Wellenlänge von 520 nm als auch für einzelne Silbernanopartikel (AgNP) und Goldnanopartikeldimere (AuNP-Dimer) bei einer Wellenlänge von 800 nm über die lokale Zerstörung der PMMA-Schicht bestimmt werden (Abb. 3.2).

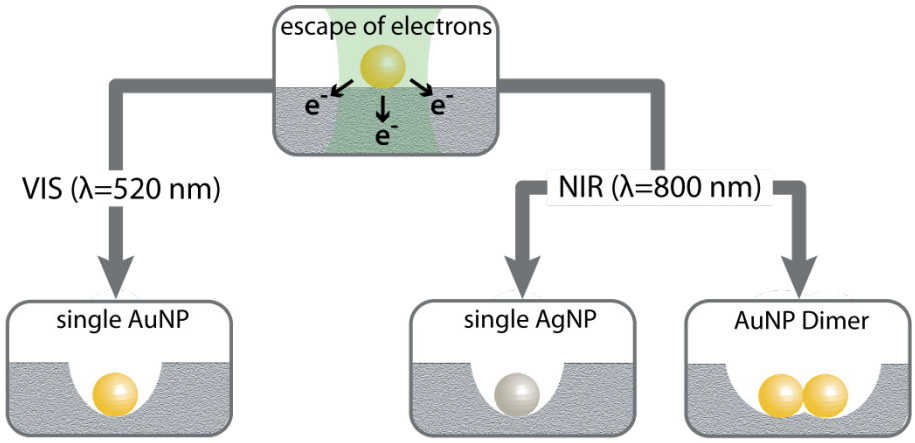

Abb.3.2. Schematische Übersicht zur lokalen Zerstörung der PMMA-Oberfläche durch die Belichtung von Silber- und Goldnanopartikeln mit fs-Laserpulsen mit einer Wellenlänge (λ) von 530 bzw. 800 nm und einer Pulsdauer (t_p) von je 100 fs.

3.2.1 fs-Laserbelichtung einzelner Gold-Nanopartikel [JW5]

Im Vergleich zu ähnlichen Arbeiten mit AuNPs wurden in der Publikation [JW5] zunächst Kontrollversuche zur unspezifischen Zerstörung des PMMAs durchgeführt. Es konnte bei einer Laserwellenlänge von 520 nm eine Laserfluenz von 1,5 mJ/cm² ermittelt werden, bei der das PMMA ohne die Verwendung von AuNPs zerstört wird. Von diesem Wert ausgehend erfolgte die Belichtung der einzelnen AuNPs mit geringeren Laserfluenzen. Da sich die verwendete Laserwellenlänge im Bereich der Plasmonenresonanz der AuNPs befindet, wird eine plasmonisch unterstützte Zweiphotonen-Anregung der Elektronen verursacht, sodass bereits bei geringen Laserfluenzen von ca. 0,3 bis 0,4 mJ/cm² lokale Zer-

störungen im PMMA auftreten (Abb. 3.3a). Diese Zerstörungen sind auf der PMMA-Oberfläche stark lokalisiert und beschränken sich lediglich auf den Bereich der belichteten AuNPs (Abb. 3.3b). Des Weiteren erfolgte zusätzlich die spektrale Charakterisierung einiger AuNPs vor und nach ihrer Belichtung mit der ermittelten Laserfluenz, analog zu der in Publikation [JW1] beschrieben Methode. Durch lokale Brechungsindexänderungen der eingesunkenen Partikel wurde eine spektrale Resonanzverschiebung von ca. 40 nm zu größeren Wellenlängen ermittelt.

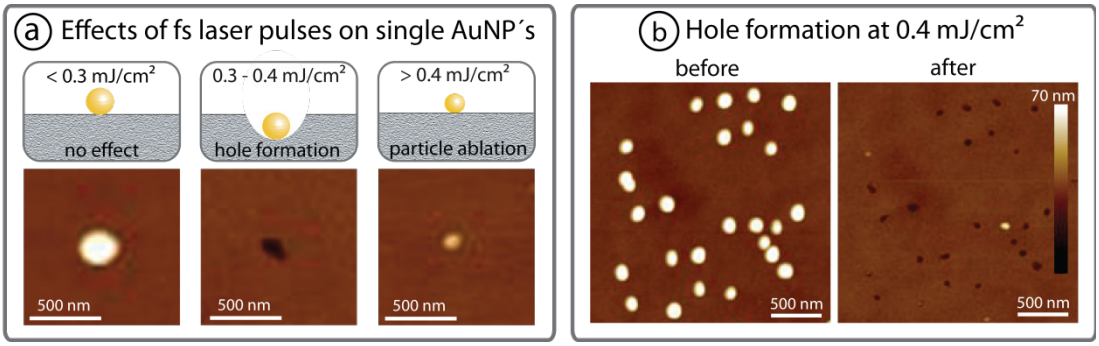

Abb. 3.3. fs-Laserbelichtung von einzelnen AuNPs bei einer Wellenlänge von 520 nm. (a) In Abhängigkeit von der Laserfluenz bleiben die AuNPs entweder unverändert, führen zur lokalen Zerstörung des PMMAs oder abladieren. (b) Effiziente Wechselwirkung und lokale Zerstörung des PMMAs an der Partikelposition bei 0,4 mJ/cm².

3.2.2 fs-Laserbelichtung von einzelnen Silber-Nanopartikeln und Goldnanopartikel-Dimeren [JW1, JW2, JW3, JW5]

Die Untersuchungen mit verschiedenen Laserfluenzen auf einzelne AgNPs [JW2, JW3] erfolgten im nahen Infrarotbereich mit einer Laserwellenlänge von 800 nm. Im Vergleich zur Belichtung einzelner AuNPs befindet sich diese Wellenlänge außerhalb der Plasmonenresonanz der AgNPs. Für eine plasmonische Anregung der AgNPs bei einer Wellenlänge von 400 nm über eine Zweiphotonenabsorption sind größere Photonendichten notwendig. Aus diesem Grund werden für eine lokale Zerstörung des PMMAs auch höhere Laserfluenzen von 3 bis 7 mJ/cm² benötigt (Abb. 3.4a).

Des Weiteren wurde diese ermittelte Laserfluenz auch zur Belichtung anisotroper Partikelformen bei einer Laserwellenlänge von 800 oder 1030 nm angewendet. Am Beispiel von AuNP-Dimeren konnte gezeigt werden, dass die lokale

Zerstörung des PMMAs von der Polarisationsrichtung der Laserstrahlung abhängig ist. Während eine parallele Ausrichtung des E-Feldes zur longitudinalen Dimer-Achse eine lokale Zerstörung des PMMAs verursacht, sind bei einer orthogonalen Ausrichtung keine sichtbaren Auswirkungen, weder auf den Dimeren noch auf die PMMA-Schicht, erkennbar (Abb. 3.4b). Somit ist es möglich, durch die Einstellung des Polarisationswinkels die PMMA-Schicht in der Umgebung von bestimmten AuNP-Dimeren auf der Probe selektiv zu manipulieren. Die Selektivität wird hierbei durch die Anregung der longitudinalen Plasmonenresonanz des AuNP-Dimers gegeben, welche sich im längerwelligen Bereich befindet und somit durch die verwendete Laserwellenlänge angeregt werden kann. Damit können die lokalen Zerstörungen in der PMMA-Schicht über die Einstellung des Polarisationswinkels selektiv induziert werden [JW1, JW5].

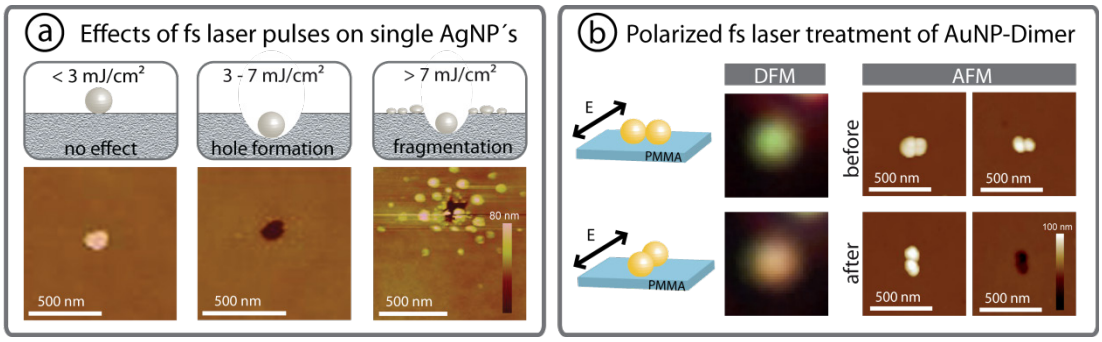

Abb. 3.4. fs-Laserbelichtung von einzelnen AgNPs und AuNP-Dimeren bei einer Wellenlänge von 800 nm. (a) Leistungsabhängige fs-Laserbelichtung von AgNPs. In Abhängigkeit der Laserfluenz bleiben die AuNPs entweder unverändert (links), führen zur lokalen Zerstörung (mitte) oder zur unspezifischen PMMA-Zerstörung durch die Fragmentation der AgNPs (rechts). (b) Polarisationsabhängige Dunkelfeldaufnahmen und fs-Laserbelichtung von AuNP-Dimeren. Eine parallele Ausrichtung des E-Feldes führt während der fs-Laserbelichtung zum Einsinken der AuNP-Dimere.

Hierbei kann eine thermisch induzierte Zerstörung des PMMAs ausgeschlossen werden. Dafür sind kurzzeitige Temperaturerhöhungen von 300 bis 400°C erforderlich[70,71]. Theoretische Berechnungen haben jedoch gezeigt, dass während der fs-Laserbelichtung an der Partikeloberfläche eine Gleichgewichts-Temperatur bereits nach 60 ns (5 Laserpulsen) eintritt und daher nur eine Temperaturerhöhung von lediglich 3°C verursacht[62], weshalb die experimentelle Ermittlung der optimalen Laserfluenz nicht auf eine thermisch induzierte Zerstörungen des PMMAs zurückzuführen ist. Vielmehr können diese durch Elektronen verursacht werden, die während der fs-Laserbelichtung aus der Par-

tikeloberfläche austreten[72-75]. Durch die optimale Einstellung der Laserfluenz konnte eine Zerstörung der Partikel durch eine Coulomb-Explosion verhindert werden. Die Partikel können somit in einem kurzen Zeitbereich (< 1 ps) als „Nano-Elektronenquellen“ dienen.

Zusammenfassend betrachtet konnten für einzelne Gold- und Silber-Nanopartikel optimale Laserfluenzbereiche ermittelt werden, die eine effiziente Wechselwirkung zwischen ihnen und ihrer Umgebung ermöglichen. Diese Wechselwirkung beruht auf der Elektronenemission aus der Partikeloberfläche und konnte über die lokale Zerstörung einer elektronensensitiven PMMA-Schicht unterhalb der belichteten Nanostruktur nachgewiesen werden. Des Weiteren war es möglich, Goldnanopartikel-Dimere selektiv über die Einstellung des Polarisationswinkels zur lokalen PMMA-Zerstörung zu nutzen. Die dabei gewonnen Erkenntnisse könnten zukünftig zur Nanostrukturierung von Polymeroberflächen angewendet werden. Im Rahmen dieser Arbeit wurden die optimierten Laserfluenzen für die Manipulation von DNA-Molekülen genutzt, dessen Auswirkungen im anschließenden Kapitel vorgestellt werden.

3.3 Untersuchung der Energietransfer-Effekte in DNA-Molekülen durch die fs-Laserbelichtung von Metall-Nanopartikeln

In diesem Teil der Arbeit werden die Auswirkungen der Nanopartikel-vermittelten Manipulation auf DNA-Moleküle vorgestellt (Abb. 3.5). Neben einer lokalen Zerstörung unterhalb des Nanopartikels [JW2, JW3, JW5], konnte erstmalig ein Anregungstransfer entlang der DNA durch die plasmonische Anregung eines AgNPs über die lokale Zerstörung des Polymers beobachtet werden [JW3]. Eine anschließende detaillierte Untersuchung des Transfers in Publikation [JW4] hat gezeigt, dass diese Anregung zu einem fluoreszenzmarkierten Akzeptor-AgNP transportiert werden kann. Des Weiteren konnte ein Anregungstransfer auch unter Verwendung von stabileren AuNP-Agglomeraten beobachtet werden, welcher jedoch stark von der Richtung des eingestrahlten E-Feldes des Lasers abhängig ist [JW5]. Im Folgenden werden die einzelnen Untersuchungen zu den genannten Ergebnissen vorgestellt.

Vor der fs-Laserbelichtung wurden zunächst fluoreszenzmarkierte λ-DNA-Moleküle mit Gold (AuNP)- bzw. Silbernanopartikeln (AgNP) auf PMMA-beschichteten Glas-Chips immobilisiert. Hierfür wurde eine Lösung, bestehend aus λ-DNA-Molekülen und Nanopartikeln auf dem Chip eingetrocknet, was zu gestreckten und mit Nanopartikeln markierten DNA-Molekülen führte[76]. Die Proben wurden mittels Fluoreszenz-, Dunkelfeld- und Rasterkraftmikroskopie charakterisiert. Die fs-Laserbelichtung erfolgte analog zu der Belichtung der Partikel im Abschnitt 3.2 mit einer Wellenlänge von 520, 800 bzw. 1030 nm und der jeweils ermittelten Laserfluenz. Die Charakterisierung der Auswirkungen auf die DNA-Moleküle bzw. der darunterliegenden PMMA-Schicht erfolgte erneut durch AFM-Messungen.

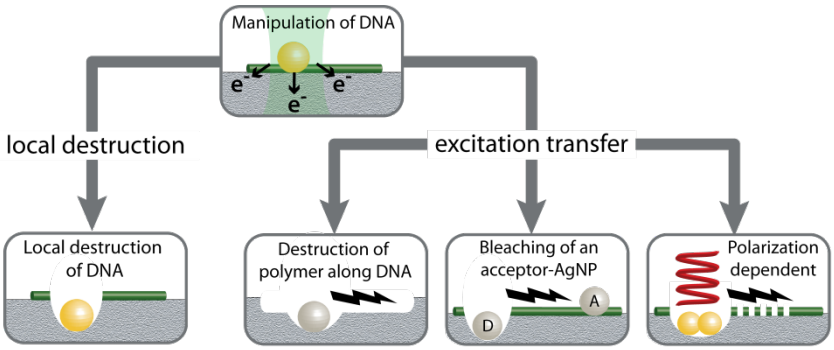

Abb.3.5. Auswirkungen der Nanopartikel-vermittelten Manipulation auf DNA.

3.3.1 Lokale Zerstörung von DNA-Molekülen [JW2, JW3, JW5]

Die Anwendung der laserinduzierten Nanopartikel-vermittelten Manipulation auf DNA-Moleküle führt zu ihrer lokalen Zerstörung im Bereich des Nanopartikels. Die Zerstörung der DNA befindet sich im Größenbereich des Nanopartikels und beschränkt sich lediglich auf DNA-Moleküle, welche sich in unmittelbarer Nähe zum Nanopartikel befinden (Abb. 3.6).

Somit ist diese Methode nicht nur auf die selektive Zerstörung von Zellen und Chromosomen limitiert, sondern kann auch auf molekularer Ebene zur nanoskaligen Zerstörung von DNA-Molekülen eingesetzt werden.

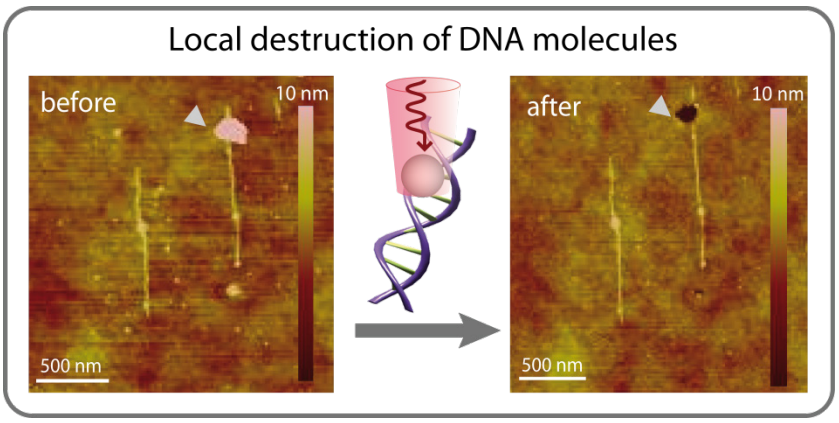

Abb. 3.6. Nanolokale Zerstörung von DNA durch die fs-Laserbelichtung eines einzelnen Metallnanopartikels.

3.3.2 Detektion des DNA-Anregungstransfers über die selektive Zerstörung eines Polymers [JW3]

Neben einer lokalen Zerstörung kann die fs-Laserbelichtung einzelner AgNPs einen Anregungstransfer entlang benachbarter DNA-Moleküle hervorrufen. Dieser Anregungstransfer erreicht eine über bisher in DNA beobachteten Elektronentransfer von wenigen Nanometern[77] deutlich darüber hinausgehende Distanz von mehreren Mikrometern und führt zu mikrometerlangen Zerstörungen (bis zu 4 µm) mit einem Durchmesser von wenigen Nanometern im PMMA. Die Strukturen besitzen eine Tiefe von ca. 4 nm und folgen der ursprünglichen DNA-Lage (Abb. 3.7). Die Kontrollexperimente zur Belichtung unmarkierter DNA-Moleküle zeigten keine sichtbaren Auswirkungen. Auch die Belichtung von AgNPs, die sich nicht direkt auf den DNA-Molekülen befanden, sondern nur wenige Nanometer (20 nm) von ihr entfernt waren, zeigten keine vergleichbaren Effekte an der DNA.

Damit können die im Abschnitt 3.1 hergestellten Nanolöcher auf viel komplexere Strukturen erweitert werden, dessen Ausmaße nicht auf die Geometrie des Partikels beschränkt sind. In diesem Zusammenhang wird eine neue Methode vorgestellt, DNA-Moleküle als Template für die parallele Herstellung von Nanostrukturen zu nutzen, welche auf der plasmonischen Anregung eines einzelnen AgNPs basiert. Insbesondere eine erfolgreiche Anwendung dieser Methode auf komplexere DNA-Strukturen, wie beispielsweise 2- oder 3-dimensionale DNA-Konstrukte (DNA-Origami)[78-81], würde neue Wege in der optischen Nanolitho-

graphie eröffnen. Somit könnten einfach und kostengünstig beliebige Strukturen parallel, mit Dimensionen weit unterhalb der Beugungsgrenze hergestellt werden. Dafür bedarf es eines besseren Verständnisses.

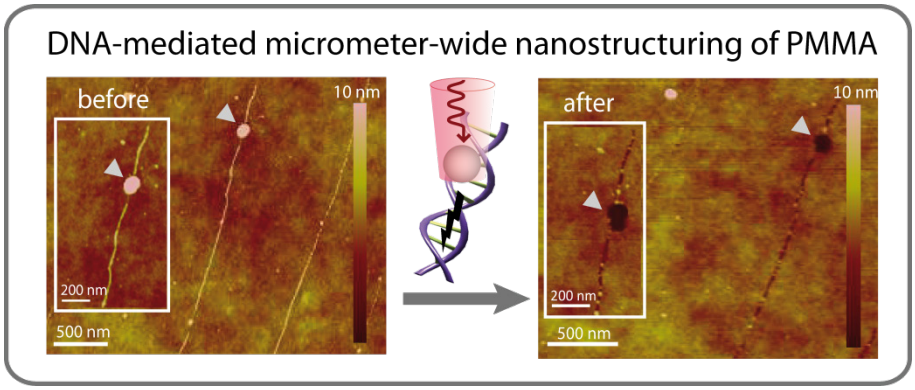

Abb. 3.7. Nanostrukturierung von PMMA durch einen plasmonisch induzierten Anregungstransfer in DNA nach der fs-Laserbelichtung eines einzelnen AgNPs. Ausgehend vom AgNP folgen die Vertiefungen der ursprünglichen Position der DNA über Längen von bis zu 4 µm.

3.3.3 Detektion des DNA-Anregungstransfers mittels Fluoreszenzexperimenten [JW4]

Ausgehend von der Elektronenemission aus der Partikeloberfläche soll geklärt werden, welcher Transferprozess entlang der DNA stattfindet und zur Zerstörung des PMMAs führt. Sowohl die Sensitivität des PMMAs gegenüber UV-Strahlung und Elektronen, als auch dessen detektierte Zerstörung entlang der DNA, lassen entweder einen optischen oder elektronischen Transferprozess vermuten. In diesem Zusammenhang wurden in der Publikation [JW4] weitere Untersuchungen durchgeführt, bei der die λ-DNA-Moleküle mit einem im UV-Bereich anregbaren Fluoreszenzfarbstoff (SYBR Green II®) markiert wurden. Anschließend wurden die DNA-Moleküle analog zur o.g. Methode gemeinsam mit AgNPs auf PMMA-beschichteten Glas-Chips immobilisiert, charakterisiert und mit fs-Laserpulsen belichtet. Hierbei lagert sich der verwendete Fluoreszenzfarbstoff auch an die AgNPs an, welches während der mikroskopischen Charakterisierung in einer intensiven Fluoreszenz der AgNPs resultierte. Während der fs-Laserbelichtung der angelagerten AgNPs konnte keine Fluoreszenz entlang der DNA detektiert werden, welche auf einen optischen Transfer in Form von anregender UV-Strahlung hingewiesen hätte. Stattdessen konnte durch einen Vergleich der Fluoreszenzaufnahmen vor- und nach der Belichtung

eine starke Abnahme der Fluoreszenzintensität im Bereich des belichteten AgNPs über eine Distanz von insgesamt 3,5 µm entlang der DNA beobachtet werden. Eine anschließende AFM-Charakterisierung dieses Bereiches zeigte eine Zerstörung der DNA von nur 400 nm, weshalb die mikrometerweite Abnahme der Fluoreszenz auf einen elektronisch-induzierten Transfer durch die plasmonisch unterstützte Elektronenemission eines AgNPs zurückgeführt werden kann (Abb. 3.8). Als Ursache für das verminderte Fluoreszenzsignal wird ein *Fluoreszenz-Bleaching* vermutet, welcher durch irreversible Schäden der Fluoreszenz-Moleküle infolge des plasmonisch-induzierten Anregungstransfers in DNA-Molekülen verursacht wird.

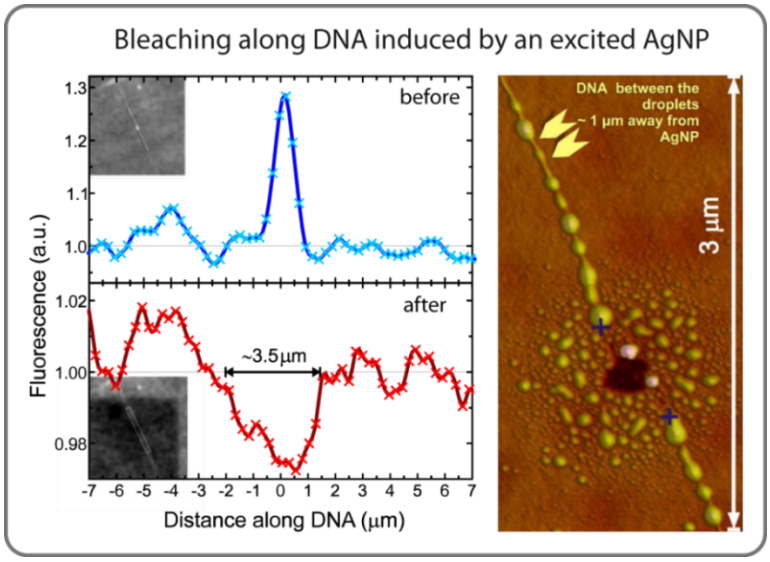

Abb. 3.8. Fluoreszenzabnahme entlang der DNA durch einen plasmonisch induzierten Anregungstransfer. (Links) Intensitätsprofil der fluoreszenzmarkierten DNA vor (blau) und nach (rot) der Belichtung. Die verstärkte Fluoreszenz am AgNP am Nullpunkt vor der Belichtung ist deutlich sichtbar. (Rechts) AFM-Aufnahme einer kurzreichweitigen Zerstörung der DNA.

Die Kontrollexperimente zur Belichtung von DNA-Molekülen als auch von AgNPs, welche weiter von der DNA entfernt sind, zeigten keine signifikante Veränderung Fluoreszenz der DNA, wodurch die notwendige unmittelbare Nähe bzw. der direkte Kontakt zur DNA für einen Transfer aus [JW3] bestätigt wird. Frühere Studien zur Untersuchung der DNA-Leitfähigkeit haben gezeigt, dass ein elektronischer Transport in einzelnen DNA-Molekülen nur über kurze Distanzen von einigen Nanometern vorkommen kann[77], und nur vereinzelt in DNA-Netzwerken und -bündeln längere Distanzen von mehreren hundert Nanome-

tern erreicht werden konnten[82]. Demnach könnten die aus der Partikeloberfläche austretenden Elektronen zur Anregung anderer Elektronen in der DNA führen, deren Anregungsenergie möglicherweise in der DNA propagieren und zur verminderten Fluoreszenz der DNA durch *Bleaching* bzw. zur Zerstörung des PMMAs führen.

Diese Hypothese des Anregungstransfers wurde in einem weiteren Experiment überprüft, bei der erneut durch einen Vergleich der Fluoreszenzaufnahmen vor und nach der fs-Laserbelichtung ein Anregungstransfer entlang der DNA demonstriert werden konnte. Im Gegensatz zum vorherigen Experiment führte die fs-Laserbelichtung eines AgNP-Agglomerats (Donor) zur starken Abnahme der Fluoreszenzintensität des fluoreszenzmarkierten unbelichteten AgNPs (Akzeptor), welcher über die DNA in einer Distanz von 5,7 µm mit dem Donor verbunden war (Abb. 3.9a). Um auszuschließen, dass es sich um eine generelle Abnahme der Fluoreszenzintensität handelt, wurden die Intensitätsänderungen mehrerer einzelner unbelichteter AgNPs nahe der DNA miteinander verglichen. Hierbei wies der Akzeptor-AgNP im Vergleich zu den Kontrollpartikeln einen über 10-fach höheren Intensitätsverlust nach der Belichtung auf (Abb. 3.9b).

Im Vergleich zu dem in [JW3] beobachteten mikrometerweiten Anregungstransfer blieb die DNA über den beobachteten Bereich größtenteils erhalten. Neben ihrer möglichen Verwendung als Template zur Herstellung von Nanostrukturen bestehen somit auch mögliche Anwendungen im Bereich der molekularen Elektronik, in der die DNA als Medium zum Transport von Informationen, z.B. von elektronischen Anregungen dient. Im Gegensatz zu früheren Arbeiten von *Braun et al.*, bei denen λ-DNA-Moleküle zwischen zwei Elektroden elektrisch aufgespannt und anschließend metallisiert wurden, um einen molekularen elektrisch leitenden Draht herzustellen[83,84], wird in der hier beschriebenen Methode der Transfer kontaktfrei über die Laserbelichtung eines Nanopartikels induziert und ohne eine Metallisierung der DNA erreicht. Somit ist sie nicht auf einen stabilen Kontakt zu äußeren Elektroden angewiesen. Aufgrund des Einsinkens des Donor-AgNPs in die PMMA-Schicht ist diese Methode bislang auf eine einmalige Nutzung beschränkt, welche durch weitere theoretische und experimentelle Studien vermieden werden könnte.

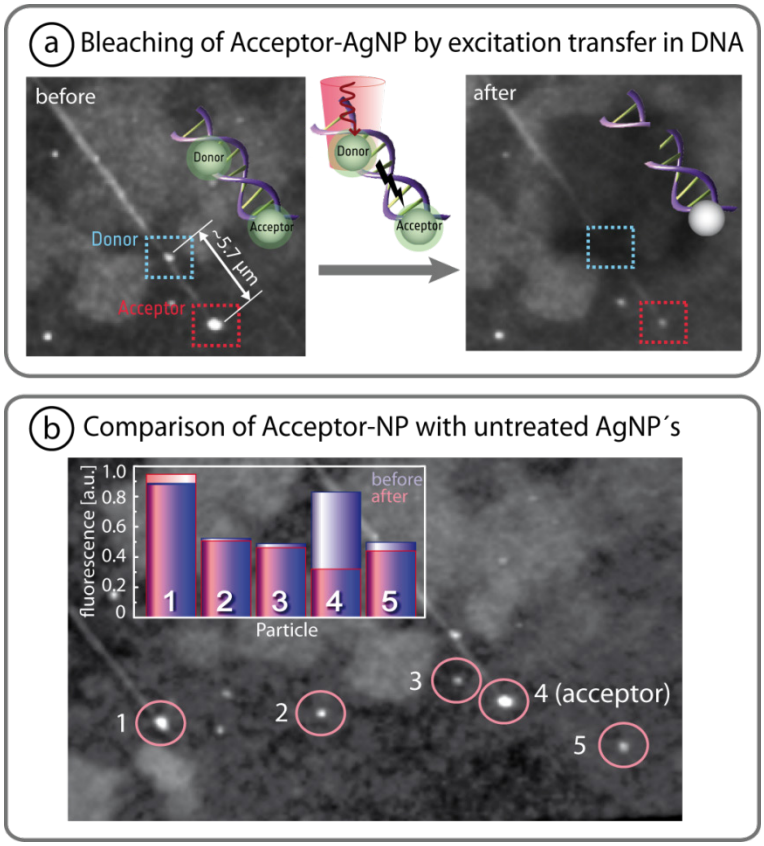

Abb. 3.9. Experimentelle Untersuchung des Anregungstransfers in DNA. (a) Durch einen induzierten Anregungstransfer kommt es zur starken Abnahme der Fluoreszenzintensität des fluoreszenzmarkierten Akzeptor-AgNPs. (b) Verglichen mit unbelichteten AgNPs (Kontrollen: Nr.1-3,5) zeigt der Akzeptor-AgNPs (Nr.4) eine klare Fluoreszenzabnahme.

3.3.4 Polarisationsabhängigkeit des DNA-Anregungstransfers [JW5]

Für eine zukünftige Anwendung ist neben der vollständigen Aufklärung eine dauerhafte Stabilität der verwendeten Nanopartikel nötig, welche mit den bisher verwendeten AgNPs nicht gegeben ist. Insbesondere die unter Umgebungsbedingungen zu beobachtende Oxidation der AgNPs kann zur stetigen Veränderung ihrer Resonanzwellenlänge führen, welche die optimale Belichtung dieser Partikel erschwert[85,86]. Im Vergleich dazu besitzen AuNPs neben ihrer Biokompatibilität den Vorteil, chemisch stabil zu sein. Aus diesem Grund wurden in [JW5] weitere Experimente mit AuNPs durchgeführt. Hierbei sollte insbesondere geklärt werden, ob die plasmonische Anregung von AuNPs mittels fs- Laser-

pulsen ebenfalls einen Anregungstransfer in benachbarten DNA-Molekülen hervorrufen kann. Ähnlich zu den vorhergehenden Experimenten erfolgte die plasmonische Anregung der AuNPs mittels fs-Laserpulsen bei einer Wellenlänge von 1030 nm. Es konnte sowohl eine lokale Zerstörung als auch eine Fragmentierung der DNA im Bereich von belichteten AuNP-Agglomeraten (Di- und Trimere) über eine Distanz von 1 µm beobachtet werden. Die Fragmentierung entlang der DNA findet hierbei nur bei einer parallelen Ausrichtung des E-Feldes zur den gestreckten DNA-Molekülen statt und ähnelt der in [JW3] induzierten Nanostruktur, welche sich durch Unterbrechungen entlang der DNA auszeichnet und auf einen Anregungstransfer hinweist. Jedoch im Vergleich zu [JW3] kommt es hierbei zu keiner Zerstörung des PMMAs unterhalb der DNA, was möglicherweise auf einen stärker lokalisierten Transfer zurückgeführt werden kann. Die Kontrollexperimente zur Belichtung von unmarkierten DNA-Molekülen, sowie auch mit AuNPs-markierter DNA mit einem Polarisationswinkel von 45° zur DNA, zeigten keine vergleichbaren Auswirkungen (Abb. 3.10).

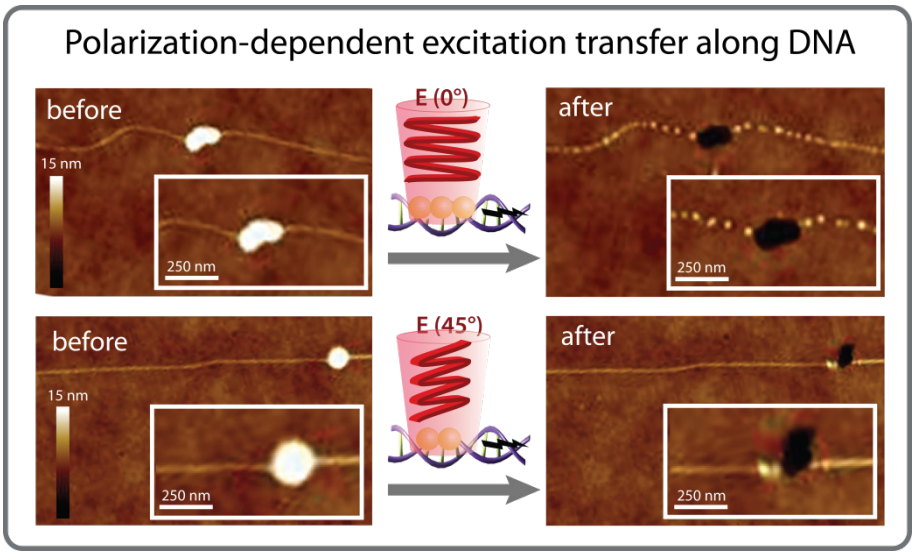

Abb. 3.10. Polarisationsabhängige fs-Laserbelichtung von AuNP-Multimeren an DNA-Molekülen. Nur eine parallele Ausrichtung des E-Feldes zur DNA führt zu lokalen Zerstörungen entlang der DNA.

Somit weisen diese Ergebnisse auf eine Abhängigkeit des Anregungstransfers von der Richtung des elektromagnetischen Feldes des Lasers hin. Ähnlich zu den in Abschnitt 3.2 belichteten AuNP-Dimeren könnte damit auch der Anregungstransfer in der DNA selektiv induziert werden.

Obwohl die vollständige Aufklärung des Mechanismus dieses entdeckten Anregungstransfers noch eine Anforderung für zukünftige Arbeiten bleibt, zeigen die Ergebnisse dieser Arbeit, dass sich auch die stabileren AuNPs für einen plasmonisch induzierten Anregungstransfer eignen und somit in zukünftige DNA-basierte elektrische Chips implementiert werden könnten.

4 Zusammenfassung und Ausblick / Summary and Outlook

In der vorliegenden Arbeit wurden die Wechselwirkungsmechanismen von Licht mit Metallnanopartikeln vorgestellt und ihre Auswirkungen auf einer Polymer-Oberfläche und an benachbarten DNA-Molekülen untersucht. Beginnend bei der selektiven Einstellung der optischen Eigenschaften metallischer Nanopartikel, über ihre leistungsabhängige optimierte fs-Laserbelichtung für die lokale Manipulation, zeigt sie schließlich die Auswirkungen der Nanopartikelvermittelten Manipulation auf molekularer Ebene anhand von DNA-Molekülen mit der Demonstration eines molekularen weitreichenden Anregungstransfers.

Im ersten Teil wurden die optischen Eigenschaften einzelner Goldnanopartikel auf einer dielektrischen/metallischen Interferenzschicht untersucht. Mittels spektroskopischer Messungen und theoretischer Berechnungen wurde gezeigt, wie das Streuverhalten einzelner Goldnanopartikel und Goldnanopartikel-Dimere selektiv durch die Veränderung der optischen Weglänge des Lichtes in der Interferenzschicht modifiziert werden kann. Im Vergleich zu ähnlichen Methoden, bei denen gesamte Partikelarrays untersucht wurden, konnten in dieser Arbeit die Auswirkungen an Einzelpartikeln charakterisiert werden. Diese Untersuchungen könnten somit als Grundlage für die Herstellung eines neuen sensorischen Verfahrens dienen, bei der die optische Detektion der Veränderung des Streuverhaltens einzelner Nanopartikeln über Brechungsindexänderungen im Fernfeld stattfinden.

Im zweiten Teil konnte unter Nutzung des Nanoantennen-Effektes erfolgreich demonstriert werden, dass eine plasmonische Anregung von Metallnanopartikeln mit intensiven fs-Laserpulsen zur Emission von Elektronen und zur lokalen Zerstörung ihrer Umgebung führt. Diese hängt von der Intensität der Laserpulse ab. Für einzelne Gold- und Silbernanopartikel konnte jeweils ein optimaler Intensitätsbereich über die Zerstörung eines elektronensensitiven Polymers experimentell ermittelt werden. Eine Anwendung auf anisotrope Goldnanopartikel-Dimere ermöglicht die selektive Manipulation ausgewählter Strukturen über die Einstellung des Polarisationswinkels der Laserstrahlung.

Darauf aufbauend erfolgte im dritten Teil die Erweiterung auf DNA-Moleküle, um die Auswirkungen der emittierten Elektronen während der plasmonischen Anregung metallischer Nanopartikel auf Biomoleküle zu untersuchen. Neben einer lokalen Zerstörung im Bereich des Nanopartikels wurde durch einen Anregungstransfer eine selektive Zerstörung des Polymers entlang des darüber liegenden Biomoleküls hervorgerufen. Damit können DNA-Moleküle als Template verwendet werden, um auch komplexe Nanostrukturen zu erzeugen. Durch weitere Studien sowie Optimierung könnte dieses Verfahren in Zukunft auch auf DNA-Superstrukturen (DNA-Origami) angewendet werden. Des Weiteren konnte auch ein zerstörungsfreier Anregungstransfer über eine Abnahme der Fluoreszenzintensität entlang der DNA bzw. an einem Akzeptor-Partikel demonstriert werden, bei der die DNA nicht über ihre gesamte Länge sichtbar beschädigt wurde. Somit könnte mit diesem Verfahren DNA in Zukunft auch zur Weiterleitung von Informationen dienen, welches insbesondere für die Miniaturisierung und Weiterentwicklung von derzeitigen Halbleiter-Chips einen von großem Vorteil wäre.

Die Übertragung der Untersuchungen auf stabilere biokompatible Goldnanopartikel-Multimere zeigte einen Anregungstransfer ausschließlich bei einer parallelen Orientierung des E-Feldes zur DNA. Neben dem Vorteil der chemischen Stabilität von Goldnanopartikeln gegenüber Silber könnten die Transferprozesse ähnlich zur o.g. Nanostrukturierung mit Dimeren selektiv über den Polarisationswinkel induziert werden.

Da photoinduzierte Elektronentransferprozesse auch in der Lage sind DNA-Schäden hervorzurufen bzw. zu reparieren, sind diese Ergebnisse hinsichtlich ihrer Anwendung nicht nur auf die Herstellung von Nanostrukturen und Biochips beschränkt, sondern könnten auch im Bereich der Krebsforschung als nanoskaliges optisches Werkzeug von Nutzen sein. Somit stellt die vollständige Aufklärung und weitere Optimierung dieses plasmonisch induzierten Anregungstransfers bis zur Anwendungsreife ein vielversprechendes Ziel für die Grundlagenforschung wie auch die Technologieentwicklung dar.

In the presented work the interaction of light with metal nanoparticles and their effects on a polymer layer and DNA molecules were investigated. Starting with the selective tuning of the particle properties, over the intensity-dependent and optimized fs-laser irradiation for the local manipulation, the work shows in the last part the effects of the nanoparticle mediated manipulation at the molecular scale using DNA molecules with the demonstration of a long-range excitation transfer.

In the first part the optical properties of single gold nanoparticles above a dielectric/metallic interference layer were investigated. In dependence on the interference path, the scattering spectra and distribution of single gold nanoparticles and dimers could be selectively modulated, which was experimentally and theoretical characterized by spectroscopic measurements, optical imaging and calculations, respectively. Compared to similar methods, where the optical properties were studied for whole particle ensembles, this work characterized the effects on the single particle level. These investigated principles could contribute to a novel sensing method for the optical detection of changes in the scattering behaviour by refractive index changes in the far-field at the single nanoparticles level.

The second part demonstrated the successful use of the nano-antenna effect, where the emission of electrons from the nanoparticles is initiated by the plasmonic excitation with fs laser pulses, leading to the local destruction of the particle surrounding. These destructions depend strongly on the laser pulse intensities. The optimal intensity range was investigated experimentally for single gold- and silver nanoparticles by the local destruction of an electron sensitive polymer. The application to anisotropic gold nanoparticle dimers allows a selective manipulation by tuning the polarization angle of the laser light.

Based on these results, this method was extended to DNA molecules to investigate the effects of the emitted electrons on biomolecules during the plasmonic excitation of metal nanoparticles. In addition to the local destruction at the particle position, an excitation transfer along the DNA is observed leading to the selective destruction of the polymer following the original position of the biomolecule. These results show the possibility for the usage of DNA molecules as template to produce complex nanostructures. By further optimization this procedure could be applied to DNA superstructures (DNA origami).

Furthermore the excitation transfer was demonstrated non-destructively by the bleaching of the DNA and of an attached acceptor particle, respectively. Therefore, the DNA was apparently not destroyed over its whole length but only at the position of the excited particle. Thus, DNA may also play a role in prospective technologies for transferring information, which would have great advantages for the miniaturization and further development of today´s semiconducting devices.

The experimental investigations with stable biocompatible gold nanoparticle multimers revealed an excitation transfer exclusively at a parallel orientation of the E-field to the DNA. In addition to the chemical stability of gold nanoparticles compared to silver, the transfer process could be induced selectively by tuning the polarization angle, like in the case of the above-named nanostructuring with dimers.

Due to the fact that electron transfer processes can induce and repair DNA damages, the application of these results is not limited to the production of nanostructures and biochips; they could also be useful in the field of cancer research as a nanoscale tool. Therefore, the complete explanation and further optimization of the observed plasmonically induced excitation transfer up to its commercial stage represents a promising aim for further research and in the development of new technologies.

5 Veröffentlichte Arbeiten

[JW1] Tuning of spectral and angular distribution of scattering from single gold nanoparticles by sub-wavelength interference layers
J. Wirth[‡], F. Garwe[‡], J. Bergmann, W. Paa, A. Csáki, O. Stranik, W. Fritzsche. Nano Letters, 2014. **14** (2): p. 570–577

[JW2] Molecular plasmonics: light meets molecules at the nanoscale
A. Csáki, T. Schneider, J. Wirth, N. Jahr, A. Steinbrück, O. Stranik, F. Garwe, R. Müller, W. Fritzsche. Philosophical Transactions of the Royal Society A: Mathematical, Physical and Engineering Sciences, 2011. **369** (1950): p. 3483-3496

[JW3] Plasmonic nanofabrication by long-range excitation transfer via DNA nanowire
J. Wirth, F. Garwe, G. Hähnel, A. Csáki, N. Jahr, O. Stranik, W. Paa, W. Fritzsche. Nano Letters, 2011. **11**(4): p. 1505-1511

[JW4] Plasmonic coupling and transfer of an excitation along a DNA nanowire
J. J. Toppari[‡], J. Wirth[‡], F. Garwe[‡], O. Stranik, A. Csáki, Joachim Bergmann, W. Paa, W. Fritzsche. ACS Nano, 2013. **7**(2): p. 1291-1298

[JW5] Plasmonically-enhanced electron escape from gold nanoparticles and their polarization-dependent excitation transfer along DNA nanowires
J. Wirth[‡], F. Garwe[‡], R. Meyer, A. Csáki, O. Stranik, W. Fritzsche. Nano Letters, 2014. **14**(7): p. 3809-3816

[‡] Geteilte Erstautorenschaft

5.1 Tuning of spectral and angular distribution of scattering from single gold nanoparticles by sub-wavelength interference layers [JW1]

	Autorenschaft der Publikation
Janina Wirth[‡]	Konzeptentwicklung Messungen und Evaluierung der Daten Diskussion des Konzepts und der Ergebnisse Diskussion und Korrektur des Manuskripts
Frank Garwe[‡]	Evaluierung der Daten Diskussion des Konzepts und der Ergebnisse Diskussion und Korrektur des Manuskripts
Joachim Bergmann	Diskussion und Korrektur des Manuskripts
Wolfgang Paa	Korrektur des Manuskripts
Andrea Csáki	Korrektur des Manuskripts
Ondrej Stranik	Durchführung der Simulationen Diskussion des Konzepts und der Ergebnisse Diskussion und Korrektur des Manuskripts
Wolfgang Fritzsche	Diskussion des Konzepts und der Ergebnisse Diskussion und Korrektur des Manuskripts

Nano Letters, 2014. **14** (2): p. 570–577

NANO LETTERS

Letter

pubs.acs.org/NanoLett

Tuning of Spectral and Angular Distribution of Scattering from Single Gold Nanoparticles by Subwavelength Interference Layers

J. Wirth, F. Garwe, J. Bergmann, W. Paa, A. Csaki, O. Stranik,* and W. Fritzsche

Leibniz Institute of Photonic Technology (IPHT), 07745 Jena, Germany

Supporting Information

ABSTRACT: Localized surface plasmon resonance (LSPR) as the resonant oscillation of conduction electrons in metal nanostructures upon light irradiation is widely used for sensing as well as nanoscale manipulation. The spectral resonance band position can be controlled mainly by nanoparticle composition, size, and geometry and is slightly influenced by the local refractive index of the near-field environment. Here we introduce another approach for tuning, based on interference modulation of the light scattered by the nanostructure. Thereby, the incoming electric field is wavelength-dependent modulated in strength and direction by interference due to a subwavelength spacer layer between nanoparticle and a gold film. Hence, the wavelength of the scattering maximum is tuned with respect to the original nanoparticle LSPR. The scattering wavelength can be adjusted by a metallic mirror layer located 100−200 nm away from the nanoparticle, in contrast to near-field gap mode techniques that work at distances up to 50 nm in the nanoparticle environment. Thereby we demonstrate, for the first time at the single nanoparticle level, that dependent on the interference spacer layer thickness, different distributions of the scattered signal can be observed, such as bell-shaped or doughnut-shaped point spread functions (PSF). The tuning effect by interference is furthermore applied to anisotropic particles (dimers), which exhibit more than one resonance peak, and to particles which are moved from air into the polymeric spacer layer to study the influence of the distance to the gold film in combination with a change of the surrounding refractive index.

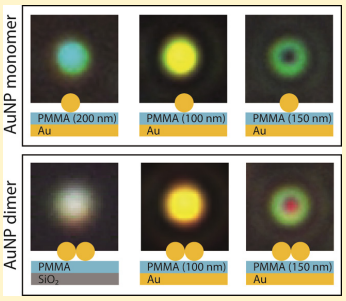

KEYWORDS: *Plasmonic nanoparticles, gold film, PMMA, polarization, interference, point spread function, light scattering, fs laser pulse*

Metal nanoparticles (NPs) show a resonant oscillation of their conduction electrons upon light irradiation[4] which leads to an increase of nanoparticle scattering. This localized surface plasmon resonance (LSPR) effect is utilized for biosensing down to the single NP level,[5] for enhancing the signal of fluorescent labels,[6] for therapeutic approaches based on either cell damages[7] or on the release of active compounds,[8] or for the coupling of laser light pulses through resonant plasmonic interactions with metal NPs into attached molecular wires.[9] Most applications are based on a resonant excitation of the particles, so that a tuning of the particles resonance to the wavelength of accessible light sources, such as lasers, is a key issue for efficient use.

Beyond the selection of plasmonic particle parameters such as composition, size, and geometry,[10] there is a search for external parameters that influence the resonance of the NPs and could be used for tuning this value. One possibility is the change of the refractive index of the dielectric medium in the evanescent near-field of NPs.[11] A metal (usually gold) film in the NP's proximity (<50 nm distance) represents another possibility. Such mirror experiments are known from fluorophores: Early Drexhage experiments with fluorescence molecules placed above a metallic mirror found affected angular distribution of fluorescence and affected fluorescence decay time.[1] Later theoretical studies by Enderlein show that the photon number of single molecule fluorescence can be influenced (more than quantum yield) by a metallic layer in the near-field of the molecules.[2] Experimental studies also show that the fluorescence emission spectrum of a single molecule can be changed by embedding it inside a tunable planar subwavelength metal microcavity.[3] Nevertheless, fluorescence involves excitation of a single electron from one electronic level to an excited state, followed by time-delayed emission of a photon with longer wavelength. This fluorescence mostly happens in conjugated molecules like dyes and is difficult to observe in large systems like metal nanoparticles where they do not have any quantized energy levels. Metal NPs exhibit an interaction of their localized surface plasmon resonance with the surface plasmon polariton in the adjacent metal layer that changes the particle resonance (gap mode).[12] Moreover, the gold film within the near-field of the NP induces a polarization of the scattered light, resulting in a doughnut-shaped PSF when imaged in the far-field.

Received: October 8, 2013
Revised: December 23, 2013
Published: January 6, 2014

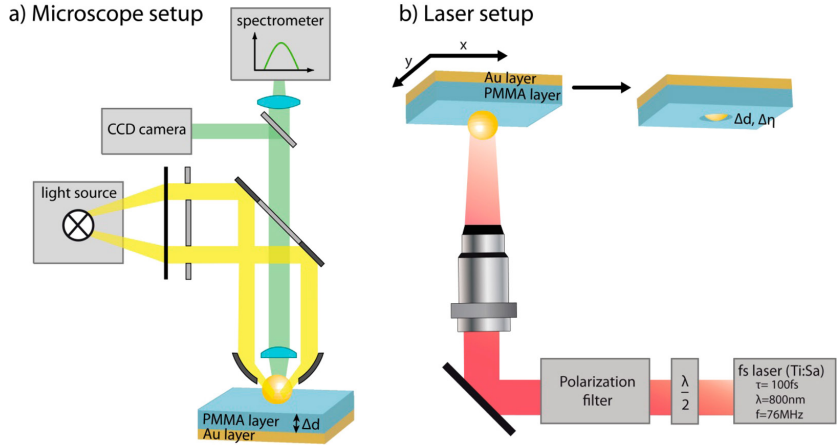

Figure 1. (a) Microscope setup for dark-field detection of the scattered light of a single NP. (b) Microscope setup for polarization-dependent femtosecond laser irradiation of single NPs, which was used for sinking of the NPs into the spacer polymer (PMMA) layer.

There are first (bio)sensing demonstrations with plasmonic NP ensembles using interferometric setups of lithographic fabricated metal nanorods placed at Bragg distance above a metal mirror,[13] of a nanoparticle layer separated from an aluminum mirror layer by an silica layer,[14] of metal spheres placed on several high- and low index materials,[15] of nanostructured slits in a metal film,[16] or of NPs on a 500 nm silica layer on top of a silicon substrate.[17] Interferometric effects could be demonstrated by a Fabry−Perot setup consisting of two gold layers or of one gold layer and particle islands[18] acting as mirrors in a distance of half of the excitation wavelength. A spectral tuning of microcavity modes by a single metal NP positioned inside this setup could be realized.[19]

In this Letter, we go even further and demonstrate the possibility to establish and characterize an interferometric technique using a single gold NP only, separated from a gold film by a polymeric subwavelength layer. The utilized interference cavity consists of a gold layer, a distance layer of subwavelength thickness (Δd) of a transparent polymer (polymethylmethacrylate, PMMA), and single gold nanoparticles (AuNPs) (Figure 1). To fabricate the nanocavity sample, a gold layer with a thickness of 200 nm was prepared on a glass coverslip by e-beam evaporation. In a next step, a polymer layer (100, 150, or 200 nm thickness) was deposited on top of this gold layer by spin coating 100 μL of a 1.6% PMMA solution in toluene, hardened by baking at 180 °C for 10 min. For the particle preparation, AuNPs were synthesized by a nine step seeded growth synthesis to get a solution containing AuNPs with a diameter of around 80 nm.[20] Afterward, for every sample with a certain PMMA thickness, a droplet of the nanoparticle solution (~10^8 NP/mL) was dried at 35 °C on the PMMA surface. Finally, all samples were washed in deionized water for 5 min and dried under nitrogen flow in atmosphere.

In our experiment for plasmonic excitation (Figure 1a), polychromatic light (halogen light source HAL 100, Carl Zeiss Jena GmbH, Jena, Germany) was focused onto the AuNPs by using a microscope (AxioImager.Z1m, Carl Zeiss Jena GmbH, Jena, Germany) with dark field objective (100 × 0.75 NA). To set the focal plane on top of the PMMA surface, the light was focused on single AuNPs in the immediate vicinity of the particles to be measured. The scattered light from the sample was collected in this dark field geometry by the same objective and detected by a CCD color camera (AxioCam MRc 5, Carl Zeiss Jena GmbH, Jena, Germany). Only the light of the particle of interest passed through a pinhole with a diameter of 75 μm. This light was coupled into a multimode fiber and directed to an Acton Research SpectraPro 2300i microspectrometer (Princeton Instruments, Trenton, NJ), for recording a spectrum of the single AuNP.

Changing the refractive index and diminishing the NP metal layer distance can be reached by inserting NP into the PMMA layer in between NP and metal layer. Sinking of AuNPs into the PMMA layer was induced using a titanium:sapphire laser (Mira Optima 900-D, Coherent Inc., Santa Clara, CA) delivering 100 fs pulses at a wavelength of 800 nm and a repetition rate of 76 MHz (Figure 1b). The femtosecond (fs) pulses were coupled to an inverse microscope (AxioObserver, Carl Zeiss Jena GmbH, Jena, Germany), which was equipped with an oil immersion objective (40 × 1.25 NA) to obtain a pulse fluence of 3 mJ/cm^2. For sample illumination the stage scanning method using a PI Nano 545 3R7 stage and a PI XYZ piezo controller (PI instruments Inc., Karlsruhe, Germany) was utilized. The scanning was done in 1 μm steps, which guarantees the excitation of all AuNPs within the area. Irradiation time at each position was 1000 ms. At the end of this procedure an area of 20 μm × 20 μm was scanned and illuminated with a uniform fs laser fluence. The AuNPs on the PMMA surface were characterized before and after fs irradiation by atomic force microscopy (Nanoscope III with Dimension 3100 head from Digital Instruments, Santa Barbara, CA, USA) as well as dark field microscopy (see Figure 1 above).

Spectra from single spherical AuNPs recorded with the microscope setup (Figure 1a) are shown in Figure 2. The PMMA spacer layer defines the interference path distance. The resulting spectrum of the scattered light from the AuNP on a 200 nm thick layer shows a strong maximum in the blue−green spectral region. When the PMMA layer thickness is reduced to 150 nm, the spectrum shifts to the green range. Here a

dx.doi.org/10.1021/nl4037438 | Nano Lett. 2014, 14, 570−577

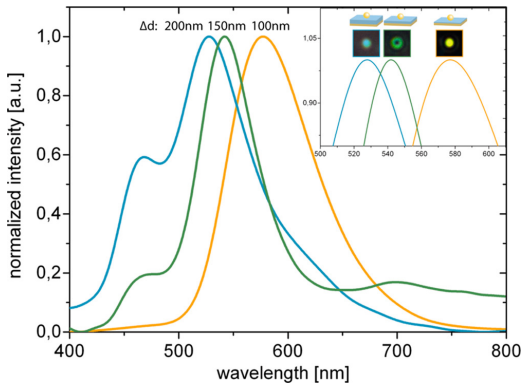

Figure 2. Scattering spectra of single AuNPs (diameter = 80 nm) on a PMMA coated Au layer. The spectrum changes in dependence of the PMMA layer thickness, Δd. With decreasing PMMA thickness Δd the scattering spectrum of the AuNP is shifting to longer wavelengths: from blue-green (Δd = 200 nm) over green (Δd = 150 nm) to yellow (Δd = 100 nm). At a distance of 150 nm the single AuNP appears as a green doughnut-shaped scattering in the dark-field image (inset).

doughnut-shaped pattern of the scattered light is visible. In case of PMMA layer of only 100 nm, which is far away from near-field interaction of AuNP and Au layer, the spectrum shifts into the yellow range.

From a theoretical point of view, the light interacts with metal nanoparticles immobilized on thin interference layers in a complex manner. To simplify the process of light interaction with immobilized NPs and to get a physical understanding of this interaction, the process is divided into three consecutive steps: In the first step, only the light interaction with the interference layers (PMMA layer/Au substrate) will be considered to calculate the resulting electromagnetic field distribution in the stratified medium. The second step describes the interaction of the resulting electromagnetic field with metal NPs. In the last step, the interaction of light originating (scattered) from the metal NP with the stratified medium will be analyzed. This separation into three steps is justified, because the AuNPs are deposited at a low density on the surface, and can be regarded as a small perturbation in the interference layers.

Experimentally, the samples were observed in the reflection dark field setup. In this configuration, unpolarized light falls onto the samples in a narrow range of inclination angles, but at azimuthal angles ranging from 0° to 360°. The inclination angles are higher than the maximum collection angle, which is defined by the objective's numerical aperture. Because the illumination light has a short coherence length and it is not tightly focused by the dark field condensor, the light collected from different azimuthal angles can be treated independently. Therefore, it is valid to calculate only the interaction of a single plane wave incident under an oblique angle onto the PMMA layer/Au substrate system. The field distribution in such a system can be analytically solved by expanding the field in each layer by a reflected and transmitted plane wave with coefficients for reflection and transmission obtained from Fresnel equations.[21]

When such a system is illuminated with a plane wave, the metal substrate acts as a reflecting mirror, and an interference pattern is created in the PMMA and in air. The average electric field amplitude and orientation strongly depend on the wavelength of the light and on the thickness of the PMMA layer.

The optical response of the metallic nanoparticle strongly depends on direction of the electric field of the incident light. As it will be shown later, there are two significant directions with different optical responses, perpendicular and parallel to the substrate. Therefore, the ratio (R_{per}) of the average electric field perpendicular to the substrate and the average electric field parallel to the substrate for both polarizations is defined as:

$$R_{per} = \frac{\left|\vec{E}^{TM}_{per}\right|}{\left|\vec{E}^{TM}_{par}\right| + \left|\vec{E}^{TM}_{par}\right| + \left|\vec{E}^{TE}_{par}\right|} \quad (1)$$

where upper superscript and lower superscript denote the electromagnetic field polarization (TE or TM) and the E-field direction (parallel or perpendicular to the sample surface), respectively.

This ratio (R_{per}) was evaluated for three different PMMA thicknesses at the future position of a AuNP and is presented in Figure 3a. In the calculation, the following parameters were

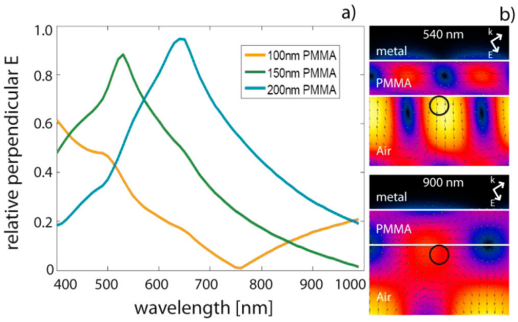

Figure 3. (a) Graph of the relative quantity of E-field in the direction perpendicular to the PMMA layer/Au substrate (vertical polarization) at a distance of 40 nm from PMMA substrate. The E-field is almost vertically oriented at plasmon resonance of the AuNPs (λ = 540 nm) in the case of 150 nm PMMA layer. (b) Electric field distribution in the air/PMMA (150 nm)/Au system illuminated with 540 nm (top) and 900 nm (bottom) light at 60°. (False color map: real part of E, arrows indicate direction of the real part of E, dark circles represents the position of the AuNP).

used: PMMA layer with a thickness of 100, 150, or 200 nm with the refractive index n = 1.49. The refractive index of gold was taken from Johnson et al.;[22] the angle of incidence of the light was set to 60°, which corresponds to the specification of the used microscope objective (NA). The field was calculated at the distance of 40 nm from the PMMA layer in air, which corresponds to the center of the used AuNP. Examples of the E-field distributions in the layers for 150 nm PMMA and for two different observation wavelengths are given in Figure 3b, where the interference pattern is clearly visible.

The graphs show that the E-field can be almost perpendicular or parallel to the PMMA layer/Au substrate for a specific wavelength and the position can be tuned by the thickness of the PMMA layer. The E-field is parallel for a 100 nm thick PMMA layer at 760 nm, and the E-field is almost perpendicular for a 150 nm thick layer at 520 nm and for a 200 nm thick layer

dx.doi.org/10.1021/nl4037438 | Nano Lett. 2014, 14, 570−577

at 650 nm. These properties of the interference layer obviously enable an excitation of specific plasmon modes in metal nanostructures.

The second step of the separation process mentioned above consists of the interaction of a spherical metal nanoparticle with a plane wave placed in homogeneous medium. This is fully described by Mie theory, which allows calculating the scattering spectra of the nanoparticle.[23] The scattering spectra of substrate-immobilized AuNP can be also calculated by Mie theory, if the effect of the PMMA layer is approximated by using an effective refractive index of the embedding medium.[24] The effective refractive index (n_{eff}) is the weighted average of refractive index of the superstrate (the medium above the substrate) and the substrate. In this approximation, the scattering spectra are independent of the direction of the *E*-field. The calculated scattering spectrum (C_{sca}) of spherical 80 nm diameter AuNP on the PMMA layer (fitted n_{eff} = 1.25) is shown in Figure 4 by the dashed line. The spectrum exhibits a peak at around 540 nm that can be associated with the known plasmon resonance of the particles.[23] In this NP size range, the plasmon resonance is still dominated by a dipole oscillation of the conductive electrons in the NP.[25]

Adding a metallic substrate to the NP/PMMA system modifies the scattering spectra of the nanoparticles significantly. In this case, the effect of the metal substrate cannot be simplified by an effective refractive index. As mentioned before, the light scattered from NPs at the plasmon resonance can be approximated by light emitted from an oscillating electric dipole. Therefore, we can apply the same mathematical methods, which were developed for the analysis of emission from a fluorescent dye close to the interface. An electric field (E) at a place (r) generated by an oscillating dipole with dipole moment (p) at the position (r_0) can be expressed by Green's function formalism[26] such as:

$$E(r) = \omega\mu\mu_0 G(r, r_0)p \tag{2}$$

where G is the Green function of the given space geometry (eq 2). The scattered power (P) is then obtained from the E-field in a simple form as:

$$P = \frac{\omega}{2} Im\{E(r_0)p^*\} \tag{3}$$

Equation 3 states that the emission power is changed if the *E*-field of the radiating dipole is modified by the interfaces (expressed by different forms of the Green function). For a dipole located at larger distances (>wavelength/5) from the metal layer, the emitted power results from the interference of the original dipole field with the reflected field from the metal substrate. This leads to the oscillatory character of the emitted power in dependence of the distance.[27]

The scattering spectrum of AuNPs with a PMMA layer and a gold substrate system (C_{sca}*) can be expressed in a first approximation as a product of the scattering spectrum of AuNPs in a homogeneous medium and the emission power of a dipole in the layered system, normalized to the emission power of a dipole in a homogeneous medium (P_0) (eq 4).

$$C^*_{sca} = C_{sca}\frac{P}{P_0} \tag{4}$$

The coefficient P/P_0 was calculated (for details of the Green function see Novotny et al.[28] and Supporting Information) for 100 and 200 nm thick PMMA layers with the dipole parallel to the interface and a 150 nm thick layer with the dipole oriented perpendicular to the interface. The results are plotted in Figure S1. The choice of dipole orientations reflects approximately the profile of the excitation field at the plasmon resonance, because the dipole plasmon mode is in the same direction as the inducing electric field (see Figure 3). The resulting scattering spectra of AuNPs on 100, 150, and 200 nm thick layers are presented in Figure 4. It can be seen that the position of the plasmon peak is changing with the thickness of the PMMA. For 200 nm PMMA the position is shifted to shorter wavelengths. For 150 nm it is almost identical, and for 100 nm it is shifted to longer wavelengths.

Dark field images of AuNPs on PMMA/metal substrate were recorded by the CCD camera of the microscope, with the signal being proportional to the square of the *E*-field. Approximating the AuNPs again by an oscillating dipole, the *E*-field can be expressed in the form of the Green function, where the total Green function is a multiplication of a Green function of the dipole in a given geometry and a transfer Green function of the microscope. In case of a dipole emitting in free space, the analytical expression for the total Green function (identical to the point spread function) can be found in.[28] These expressions were used to calculate the images from AuNPs, where the influence of the PMMA layer/Au substrate was expressed only by the orientation of the dipole. In the case of 100 nm/200 nm PMMA, the orientation was set parallel to the substrate, and for 150 nm PMMA, the orientation was set perpendicular to the substrate. The images of the AuNPs at the given plasmon wavelengths (modified by the PMMA/gold layer) are presented in the inset of Figure 4. It can be seen that images of AuNPs on

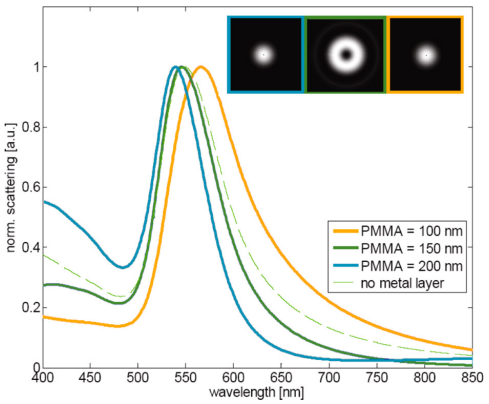

Figure 4. Calculated scattering spectra of single 80 nm AuNPs placed on a PMMA layer (Δd = 100, 150, 200 nm)/Au substrate in a homogeneous medium with an effective refractive index n_{eff} = 1.25. Inset: Calculated image of AuNPs placed on PMMA/Au substrate for the utilized microscope system (cf. Figure 1a, 100× objective, 0.75 NA).

100 and 200 nm PMMA result in bell-shaped profiles, but the image of AuNPs on 150 nm PMMA resembles a doughnut-shaped profile. The reason for this doughnut shape in the case of 150 nm PMMA is a destructive interference at the center of the image of the radially polarized *E*-field of the perpendicular dipole. A comparison with the experiment proves that even the simplified Green function yields good qualitative results and that the PMMA layer/Au substrate does not change the radially polarized character of the *E*-field.

dx.doi.org/10.1021/nl4037438 | Nano Lett. 2014, 14, 570−577

To prove the high local interference character of the scattered light of another particle shape and another particle environment, two further experiments were carried out. Figure 5 shows the spectrum and the dark field image from a single

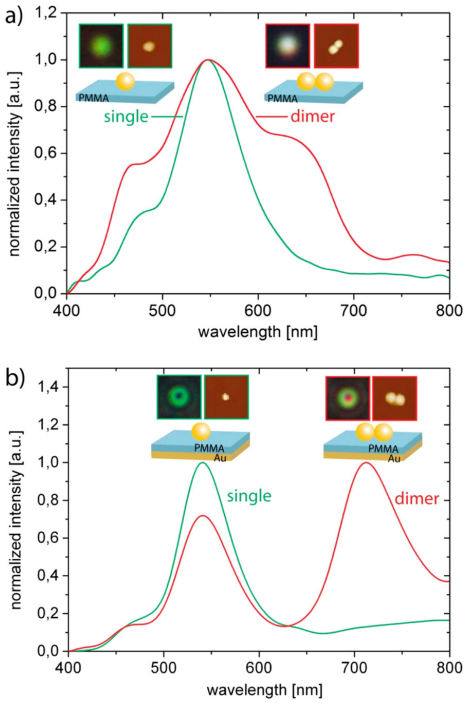

Figure 5. Effect of gold mirror layer. (a) Spectrum, dark field, and AFM image of a single AuNP and an AuNP dimer on PMMA. The well-known LSPR band at 550 nm is observed in both cases; the dimer shows additionally a second longer wavelength band. (b) Comparable data for a single AuNP and a AuNP dimer on PMMA 150 nm above a gold mirror layer. The much stronger red-shift of the second band of the dimer (compared to the case in a) can be explained by the influence of particle size ratios and distance onto the band position. In the dark field image, the single AuNP now results in a green doughnut-shaped PSF. The AuNP dimer shows a similar green doughnut but filled with a red bell-shaped PSF.

AuNP on a 150 nm PMMA layer without the Au layer (Figure 5a) in comparison with a single and a dimer AuNP on top of a 150 nm PMMA layer/Au substrate (Figure 5b). Single AuNPs on PMMA substrate show the well-known LSPR band at 550 nm. The scattered light is detected as a green bell shaped point spread function (PSF) (Figure 5a). In contrast, single AuNPs on the PMMA layer/Au substrate show a green doughnut shaped scattering (Figure 5b) as explained in the previous section. For AuNP dimer on PMMA without Au layer, the LSPR shifts into the red range of the spectrum using parallel polarization of the excitation light in relation to the dimer axis (Figure 7). At polarization perpendicular to the dimer axis, the LSPR remains in the green spectral range. Using unpolarized white light for excitation, the scattered light of AuNP dimers show both the LSPR in the red spectral range (red bell-shaped PSF in the center) as well as in the green spectral range (the green doughnut-shaped PSF around the red center) known from single AuNPs on the same layer system. The red curve in Figure 5b shows the spectrum of this arrangement.

In the case of dimers of metallic NPs the Mie theory cannot be used, so that numerical methods are required to calculate scattering spectra.[29] A finite element method implemented in the commercial software COMSOL was used (see Supporting Information for the details of the calculation). The resulting *E*-field distributions with scattering cross sections for three different orientations of the incident field are presented in Figure 6. The effect of the PMMA layer was again incorporated

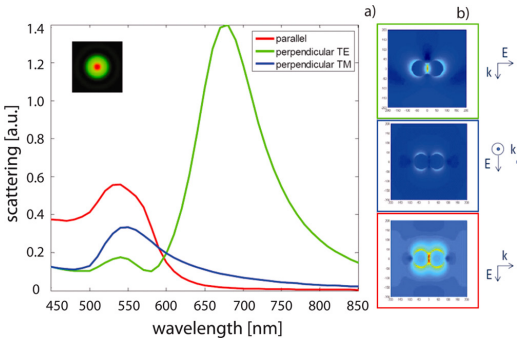

Figure 6. (a) Calculated scattering spectra of an 80 nm AuNP dimer with 2 nm interparticle separation in a homogeneous medium (n_{eff} = 1.25) for different polarization of the excitation light. Inset: Calculated image of an AuNP dimer placed on a 150 nm PMMA layer/Au. (b) Electric field representations ($\log(1 + E^2)$) around the AuNP dimer at the plasmon resonances for different polarization of the excitation light (indicated by vectors).

into the effective refractive index n_{eff} = 1.25, and the separation of the two AuNPs was set to 2 nm. The AuNP dimers exhibit a plasmon peak around 670 nm for an *E*-field parallel to the dimer axis (green curve). The dimer axis is fixed parallel to the PMMA layer. The AuNP dimers also exhibit a peak around 540 nm, which corresponds to the plasmon resonance of a single AuNP for both parallel and perpendicular directions of the *E*-field with respect to the PMMA substrate (red and blue curves). From Figure 3 and Figure 6 we conclude that a AuNP dimer placed on a 150 nm thick PMMA layer/Au substrate can be approximated as a combination of a perpendicular dipole scattering at 540 nm and a parallel dipole scattering at 670 nm. The dark field image of the dimer in such an approximation is shown in the inset of Figure 6.

The spectral change of the plasmon mode around 670 nm in AuNP dimers due to the presence of the PMMA layer/Au substrate was calculated. The similar procedure as in the case of the plasmon mode in single AuNP and described earlier was used. However, now the plasmon mode around 670 nm in AuNP dimers is restricted to oscillate always parallel to the interface. In eq 4, the scattering cross section from the numerical simulation of the AuNP dimers (green curve in Figure 6) was used. The resulting calculated scattering spectra of AuNPs dimers with 2 nm separation placed on a PMMA layer (Δd = 100, 150, 200 nm)/Au substrate and in homogeneous medium (n_{eff} = 1.25) for the case of plasmon excitation at 670 nm are presented in Figures S3 (in the Supporting Information). It is clearly visible that the position of

dx.doi.org/10.1021/nl4037438 | *Nano Lett.* 2014, 14, 570–577

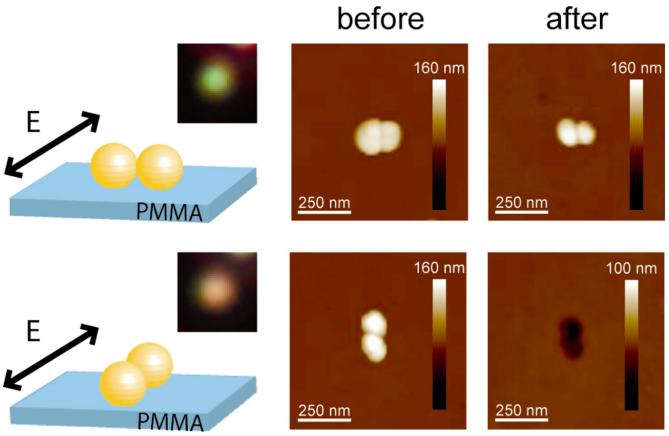

Figure 7. Effect of the polarization of incoming light. Top: Incident white light polarized perpendicular to the dimer axis results in LSPR and in increased scattered light at 530 nm (dark field image, left). AFM imaging does not show any damaging effect of the laser pulse irradiation (small apparent changes can be probably attributed to changes in scanning tip quality). Bottom: Laser light polarized parallel to the dimer axis shifts the LSPR, and an increased scattered light in the red spectral range is observed in the dark field image (left). AFM images show that the dimer sinks into the PMMA layer (right).

the plasmon peak is changing with the thickness of the PMMA. For 200 nm PMMA, the position is shifted to shorter wavelengths. For 150 nm it is shifted to longer wavelengths, and for 100 nm it is almost identical.

The dark field images of dimer AuNP on the top of 100 and 200 nm PMMA layer/Au substrate system together with the samples' topological characterization are presented in Figure S2 (in the Supporting Information). In these cases, the both plasmon resonances (~ 540 nm and 670 nm) cannot be spatially separated in the dark field image, because they both emit as bell-shaped PSF and so these overlap. This indicates that both plasmon oscillations are parallel to the substrate. For 100 nm PMMA, the plasmon resonance at longer wavelengths is enhanced (see Figures S1 and S3, orange (red) curve), but for 200 nm PMMA, the plasmon resonance at longer wavelengths is suppressed (see Figures S1 and S3, blue (black) curve).

AFM images in Figure 7 reveal that also AuNP dimers, excited by fs laser light parallel to the dimer axis, sink into the PMMA layer (dark area). The simple temperature effect in the immediate vicinity of metal nanoparticles can be excluded. Femtosecond laser illumination with fluences below the ablation threshold causes a temperature increase of 40 K in maximum.[30] This is too low for a thermally induced sinking of the metal nanoparticle into the PMMA layer, as confirmed by experimental determination of the required temperature of at least 300 °C.[31] An accumulated temperature raise during irradiation by femtosecond laser pulses with 76 MHz repetition rate can be excluded as shown by FEM calculations of heat conduction that result in an accumulated temperature increase of 3.5 K.[30] Excluding temperature effects as discussed before, we conclude that LSPR supports the high electric field of the fs laser pulses and leads to the possibility for electrons to override the work function of the gold in nanoparticles. These highly excited free electrons destroy the PMMA molecules around the dimer nanoparticle in a highly localized manner.[9] Hence, using polarized fs laser pulses at a wavelength of 800 nm, AuNP dimers can be selectively chosen for LSPR supported highly localized damage of the PMMA layer during irradiation.

Figure 8a shows the dark field image of a mixture of single AuNPs and AuNP dimers on top of a 150 nm PMMA layer on gold before and after fs laser irradiation. In the image of the single AuNP, the spectral doughnut-shaped scattering does not change after irradiation. Also the AFM images show no significant shape change or sinking of these single AuNPs. In contrast, the AuNP dimers also present in the sample show before fs laser pulse irradiation the typical dark field image at the red and green frequency range. However, after irradiation, these AuNP dimers sink into the PMMA (see SEM image, Figure 8b). The dark field image of the dimers changed its appearance. The scattering spectrum of AuNP dimer changes its PSF from doughnut-shaped to bell-shaped (see Figure 8a dark-field image before and after). Furthermore, the spectrum is changed from IR to shorter wavelengths (yellow/red) (see Figure 8b, red curve), so a yellowish bell-shaped PSF can be observed (see Figure 8a dark-field image after, Figure 8b red bordered dark field image). This could be explained by geometrical changes of the nanoparticle, which cannot be resolved by the utilized characterization techniques. The band position could be also influenced by the changed particle environment (from top of PMMA into PMMA).

In the discussed case of dimers, irradiation results in two effects which both influence the final spectral properties: Sinking into the polymer (which changes the refractive index around the NP, but at the same time the distance between NP and gold mirror layer), and possibly a change in shape and/or orientation of the particle pair. The first effect would induce a red shift due to the increase of the refractive index, the latter can result in a quite complex change. Because the applied characterization techniques do not sufficiently resolve position and shape of the particles, one can only speculate about the various changes. Figure 9 shows another example of a dimer and its behavior upon irradiation. While in Figure 8 the dimer changes dramatically due to laser light treatment, resulting in just one remaining particle visible in SEM afterward, the dimer

dx.doi.org/10.1021/nl4037438 | Nano Lett. 2014, 14, 570−577

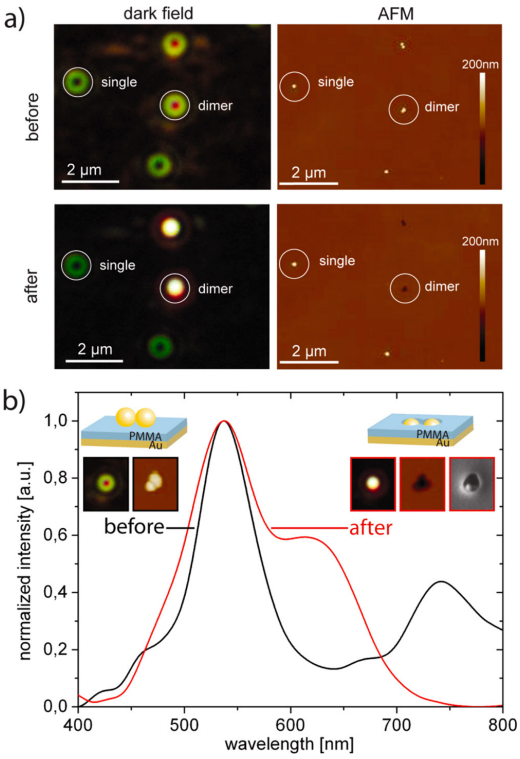

Figure 8. Selective laser light interaction with dimer particles. Dark field and AFM image as well as UV–VIS scattering spectrum of single and dimer AuNPs on PMMA 150 nm above a gold layer before and after fs laser pulse irradiation. The AuNP dimer exhibits typical red bell-shaped and green doughnut-shaped scattering before fs laser irradiation (black curve, cf. Figure 5b). Single AuNPs do not sink into the PMMA layer, and their green doughnut shape does not change upon fs pulse irradiation. The AuNP dimers sink into the PMMA layer, which certainly contributes by the resulting change in the particle-mirror distance to the modification of the PSF.

in Figure 9 is afterward still visible in the AFM (which points to a decreased sinking) as two particles in the same arrangement.

In conclusion, the influence of an interference layer arrangement consisting of a PMMA spacer layer and a reflecting gold layer on the scattering behavior of gold nanoparticles (in a distance to the gold layer beyond the evanescent near-field) was demonstrated. The scattered light spectrum and the shape of the point-spread function observed in the far-field can be tuned by choice of the PMMA spacer layer thickness as well as the nanoparticle near-field environment (matrix) and the nanoparticle shape. Moreover, the anisotropy of dimer particles allows to selectively address particles of interest by light of a selected plane of polarization. The presented results add new methods to the nanoplasmonic toolbox which allows for a quite specific spectral as well as orientational far-field selection of single functional nanoparticle units for application in fields like ultrasensitive molecular analytics or nano-optics.

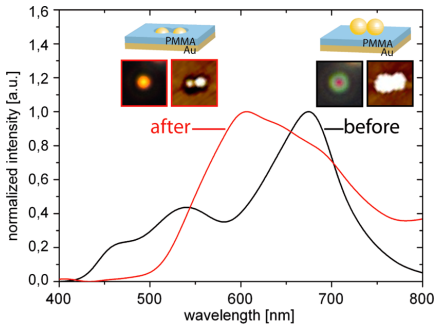

Figure 9. Dark field and AFM images with spectra of an AuNP dimer on PMMA 150 nm above a gold layer before and after fs laser irradiation. Before fs laser irradiation, the AuNP dimer exhibits a typical spectrum (black curve). After fs irradiation (red curve) the dimer itself does not change the shape significantly; however a peak forms at 600 nm, and a shoulder becomes visible at 700 nm (which could be the red-shifted peak from 680 nm visible before, due to refractive index changes from air to PMMA). The distance between dimer and Au layer decreases (Δd = 100 nm assuming negligible ablation, because AFM height measurements yielded 30 nm afterward) due to the sinking of the dimer into the PMMA layer. The green doughnut-shaped scattering changes into the yellow spectral range with bell-shaped scattering (see also Figure 2).

■ ASSOCIATED CONTENT

Supporting Information

Calculated efficiency of an emitting dipole on the PMMA/Au substrate system and dark field images of a dimer AuNP on 100 and 200 nm PMMA/Au substrate systems; calculated scattering spectra of AuNP dimers placed on a PMMA/Au substrate system; details of numerical simulation of the AuNP dimers and expressions for calculation of modified emitted power by dipole on the PMMA/Au substrate system. This material is available free of charge via the Internet at http://pubs.acs.org.

■ AUTHOR INFORMATION

Corresponding Author

*E-mail: ondrej.stranik@ipht-jena.de.

Author Contributions

J.W. and F.G. contributed equally.

Notes

The authors declare no competing financial interest.

■ ACKNOWLEDGMENTS

The authors thank Rainer Heintzmann for enlightening discussions. Furthermore, we thank Matthias Zeisberger for the access to the simulation software. The helpful assistance of Franka Jahn (IPHT Jena, Germany) for SEM images, Pedro Quaresma (FCUP, FTC/UNL, Porto and Lisboa, Portugal) for the synthesis of nanoparticles, and André Dathe for assistance during imaging spectrometer measurements are gratefully acknowledged. This work was financially supported by the German Research Foundation DFG (FR 1348/19-1), Beutenberg Fellowship (MicroInter, TMWFK PE-113-1), and DAAD (ID 57036145).

■ REFERENCES

(1) Drexhage, K. Influence of a dielectric interface on fluorescence decay time. *J. Lumin.* **1970**, *1*, 693–701.

(2) Enderlein, J. Single-molecule fluorescence near a metal layer. *Chem. Phys.* **1999**, *247*, 1−9.
(3) Chizhik, A.; Schleifenbaum, F.; Gutbrod, R.; Chizhik, A.; Khoptyar, D.; Meixner, A. J.; Enderlein, J. Tuning the fluorescence emission spectra of a single molecule with a variable optical subwavelength metal microcavity. *Phys. Rev. Lett.* **2009**, *102*, 073002.
(4) Kelly, K. L.; Coronado, E.; Zhao, L. L.; Schatz, G. C. The optical properties of metal nanoparticles: The influence of size, shape, and dielectric environment. *J. Phys. Chem. B* **2003**, *107*, 668−677.
(5) Csaki, A.; Schneider, T.; Wirth, J.; Jahr, N.; Steinbruck, A.; Stranik, O.; Garwe, F.; Muller, R.; Fritzsche, W. Molecular plasmonics: light meets molecules at the nanoscale. *Philos. Trans. R. Soc. A* **2011**, *369*, 3483−3496.
(6) Lakowicz, J. R. Plasmonics in biology and plasmon-controlled fluorescence. *Plasmonics* **2006**, *1*, 5−33.
(7) Jain, P. K.; Huang, X. H.; El-Sayed, I. H.; El-Sayed, M. A. Noble Metals on the Nanoscale: Optical and Photothermal Properties and Some Applications in Imaging, Sensing, Biology, and Medicine. *Acc. Chem. Res.* **2008**, *41*, 1578−1586.
(8) Braun, G. B.; Pallaoro, A.; Wu, G. H.; Missirlis, D.; Zasadzinski, J. A.; Tirrell, M.; Reich, N. O. Laser-Activated Gene Silencing via Gold Nanoshell-siRNA Conjugates. *ACS Nano* **2009**, *3*, 2007−2015.
(9) Wirth, J.; Garwe, F.; Hahnel, G.; Csaki, A.; Jahr, N.; Stranik, O.; Paa, W.; Fritzsche, W. Plasmonic Nanofabrication by Long-Range Excitation Transfer via DNA Nanowire. *Nano Lett.* **2011**, *11*, 1505−1511.
(10) Chen, H. J.; Kou, X. S.; Yang, Z.; Ni, W. H.; Wang, J. F. Shape- and size-dependent refractive index sensitivity of gold nanoparticles. *Langmuir* **2008**, *24*, 5233−5237.
(11) Mock, J. J.; Smith, D. R.; Schultz, S. Local refractive index dependence of plasmon resonance spectra from individual nanoparticles. *Nano Lett.* **2003**, *3*, 485−491.
(12) Mock, J. J.; Hill, R. T.; Degiron, A.; Zauscher, S.; Chilkoti, A.; Smith, D. R. Distance-dependent plasmon resonant coupling between a gold nanoparticle and gold film. *Nano Lett.* **2008**, *8*, 2245−2252.
(13) Ameling, R.; Langguth, L.; Hentschel, M.; Mesch, M.; Braun, P. V.; Giessen, H. Cavity-enhanced localized plasmon resonance sensing. *Appl. Phys. Lett.* **2010**, *97*, 253116−253116-3.
(14) Sannomiya, T.; Balmer, T. E.; Hafner, C.; Heuberger, M.; Voros, J. Optical sensing and determination of complex reflection coefficients of plasmonic structures using transmission interferometric plasmonic sensor. *Rev. Sci. Instrum.* **2010**, *81*, 053102−053102-9.
(15) Schmidt, M. A.; Lei, D. Y.; Wondraczek, L.; Nazabal, V.; Maier, S. A. Hybrid nanoparticle−microcavity-based plasmonic nanosensors with improved detection resolution and extended remote-sensing ability. *Nat. Commun.* **2012**, *3*, 1108.
(16) Feng, J.; Siu, V. S.; Roelke, A.; Mehta, V.; Rhieu, S. Y.; Palmore, G. T. R.; Pacifici, D. Nanoscale plasmonic interferometers for multispectral, high-throughput biochemical sensing. *Nano Lett.* **2012**, *12*, 602−609.
(17) Hiep, H. M.; Yoshikawa, H.; Saito, M.; Tamiya, E. An interference localized surface plasmon resonance biosensor based on the photonic structure of Au nanoparticles and SiO_2/Si multilayers. *ACS Nano* **2009**, *3*, 446−452.
(18) Schalkhammer, T.; Lobmaier, C.; Pittner, F.; Leitner, A.; Brunner, H.; Aussenegg, F. R. The use of metal-island-coated pH-sensitive swelling polymers for biosensor applications. *Sens. Actuators, B* **1995**, *24*, 166−172.
(19) Mitra, A.; Harutyunyan, H.; Palomba, S.; Novotny, L. Tuning the cavity modes of a Fabry-Perot resonator using gold nanoparticles. *Opt. Lett.* **2010**, *35*, 953−955.
(20) Bastus, N. G.; Comenge, J.; Puntes, V. Kinetically Controlled Seeded Growth Synthesis of Citrate-Stabilized Gold Nanoparticles of up to 200 nm: Size Focusing versus Ostwald Ripening. *Langmuir* **2011**, *27*, 11098−11105.
(21) Orfanidis, S. J. *Electromagnetic waves and antennas*; Rutgers University: New Brunswick, NJ, 2002.
(22) Johnson, P. B.; Christy, R.-W. Optical constants of the noble metals. *Phys. Rev. B* **1972**, *6*, 4370.
(23) Bohren, C. F.; Huffman, D. R. Absorption and scattering by a sphere. In *Absorption and Scattering of Light by Small Particles*; Wiley: New York, 1983; pp 82−129.
(24) Novo, C.; Funston, A. M.; Pastoriza-Santos, I.; Liz-Marzan, L. M.; Mulvaney, P. Influence of the medium refractive index on the optical properties of single gold triangular prisms on a substrate. *J. Phys. Chem. C* **2008**, *112*, 3−7.
(25) Kelly, K. L.; Coronado, E.; Zhao, L. L.; Schatz, G. C. The optical properties of metal nanoparticles: the influence of size, shape, and dielectric environment. *J. Phys. Chem. B* **2003**, *107*, 668−677.
(26) Höppener, C.; Novotny, L. Exploiting the light-metal interaction for biomolecular sensing and imaging. *Q. Rev. Biophys.* **2012**, *45*, 209−255.
(27) Bras, M.; Dugas, V.; Bessueille, F.; Cloarec, J.; Martin, J.; Cabrera, M.; Chauvet, J.; Souteyrand, E.; Garrigues, M. Optimisation of a silicon/silicon dioxide substrate for a fluorescence DNA microarray. *Biosens. Bioelectron.* **2004**, *20*, 797−806.
(28) Novotny, L.; Hecht, B. *Principles of nano-optics*; Cambridge University Press: Cambridge, U.K., 2012.
(29) Karamehmedović, M.; Schuh, R.; Schmidt, V.; Wriedt, T.; Matyssek, C.; Hergert, W.; Stalmashonak, A.; Seifert, G.; Stranik, O. Comparison of numerical methods in near-field computation for metallic nanoparticles. *Opt. Express* **2011**, *19*, 8939−8953.
(30) Garwe, F.; Bauerschäfer, U.; Csaki, A.; Steinbrück, A.; Ritter, K.; Bochmann, A.; Bergmann, J.; Weise, A.; Akimov, D.; Maubach, G. Optically controlled thermal management on the nanometer length scale. *Nanotechnology* **2008**, *19*, 055207.
(31) Lantz, M. A.; Gotsmann, B.; Durig, U. T.; Vettiger, P.; Nakayama, Y.; Shimizu, T.; Tokumoto, H. Carbon nanotube tips for thermomechanical data storage. *Appl. Phys. Lett.* **2003**, *83*, 1266−1268.

5.2 Molecular plasmonics: light meets molecules at the nanoscale [JW2]

	Autorenschaft der Publikation
Andrea Csáki	Messungen und Evaluierung der Daten der NLD-Technik, Diskussion und Korrektur des Manuskripts
Thomas Schneider	Messungen und Evaluierung der Daten der Einzelnanopartikelsensorik
Janina Wirth	Diskussion und Konzept der Ergebnisse für die Nanoantennen Korrektur des Manuskripts
Norbert Jahr	Messungen und Evaluierung der Daten der Einzelnanopartikelsensorik mit Hybridnanostrukturen
Andrea Steinbrück	Synthese von Nanopartikeln Korrektur des Manuskripts
Ondrej Stranik	Durchführung der theoretischen Simulationen Diskussion und Korrektur des Manuskripts
Frank Garwe	Diskussion und Konzept der Ergebnisse für die Nanoantennen Korrektur des Manuskripts
Robert Müller	Korrektur des Manuskripts
Wolfgang Fritzsche	Entwicklung des Konzepts Diskussion und Korrektur des Manuskripts

Philosophical Transactions of the Royal Society A: Mathematical, Physical and Engineering Sciences, 2011. **369** (1950): p. 3483-3496.

PHILOSOPHICAL TRANSACTIONS OF THE ROYAL SOCIETY A

Phil. Trans. R. Soc. A (2011) **369**, 3483–3496
doi:10.1098/rsta.2011.0145

Review

Molecular plasmonics: light meets molecules at the nanoscale

By Andrea Csaki, Thomas Schneider, Janina Wirth, Norbert Jahr, Andrea Steinbrück†, Ondrej Stranik, Frank Garwe, Robert Müller and Wolfgang Fritzsche*

Nano Biophotonics Department, Institute of Photonic Technology (IPHT), PO Box 100239, 07702 Jena, Germany

Certain metal nanoparticles exhibit the effect of localized surface plasmon resonance when interacting with light, based on collective oscillations of their conduction electrons. The interaction of this effect with molecules is of great interest for a variety of research disciplines, both in optics and in the life sciences. This paper attempts to describe and structure this emerging field of molecular plasmonics, situated between the molecular world and plasmonic effects in metal nanostructures, and demonstrates the potential of these developments for a variety of applications.

Keywords: molecular plasmonics; metal nanostructures; gold nanoparticles; localized surface plasmon resonance

1. Introduction

The detection and quantification of minute amounts of (bio)molecules are key requirements in a wide variety of applications in medicine and the life sciences, environmental science, food production and other areas. The development of novel sensor technology that fulfils this purpose even outside of specialized laboratories and/or with significantly decreased costs is the driving force for research in this field. Other typical requirements for such technologies are the parallelization of several assays into one measurement and the reduction of the sample volume—both points demanding a miniaturization of the whole measurement set-up. Besides the further development of established technologies in this direction, also novel approaches may emerge that could fulfil these requirements. A joint feature of many of these developments is high sensitivity towards just a few molecules, which is usually achieved by miniaturization of the sensor's core part, the transducer itself. In the case of affinity sensors, which are often used in molecular analytics due to their high specificity, the sensitivity is increased by smaller sensors that more easily react to the presence of analyte molecules.

*Author for correspondence (fritzsche@ipht-jena.de).
†Present address: Chemistry Division, Los Alamos National Laboratory, Los Alamos, NM 87545, USA.

One contribution of 9 to a Theo Murphy Meeting Issue 'Metallic metamaterials and plasmonics'.

Typical examples are nanowire sensors, where the electrical conductivity of very thin structures is influenced by the binding of molecules. This influence of analyte molecules on the mobility of electrons is somehow comparable with the effect that is used in the case of localized surface plasmon sensors, especially when working with a few or even single particles.

The phenomenon of localized surface plasmon resonance (LSPR) is based on the interaction of the conduction electrons of metal nanostructures with incoming light [1]. The electromagnetic waves induce an oscillation of these electrons, and resonances can be observed. These resonances depend on parameters such as the kind of metal and its composition (in the case of a mixture), the geometry (size, shape) and the immediate environment. The last is the basis for its potential use as a sensor: for example, by using an affinity layer, certain molecules bind to the surface of such a structure, influencing and shifting the resonance, which can be observed and used as the sensed signal for readout.

Molecular plasmonics represents the field that deals with localized surface (also called particle) plasmon resonance effects in interactions with molecular components (usually bound to the surface of metal nanostructures). The observed effects can be used for novel conjugates for nano-optics (here the molecules act as a tool) as well as for biomolecular analytics aimed at molecular analytes.

This paper gives an overview of the typical approaches to prepare such structures for use as sensors, to functionalize them in order to achieve the required specificity, to use them in bioassays and possibly to integrate them into analytical systems.

2. Synthesis and (bio)conjugation of nanoparticles

Molecular plasmonics requires metal nanostructures. They are accessible in principle by two approaches, either starting from larger structures using lithographic techniques (the 'top-down' strategy) or by assembly of rather small units, e.g. atoms and molecules (the 'bottom-up' strategy). These two approaches exhibit differences regarding the required equipment, the throughput (parallelization), the crystallinity (and thereby quality) of single structures as well as the ability for integration into a technical environment.

Since the days of Faraday [2], wet chemical synthesis of metal (especially gold) nanoparticles has been used. Therefore, metal (gold) salts are reduced by reducing agents in solution. Lately, citrate is probably the most common reducing agent [3], because these ions act at the same time to stabilize the synthesized particles. In the synthesis, the final size of the particles is usually determined by the ratio of metal salt and reducing agent. The first part of the reaction includes the formation of seeds, which later grow. For a fixed amount of metal salt, the number of seeds determines the final size, because the more seeds that exist, the less metal is accessible for further growth for each particle. These reactions lead to an ensemble of particles of approximately the same size with a quite narrow size distribution. Other bottom-up approaches are less common, such as particle preparation in the gas [4,5] or the solid [6,7] (polymer, glass) phases.

Instead of chemical means, as in the bottom-up approach, the top-down technology is based on physical technologies similar to the ones used in the microelectronics industry, e.g. for integrated circuit production. It is based

on photolithography, where light is used to pattern a light-sensitive layer (photoresist) on a thin layer of metal, for example, and this resist pattern is then transferred into the metal. For nanostructures as required for the LSPR effect, light is usually replaced by an electron beam (e-beam) in order to realize smaller structures in the lower nanometre range. This step extends the accessible structure size. However, it also replaces the rather parallel photolithography (an area is irradiated in one exposure) by the serial e-beam, which in principle writes structures point by point. This slows down the fabrication significantly and makes it rather low throughput and thereby expensive. On the other hand, this technology is compatible with standard microfabrication, so e-beam structures can be positioned into chip layouts at desired locations, which is not easily possible for chemically synthesized particles. The potential of this technology is further enhanced by emerging replication technologies, which use methods like stamping or imprinting in order to replicate nanoscale features created by e-beam technology, thereby leading to a much higher throughput and significantly decreased costs. Other emerging technologies that replace the complicated e-beam technology are nanosphere lithography and scanning probe microscopy (SPM) techniques. Nanosphere lithography [8–10] actually relies mostly on microspheres (polymer beads of several hundred nanometres up to about some micrometres diameter), which are densely packed in a monolayer and used as a sputter mask. Then material (e.g. metal) is deposited on top of the monolayer, and would only deposit as islands on the surface in between the particles. These islands are preserved in a subsequent step of polymer bead removal, and represent the desired nanostructures. In their simplest set-up, they show a triangular shape with sharp corners. Other nanosphere approaches use individual spheres for anisotropic sputtering (usually using a low angle) in order to produce crescent structures, or for lift-off masks in the sputtering of a metal layer, leading to nanometre holes in a metal film. So nanosphere lithography is a rather parallel approach, in contrast to SPM. These techniques are based on a probe that is raster-scanned over the sample surface, and used to probe local properties with an extreme lateral resolution (comparable with that of the electron microscope) but under ambient conditions (or even in liquids). The first development was the scanning tunnelling microscope, probing the tunnelling current between probe and sample surface [11]; the next main success was the scanning force microscope (also called atomic force microscope, AFM) [12]. The main features of this family are not only the high (sub-nanometre!) precision of probe positioning, but also the possible visualization in between manipulation steps in one and the same instrument. Nanomanipulation of the surface can be by voltage pulses (inducing, e.g., local oxidation), mechanically ('scratching'), transfer of organic films (self-assembled monolayer of thiolated molecules) or optically (analogous to photolithography, but with a resolution below 50 nm). Although these techniques are quite flexible and the basic instrumentation is increasingly to be found in nanotechnology laboratories, it is still not an established standard procedure and it is quite laborious to fabricate a plasmonic structure of defined properties by this approach.

In order to arrange particles produced by bottom-up technologies, several methods for an integration step are under consideration. If a regular arrangement is needed, one can densely pack the particles in a monolayer, leading to a hexagonal pattern [13,14]. If a certain distance is needed in between the particles,

then techniques based on block polymers [15], phase interfaces [16] or (sequential) adsorption [17] are possible. For an arrangement in a defined pattern, templated adsorption is possible, where the lateral positions have to be somehow predefined by chemical and/or topographical modifications of the substrate [18,19], and this arrangement can be transferred by stamping [20]. Single structures made of nanoparticles are possible by electrostatic [21] or dielectrophoretic [22] trapping. However, templates based on two-dimensional arrangements of biomolecules such as crystalline bacterial cell surface layers [23] or DNA [24–26] have also been used for the defined positioning of metal nanoparticles.

3. Post-processing and biofunctionalization

Particles can be further modified after fabrication—e.g. by additional metal layers or by light-induced reshaping—prior to biofunctionalization. These steps can be used to further tune the resonance band of the particles and/or for stabilization purposes. Often a silver deposition step is applied, based on a reaction similar to wet chemical particle synthesis: the reduction of metal salt in solution. This reaction occurs preferentially on noble metal surfaces, so that silver deposits specifically onto the gold nanoparticles that are usually used as seeds [27]. As a result, the gold core is sequentially covered by a silver shell, which changes the optical properties of the particles, and thereby the solution changes its colour gradually from reddish to yellow [28]. This step increases the diameter [29] and thereby the optical contrast, allowing for a simple single-particle detection in bright field optical microscopy [30] or by electrical means when a continuous silver layer is formed between prestructured electrodes [31]. Even several shells (such as Au/Ag/Au) have been demonstrated [32]. Other typical modification steps are possible, for example, a silica shell, which stabilizes the whole system by isolating the metal core (with its affinity to certain proteins) from the surrounding solution. Such a passivation makes sense when molecular components (dyes) attached to the metal core, as in the case of Raman markers [33,34], should have minimal interactions with molecules in the solution surrounding the particle. Moreover, it separates the plasmonic functional unit from the bioaffinity (such as antibodies) part. On the other hand, a silica shell opens the way to using the well-established siloxane surface chemistry (known from the DNA microarray field) for biofunctionalization of these particles.

In order to combine the plasmonic nanostructures with the molecular world, techniques for the defined attachment of (bio)molecules to plasmonic structures are required. Probably the most used system is the one of thiol–gold, based on the high affinity of sulphur (such as in a thiol group) to gold (or silver) surfaces. It was well studied about three decades ago for self-assembled monolayers of alkane thiols using SPM [35], and has since been extended using thiolated derivatives of various molecules (such as DNA) for attachment to plasmonic nanostructures. Even older are techniques to attach proteins to gold nanoparticles for electron microscopy, which are usually based on the same sulphur–gold affinity [35]. Besides thiol, amino groups also show a certain affinity to gold surfaces and have been used to attach biomolecules, such as DNA, to gold nanoparticles [36,37]. A silica shell, as already discussed, allows the use of conjugation chemistry, widely (also commercially) established in the field of DNA and protein microarrays, where even ready-prepared substrates can be ordered to realize reproducible results.

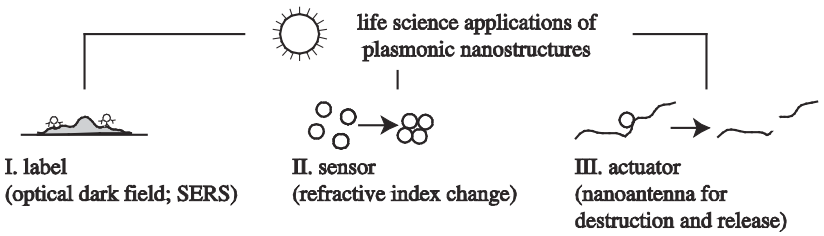

Figure 1. Life science applications of LSPR include the use of plasmonic particles as labels (for both optical as well as SERS contrast), as refractive index sensors and as a nanoantenna for the manipulation of biological structures.

4. Life science applications of localized surface plasmon resonance

Plasmonic nanostructures can be used for labelling purposes, as affinity biosensors or for light-controlled thermal manipulation of biological material (figure 1).

The use of plasmonic nanostructures as labels is based on the significant scattering efficiency of metal nanostructures, which allows for a rather simple detection of metal nanoparticles even by optical means [38–40]. By attachment of targeting molecules onto the nanoparticle, it can be directed towards the location of interest, such as on a tissue section or in cells. Additionally, local field enhancement at metal nanostructures allows also for the use as tip-enhanced Raman scattering (TERS) tips [41] or surface-enhanced Raman scattering (SERS) labels by attaching Raman-active dye molecules onto such nanostructures [34]. In contrast to the rather wide bands of fluorescence labels, the narrow Raman bands should allow a significantly higher multiplexing.

For affinity biosensors, specificity of plasmonic nanostructure sensors is usually realized using capture molecules, which specifically bind to the analyte of interest. In the case of proteinaceous analytes, antibodies or molecules with antibody-like properties are used; for DNA detection, DNA (or analogous molecules such as peptide nucleic acid) with a complementary base sequence is used. These capture molecules have to be conjugated to the sensor structure (for plasmonic sensors, usually metal nanostructures). Figure 2 gives an overview of possible schemes for molecular detection based on sensing refractive index change. The signal could be induced by the approach of a second particle in the vicinity (distance in the range of the diameter), so that particle–particle interactions determine the signal, as depicted in the left part of the scheme. The simplest approach (which was also the starting point of the plasmonic nanostructure sensing field) is to detect molecules that bridge biofunctionalized particles leading to aggregation (figure 2*a*) [42]. Thereby, the resonances typical for separated particles (such as about 520 nm for gold particles) shift dramatically (and even observable to the naked eye) to the blue. This process can be reversed by a respective design of the bioassay, so, for example, one can detect molecules that restrict (cut) certain molecules bridging particles, leading to a dissociation of particle aggregates (figure 2*b*) [43]. Again, the significant colour change can be followed easily even in small droplets.

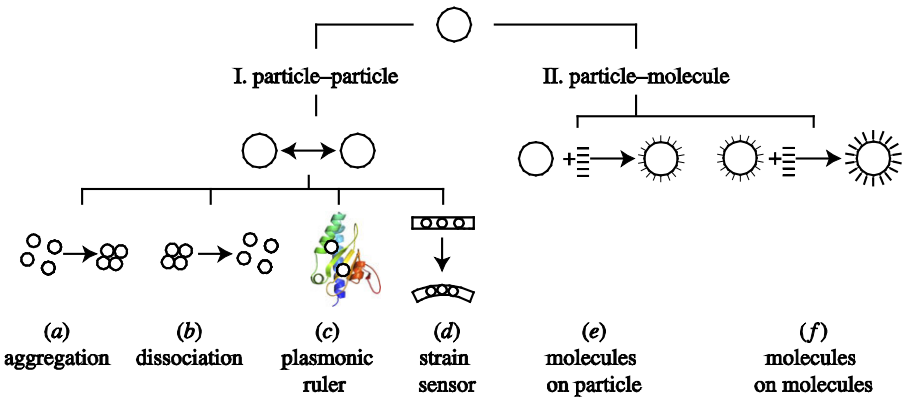

Figure 2. Applications of plasmonic particles as sensors. (Online version in colour.)

Bioassays based on aggregation or dissociation of metal nanoparticles are based on the endpoints of nanoparticle approach: they are either close together or (in a first approximation) rather distant from each other. The intermediate states can be used in order to determine distances in the lower nanometre range even in the far field, by measuring the resonance band of such a nanoparticle pair. This approach is comparable with the application of fluorescence (or Förster) resonance energy transfer, where a fluorescence donor and an acceptor are positioned on two points of a molecule and the distance is determined by the measured energy transfer (the smaller the distance, the larger the transfer). In the case of metal nanoparticles, the approach leads to a shift of the resonance band (as observed already in the case of aggregation); for gold, it would be from the red to the blue region. For particles of known plasmonic properties, the measured position of the resonance band can be used to calculate the distance in between this particle pair (figure 2*c*). Based on the same effect, but quite different from the applications, are strain sensors (e.g. for cell growth substrates) based on embedded particles, which change their interparticle distance due to the applied strain. Using spectroscopic readout, the distance change can be determined (figure 2*d*).

In addition, not only does the approach of a second particle change the resonance in an observed particle, but also even small changes in the vicinity as caused by the adsorption of a molecule resulting in a molecular (sub)monolayer (figure 2*e*) or the subsequent attachment of a second layer specifically bound to the first one (figure 2*f*). The latter process is the basis for the specificity of biosensors, when the first layer consists of capture molecules (specifically binding a given analyte).

5. Single nanoparticle applications

(*a*) *Biosensor*

The process of molecular binding results in changes in the spectroscopic properties of the particles, which can be measured not only by ensemble but also by single-particle measurements. The miniaturization of bioanalytical assays down

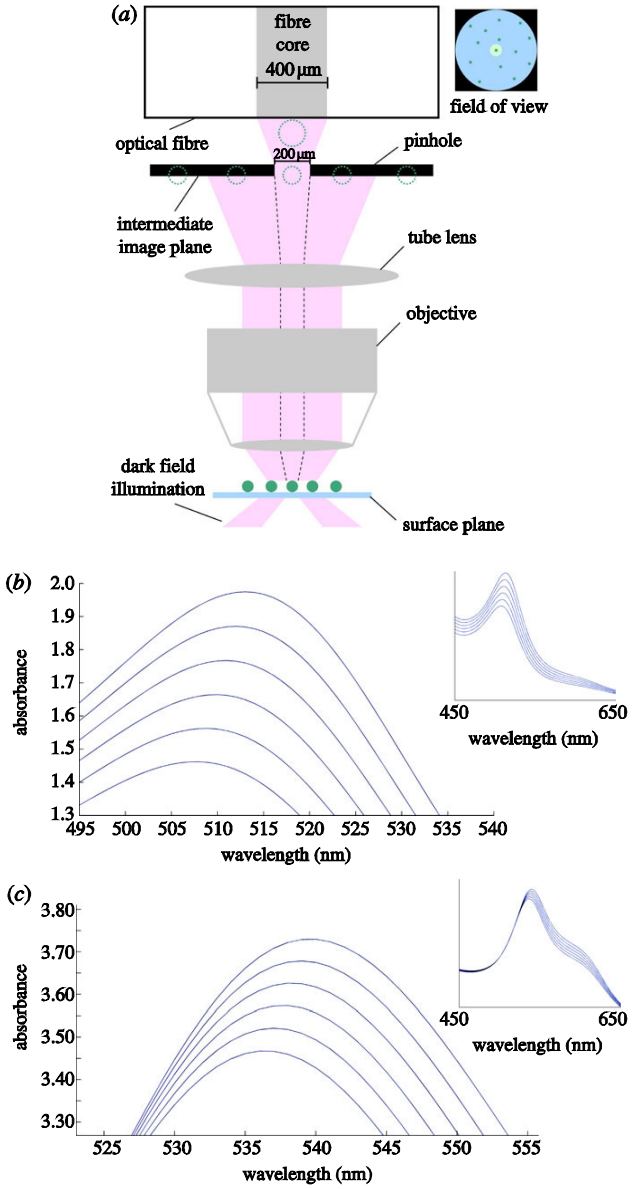

Figure 3. Microspectroscopy of single particles—instrumentation and simulations. (*a*) Set-up with dark field illumination and pinhole that collects light just from a single particle (cf. inset: particle in the centre of the field of view). (*b*,*c*) Simulation (using MiePlot v4108) of the spectroscopic effect of protein adsorption (IgG with refractive index of 1.53 and a 15 nm thickness) onto a 80 nm spherical gold nanoparticle resulting in various (0, 20, 40, 60, 80 and 100%) coverages for measurements in (*b*) air and (*c*) water. With increasing protein coverage, a shift of the peak can be observed from 508 to 514 nm (air) and from 536 to 540 nm (water). (Online version in colour.)

to single-particle sensors holds great promise for miniaturization and also for ultrasensitivity, with implications for a parallelization as required for many potential applications. So the demonstration of successful measurements of molecular binding events on this level marked an important step in the field of molecular plasmonics [44,45]. How is this single-particle microspectroscopy realized? Typically, a scattering (dark field excitation) set-up with dark field illumination is used, as introduced by Siedentopf and shown in figure 3 [46,47]. The light comes from the side at an angle, and reaches the objective only when scattered. Owing to the very high scattering efficiency of metal nanoparticles, particles of sub-wavelength dimensions can be detected in this microscopic set-up and spectroscopically characterized separately from the surrounding particles using a pinhole that collects light only from a certain region (marked in the field of view). The collected light is then guided by a glass fibre to a spectrometer. Typically, particles are visible in such set-ups down to diameters of approximately 30 and 15 nm for gold and silver, respectively. However, this technique is not limited to noble metal structures—other nanostructures such as individual Si nanowires can also be detected and characterized by it [48].

What are the expected results from measurements using such a single-particle microspectroscopy set-up? Figure 3*b*,*c* shows simulations for the effect of protein adsorption of the peak shift of gold nanoparticles (80 nm spheres). The increasing adsorption leads to a shift in the range of a few nanometres; the shift is more pronounced when measured in air compared with water. Because the resolution of such spectroscopic set-ups is usually around or even below 1 nm, these shifts should be detectable in the experiment.

An experiment demonstrating detection of proteins on a single nanoparticle level is presented in figure 4. A single gold nanoparticle was deposited on a glass substrate. In the first step, this nanoparticle was spectroscopically as well as topologically characterized. The size of the nanoparticle was 78 nm as determined by an AFM height measurement. The nanoparticle exhibited a clear plasmon resonance peak at 546 nm. In the next step, antibodies were attached to the nanoparticle, which caused a shift of the plasmon peak to 552 nm. In the last step, the nanoparticle sensor with immobilized antibodies was immersed in a test solution with antigen. This led to the specific binding of the antigen to the nanoparticles and it caused a further shift of the plasmon resonance to 569 nm.

The experimental value of the plasmon shift of around 6 nm caused by adsorption of a layer of antibodies to the nanoparticle (first layer in figure 4) is in good agreement with the calculated value in figure 3*b*. The calculation also correctly predicts the increase in the intensity of the plasmon peak upon binding of molecules (as also apparent in the dark field image of the particle after every step in figure 3*b*), which is because of the higher polarizability of the attached molecules. The discrepancy in the position of the plasmon peak is caused by the simplicity of the model, in which the effect of a substrate was not considered.

These single-particle spectroscopy demonstrations show the potential for nanosensors, which can be envisioned as intracellular sensors, comparable with the fluorescence approaches in this field sometimes already incorporating gold cores [49]. Such sensors could detect the presence of certain analytes of interest inside cells or sense certain physicochemical parameters such as pH with a sub-wavelength lateral resolution.

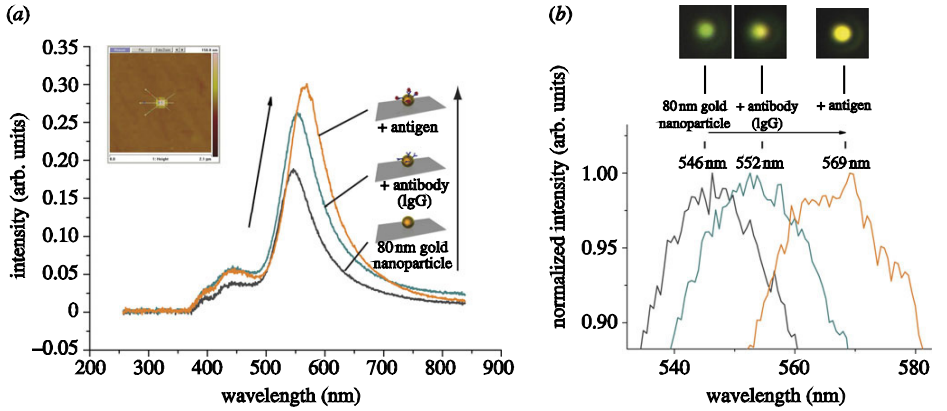

Figure 4. Microspectroscopy of single particles—experimental data. (*a*) A gold nanoparticle of 78 nm diameter (as measured by AFM, cf. inset) was characterized by single-particle microspectroscopy in its original state, then after binding of antibodies (IgG), and again after binding of antigen onto the antibody–particle conjugates. Every state leads to peak growth and shift to longer wavelength. (*b*) The peak shift is clearly visible in these zoomed spectra. The respective dark field images show a colour as well as an intensity change. The amplitude seems to increase with every added molecular layer. (Online version in colour.)

(*b*) *Nanoantenna*

A third field of life science applications of LSPR effects is using the nanoantenna character of particles: under femtosecond laser irradiation, they can collect the incoming energy and convert it into heat and/or destruction. This process can be highly selective, so that the surrounding area is not influenced at all. That light influences the behaviour of metal nanoparticles is well known: laser light can trap particles and fix them on the substrate surface [50], but can (as pulses) also change the size and shape [51], leading to approaches for tailoring the size by light [52]. On the other hand, the temperature increase induced by laser irradiation of particles can be used to induce changes in polymeric structures in the vicinity or to release attached molecules, which could, for example, be used for drug release [53] or to release RNA or DNA in order to control gene activity [54–56]. This manipulation ability can be extended to tissue [57], cells [58] and even subcellular structures (such as chromosomes) [59] or protein aggregates [60]. An important point in all applications is the parallel approach: the laser does not have to be focused down to illuminate only a single particle, but the whole sample is irradiated either by beam widening or by scanning the beam over the substrate. The extreme (nanometre-scale) localization of the damaging effects is realized by the antenna effect—significant energy conversion only occurs at the nanoparticles, and is limited to this size scale. This could be nicely demonstrated by the limited size of the holes (comparable with the size of the nanoantenna particle) that were introduced by laser pulses onto nanoparticles sequence-specifically attached to metaphase chromosomes by *in situ* hybridization [59].

Our goal is the manipulation of individual DNA molecules using this approach. We would like to combine the potential of DNA-guided specific binding of particles [36,37,61] with the nanoantenna effect. Therefore, we studied the laser light effect

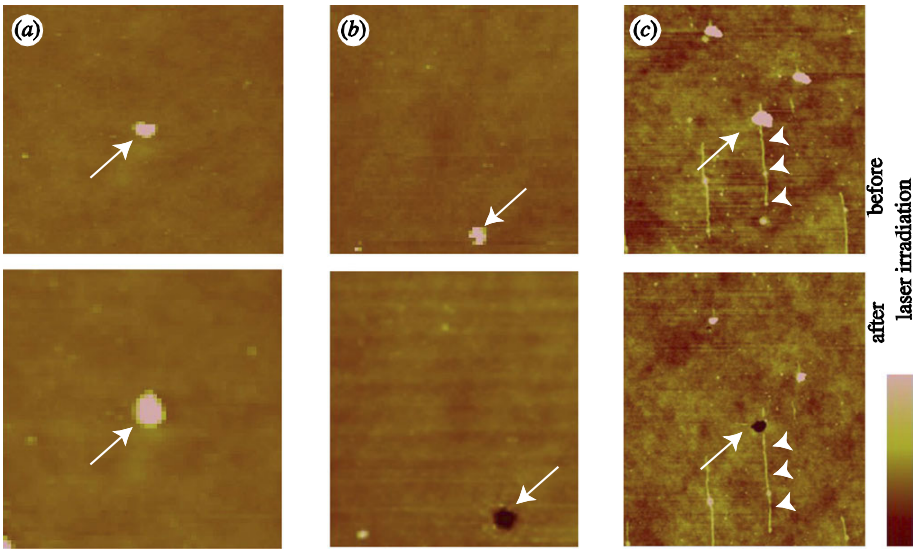

Figure 5. Manipulation of single DNA molecules using the antenna effect on plasmonic particles. (*a*) Control sample. Pulsed laser light is able to induce damage limited to the immediate surrounding of metal nanoparticles. (*b*) Particle on a polymer (PMMA) film before (top) and after (bottom) laser irradiation. The light-induced, particle-mediated damage (hole) is clearly visible. This effect was used to manipulate DNA molecules (on PMMA layer) by positioning silver particles on such molecules. (*c*) Laser irradiation damaged the particle (arrow), and thereby the DNA (arrow heads). Height scale: (*a*,*b*) 40 nm and (*c*) 20 nm. (Online version in colour.)

on metal nanoparticles, also in combination with DNA. The laser effect could be visualized by immobilization of particles onto polymer-coated substrates [62]. Poly(methyl methacrylate) (PMMA) was chosen as polymer material, owing to its established layer fabrication technique (using spin coating). AFM imaging was used to follow possible structural changes of metal nanoparticles induced by the laser pulses. Therefore, the particles were imaged before laser irradiation (figure 5, upper row), to get the original state. Then a defined (number of pulses, pulse length and amplitude) irradiation was applied, prior to further AFM imaging in order to determine possible topographical changes (figure 5, lower row). In figure 5*b*, the laser effect on an Ag nanoparticle is studied: compared with the particle before irradiation (top), after laser manipulation the particle disappeared and a hole with approximately the particle dimensions is observed (bottom). Now, this technology was applied to nanoparticles attached to DNA, which is visible as a rod-like structure and marked by arrow heads (figure 5*c*). The irradiation leads to a highly localized destruction of the particle as well as the material (such as DNA) in the vicinity, demonstrating the realization of molecular manipulation using optical control and the nanoantenna effect on plasmonic metal nanoparticles. Under certain conditions, transport of this discussed laser-based excitation of nanoparticles can be observed along DNA bundles over distances of several micrometres. This effect is documented in nanometre-deep trenches along the original position of the DNA bundles, these bundles themselves having disappeared after irradiation [63].

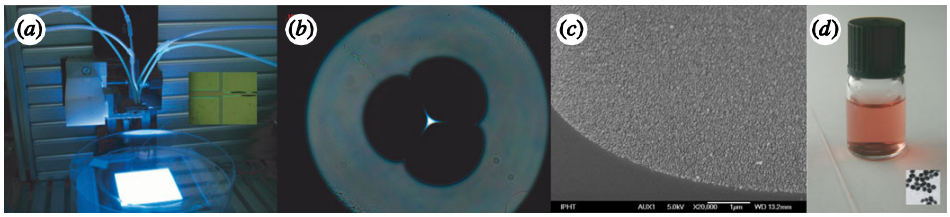

Figure 6. Functionalization of microstructured glass fibres by plasmonic particles [64]. A microfluidic set-up (*a*) is used to pump the various solutions needed for chemical activation and particle attachment into microstructured glass fibres (*b*: cross section). The internal walls of the air channels in such fibres will be covered by particles as visible in this scanning electron microscopy image in (*c*). As a result, the fibre (*d*: left) exhibits plasmonic properties comparable with the solution of these particles (*d*: centre and as TEM image in the inset). (Online version in colour.)

6. Conclusion and outlook

Plasmonic effects based on localized surface (or particle) plasmon resonance and directed towards molecules and molecular conjugates represent an emerging field between nano-optics and the life sciences, with a great potential for applications especially in diagnostics and therapy. Further progress will be supported by even more interdisciplinary approaches, including fields such as microfluidics for both sample pre-processing and separation, as well as for the core bioassay realization itself, or the combination of these plasmonic functional structures with other optical components like special glass fibres (such as microstructured optical fibres). These fibres represent a promising platform technology for fully integrated next-generation plasmonic devices; and the combination with plasmonic nanoparticles (cf. figure 6) will open novel applications especially in applications for use as sensors.

In the future, we will certainly witness a growing number of life science applications established around a core process combining LSPR effects with molecular components. 'Molecular plasmonics' has had its first showing and thereby marked its great potential for future developments. Fuelled by the exploding interest in ultrasensitive bioanalytics and nano-optics, the future looks bright for this young and promising field.

The authors would like to thank Franka Jahn for assistance with scanning and transmission electron microscope imaging, and Ines Latka, Thomas Henkel, Kerstin Schröder, Kay Schuster and Anka Schwuchow for sample preparation and discussions in the framework of the IPHT Innovation Project 2009. Funding by DFG (Fr1348/12-1) and by TMWFK (MikroInter and MikroPlex PE-113-1) is acknowledged.

References

1 Kreibig, U. & Vollmer, M. 1995 *Optical properties of metal clusters*. Springer Series in Material Science, vol. 25. Berlin, Germany: Springer.
2 Faraday, M. 1857 Experimental relations of gold (and other metals) to light. *Phil. Trans. R. Soc.* **147**, 145–181. (doi:10.1098/rstl.1857.0011)
3 Turkevich, J., Cooper, P. S. & Hillier, J. 1951 A study of the nucleation and growth processes in the synthesis of colloidal gold. *Discuss. Faraday Soc.* **11**, 55–75. (doi:10.1039/df9511100055)

4 Kruis, F. E., Fisan, H. & Peled, A. 1998 Synthesis of nanoparticles in the gas phase for electronic, optical and magnetic applications: a review. *J. Aerosol. Sci.* **29**, 511–535. (doi:10.1016/S0021-8502(97)10032-5)

5 Swihart, M. T. 2003 Vapor-phase synthesis of nanoparticles. *Curr. Opin. Colloid Interface Sci.* **8**, 127–133. (doi:10.1016/S1359-0294(03)00007-4)

6 Fritzsche, W., Porwol, H., Wiegand, A., Bornmann, S. & Köhler, J. M. 1998 *In-situ* formation of Ag-containing nanoparticles in thin polymer films. *Nanostruct. Mater.* **10**, 89–97. (doi:10.1016/S0965-9773(98)00023-3)

7 Seifert, G., Kaempfe, M., Berg, K.-J. & Graener, H. 2001 Production of 'dichroitic' gratings in glasses containing silver nanoparticles via particle deformation with ultrashort laser pulses. *Appl. Phys. B* **73**, 355–359. (doi:10.1007/s003400100652)

8 Deckman, H. W. & Dunsmuir, J. H. 1982 Natural lithography. *Appl. Phys. Lett.* **41**, 377–379. (doi:10.1063/1.93501)

9 Fischer, U. C. & Zingsheim, H. P. 1981 Submicroscopic pattern replication with visible light. *J. Vac. Sci. Technol.* **19**, 881–885. (doi:10.1116/1.571227)

10 Hulteen, J. C. & Van Duyne, R. P. 1995 Nanosphere lithography: a materials general fabrication process for periodic particle array surfaces. *J. Vac. Sci. Technol. A* **13**, 1553–1558. (doi:10.1116/1.579726)

11 Binnig, G., Rohrer, H., Gerber, C. & Weibel, E. 1983 7×7 reconstruction on Si(111) resolved in real space. *Phys. Rev. Lett.* **50**, 120–123. (doi:10.1103/PhysRevLett.50.120)

12 Binnig, G., Quate, C. F. & Gerber, C. 1986 Atomic force microscope. *Phys. Rev. Lett.* **56**, 930–933. (doi:10.1103/PhysRevLett.56.930)

13 Giersig, M. & Mulvaney, P. 1993 Preparation of ordered colloid monolayers by electrophoretic deposition. *Langmuir* **9**, 3408–3413. (doi:10.1021/la00036a014)

14 Osifchin, R. G., Mahoney, W. J., Bielefeld, J. D., Andres, R. P., Henderson, J. I. & Kubiak, C. P. 1995 Synthesis of a quantum dot superlattice using molecularly linked metal clusters. *Superlatt. Microstruct.* **18**, 283–289. (doi:10.1006/spmi.1995.1113)

15 Spatz, J. P., Roescher, A. & Möller, M. 1996 Gold nanoparticles in micellar poly(styrene)-*b*-poly(ethylene oxide) films—size and interparticle distance control in monoparticulate films. *Adv. Mater.* **8**, 337–340. (doi:10.1002/adma.19960080411)

16 Isa, L., Amstadt, E., Textor, M. & Reimhult, E. 2010 Self-assembly of iron oxide–poly(ethylene glycol) core–shell nanoparticles at liquid–liquid interfaces. *Chimia* **64**, 145–149. (doi:10.2533/chimia.2010.145)

17 Csáki, A., Möller, R., Straube, W., Köhler, J. M. & Fritzsche, W. 2001 DNA monolayer on gold substrates characterized by nanoparticle labeling and scanning force microscopy. *Nucl. Acids Res.* **29**, e81. (doi:10.1093/nar/29.16.e81)

18 Cui, Y., Björk, M. T., Liddle, J. A., Sönnichsen, C., Boussert, B. & Alivisatos, A. P. 2004 Integration of colloidal nanocrystals into lithographically patterned devices. *Nano Lett.* **4**, 1093–1098. (doi:10.1021/nl049488i)

19 Yin, Y., Lu, Y., Gates, B. & Xia, Y. 2001 Template-assisted self-assembly: a practical route to complex aggregates of monodispersed colloids with well-defined sizes, shapes, and structures. *J. Am. Chem. Soc.* **123**, 8718–8729. (doi:10.1021/ja011048v)

20 Kraus, T., Malaquin, L., Schmid, H., Riess, W., Spencer, N. D. & Wolf, H. 2007 Nanoparticle printing with single-particle resolution. *Nat. Nanotechnol.* **2**, 570–576. (doi:10.1038/nnano.2007.262)

21 Bezryadin, A., Dekker, C. & Schmid, G. 1997 Electrostatic trapping of single conducting nanoparticles between nanoelectrodes. *Appl. Phys. Lett.* **71**, 1273–1275. (doi:10.1063/1.119871)

22 Kretschmer, R. & Fritzsche, W. 2004 Pearl chain formation of nanoparticles in microelectrode gaps by dielectrophoresis. *Langmuir* **20**, 11 797–11 801. (doi:10.1021/la0482352)

23 Sleytr, U. B., Sára, M., Pum, D. & Schuster, B. 2001 Characterization and use of crystalline bacterial cell surface layers. *Prog. Surf. Sci.* **68**, 231–278. (doi:10.1016/S0079-6816(01)00008-9)

24 Han, W., Mou, J., Sheng, J., Yang, J. & Shao, Z. 1995 Cryo atomic force microscopy: a new approach for biological imaging at high resolution. *Biochemistry* **34**, 8215–8220. (doi:10.1021/bi00026a001)

25 Rothemund, P. W. 2006 Folding DNA to create nanoscale shapes and patterns. *Nature* **440**, 297–302. (doi:10.1038/nature04586)
26 Seeman, N. C. 1995 Molecular craftwork with DNA. *Chem. Intelligencer* **1**, 38–47.
27 Danscher, G. 1981 Localization of gold in biological tissue. *Histochemistry* **71**, 81–88. (doi:10.1007/BF00592572)
28 Steinbrück, A., Csaki, A., Festag, G. & Fritzsche, W. 2006 Preparation and optical characterization of core–shell bi-metal nanoparticles. *Plasmonics* **1**, 79–85. (doi:10.1007/s11468-005-9000-5)
29 Festag, G., Steinbrück, A., Csaki, A., Möller, R. & Fritzsche, W. 2007 Single particle studies of the autocatalytic metal deposition onto surface-bound gold nanoparticles reveal a linear growth. *Nanotechnology* **18**, 015502. (doi:10.1088/0957-4484/18/1/015502)
30 Csáki, A., Kaplanek, P., Möller, R. & Fritzsche, W. 2003 Single particle sensitivity in the optical detection of individual DNA-conjugated nanoparticle after metal enhancement. *Nanotechnology* **14**, 1262–1268. (doi:10.1088/0957-4484/14/12/006)
31 Möller, R., Csáki, A., Köhler, J. M. & Fritzsche, W. 2001 Electrical classification of the concentration of bioconjugated metal colloids after surface adsorption and silver enhancement. *Langmuir* **17**, 5426–5430. (doi:10.1021/la0102408)
32 Knauer, A., Thete, A., Li, S. Y., Romanus, H., Csaki, A., Fritzsche, W. & Köhler, J. M. 2011 Au/Ag/Au double shell nanoparticles with narrow size distribution obtained by continuous micro segmented flow synthesis. *Chem. Eng. J.* **166**, 1164–1169. (doi:10.1016/j.cej.2010.12.028)
33 Mulvaney, S. P., Musick, M. D., Keating, C. D. & Natan, M. J. 2003 Glass-coated, analyte-tagged nanoparticles: a new tagging system based on detection with surface-enhanced Raman scattering. *Langmuir* **19**, 4784–4790. (doi:10.1021/la026706j)
34 Schlücker, S. 2009 SERS microscopy: nanoparticle probes and biomedical applications. *ChemPhysChem* **10**, 1344–1354. (doi:10.1002/cphc.200900119)
35 Nuzzo, R. G. & Allara, D. L. 1983 Adsorption of bifunctional organic disulfides on gold surfaces. *J. Am. Chem. Soc.* **105**, 4481–4483. (doi:10.1021/ja00351a063)
36 Steinbrück, A., Csaki, A., Ritter, K., Leich, M., Köhler, J. M. & Fritzsche, W. 2008 Gold–silver and silver–silver nanoparticle constructs based on DNA hybridization of thiol and amino functionalized oligonucleotides. *J. Biophotonics* **1**, 104–113. (doi:10.1002/jbio.200810003)
37 Steinbrück, A., Csaki, A., Ritter, K., Leich, M., Köhler, J. M. & Fritzsche, W. 2008 Gold and gold–silver core–shell nanoparticle constructs with defined size based on DNA hybridization. *J. Nanoparticle Res.* **11**, 623–633. (doi:10.1007/s11051-008-9401-4)
38 Reichert, J., Csáki, A., Köhler, J. M. & Fritzsche, W. 2000 Chip-based optical detection of DNA-hybridization by means of nanobead labeling. *Anal. Chem.* **72**, 6025–6029. (doi:10.1021/ac000567y)
39 Schultz, S., Smith, D. R., Mock, J. J. & Schultz, D. A. 2000 Single-target molecule detection with multicolor optical immunolabels. *Proc. Natl Acad. Sci. USA* **97**, 996–1001. (doi:10.1073/pnas.97.3.996)
40 Yguerabide, J. & Yguerabide, E. E. 1998 Light-scattering submicroscopic particles as highly fluorescent analogs and their use as tracer labels in clinical and biological applications. II. Experimental characterization. *Anal. Biochem.* **262**, 157–176. (doi:10.1006/abio.1998.2760)
41 Deckert-Gaudig, T., Bailo, E. & Deckert, V. 2008 Perspectives for spatially resolved molecular spectroscopy—Raman on the nanometer scale. *J. Biophotonics* **1**, 377–389. (doi:10.1002/jbio.200810019)
42 Elghanian, R., Storhoff, J. J., Mucic, R. C., Letsinger, R. L. & Mirkin, C. A. 1997 Selective colorimetric detection of polynucleotides based on the distance-dependent optical properties of gold nanoparticles. *Science* **277**, 1078–1081. (doi:10.1126/science.277.5329.1078)
43 Xu, X., Han, M. S. & Mirkin, C. A. 2007 A gold-nanoparticle-based real-time colorimetric screening method for endonuclease activity and inhibition. *Angew. Chem. Int. Edn. Engl.* **46**, 3468–3470. (doi:10.1002/anie.200605249)
44 McFarland, A. D. & Van Duyne, R. P. 2003 Single silver nanoparticles as real-time optical sensors with zeptomole sensitivity. *Nano Lett.* **3**, 1057–1062. (doi:10.1021/nl034372s)
45 Raschke, G., Kowarik, S., Franzl, T., Sönnichsen, C., Klar, T. A., Feldmann, J., Nichtl, A. & Kurzinger, K. 2003 Biomolecular recognition based on single gold nanoparticle light scattering. *Nano Lett.* **3**, 935–938. (doi:10.1021/nl034223+)

46 Siedentopf, H. & Zsigmondy, R. 1902 Über Sichtbarmachung und Größenbestimmung ultramikroskopischer Teilchen, mit besonderer Anwendung auf Goldrubingläser. *Ann. Physik* **315**, 1–39. (doi:10.1002/andp.19023150102)

47 Sönnichsen, C. & Fritzsche, W. 2007 *100 years of nanoscience with the ultramicroscope: the work of Richard Zsigmondy*. Aachen, Germany: Shaker.

48 Brönstrup, G., Jahr, N., Leiterer, C., Csaki, A., Fritzsche, W. & Christiansen, S. 2010 Optical properties of individual silicon nanowires for photonic devices. *ACS Nano* **4**, 7113–7122. (doi:10.1021/nn101076t)

49 Stanca, S. E., Nietzsche, S., Fritzsche, W., Cranfield, C. G. & Biskup, C. 2010 Intracellular ion monitoring using a gold-core polymer-shell nanosensor architecture. *Nanotechnology* **21**, 055501. (doi:10.1088/0957-4484/21/5/055501)

50 Ito, S., Yoshikawa, H. & Masuhara, H. 2002 Laser manipulation and fixation of single gold nanoparticles in solution at room temperature. *Appl. Phys. Lett.* **80**, 482–484. (doi:10.1063/1.1432753)

51 Kurita, H., Takami, A. & Koda, S. 1998 Size reduction of gold particles in aqueous solution by pulsed laser irradiation. *Appl. Phys. Lett.* **72**, 789–791. (doi:10.1063/1.120894)

52 Hubenthal, F. 2009 Nanoparticles and their tailoring with laser light. *Eur. J. Phys.* **30**, S49–S61. (doi:10.1088/0143-0807/30/4/S05)

53 Sershen, S. R., Westcott, S. L., Halas, N. J. & West, J. L. 2000 Temperature-sensitive poymer–nanoshell composites for photothermally modulated drug delivery. *J. Biomed. Mater. Res.* **51**, 293–298. (doi:10.1002/1097-4636(20000905)51:3<293::AID-JBM1>3.0.CO;2-T)

54 Braun, G. B., Pallaoro, A., Wu, G. H., Missirlis, D., Zasadzinski, J. A., Tirrell, M. & Reich, N. O. 2009 Laser-activated gene silencing via gold nanoshell–siRNA conjugates. *ACS Nano* **3**, 2007–2015. (doi:10.1021/nn900469q)

55 Lee, S. E., Liu, G. L., Kim, F. & Lee, L. P. 2009 Remote optical switch for localized and selective control of gene interference. *Nano Lett.* **9**, 562–570. (doi:10.1021/nl802689k)

56 Wijaya, A., Schaffer, S. B., Pallares, I. G. & Hamad-Schifferli, K. 2009 Selective release of multiple DNA oligonucleotides from gold nanorods. *ACS Nano* **3**, 80–86. (doi:10.1021/nn800702n)

57 Hirsch, L. R., Stafford, R. J., Bankson, J. A., Sershen, S. R., Rivera, B., Price, R. E., Hazle, J. D. & Halas, N. J. 2003 Nanoshell-mediated near-infrared thermal therapy of tumors under magnetic guidance. *Proc. Natl Acad. Sci. USA* **100**, 13 549–13 554. (doi:10.1073/pnas.2232479100)

58 Hüttmann, G., Radt, B., Serbin, J., Lange, B. I. & Birngruber, R. 2002 High precision cell surgery with nanoparticles? *Med. Laser Appl.* **17**, 9–14. (doi:10.1078/1615-1615-00039)

59 Csaki, A., Garwe, F., Steinbrück, A., Maubach, G., Festag, G., Weise, A., Riemann, I., König, K. & Fritzsche, W. 2007 A parallel approach for subwavelength molecular surgery using gene-specific positioned metal nanoparticles as laser light antennas. *Nano Lett.* **7**, 247–253. (doi:10.1021/nl061966x)

60 Kogan, M. J., Bastus, N. G., Amigo, R., Grillo-Bosch, D., Araya, E., Turiel, A., Labarta, A., Giralt, E. & Puntes, V. F. 2006 Nanoparticle-mediated local and remote manipulation of protein aggregation. *Nano Lett.* **6**, 110–115. (doi:10.1021/nl0516862)

61 Csáki, A., Maubach, G., Born, D., Reichert, J. & Fritzsche, W. 2002 DNA-based molecular nanotechnology. *Single Mol.* **3**, 275–280. (doi:10.1002/1438-5171(200211)3:5/6<275::AID-SIMO275>3.0.CO;2-0)

62 Garwe, F. *et al.* 2008 Optically controlled thermal management on the nanometer length scale. *Nanotechnology* **19**, 055207. (doi:10.1088/0957-4484/19/05/055207)

63 Wirth, J., Garwe, F., Hähnel, G., Csaki, A., Jahr, N., Stranik, O., Paa, W. & Fritzsche, W. 2011 Plasmonic nanofabrication by long-range excitation transfer via DNA nanowire. *Nano Lett.* **11**, 1505–1511. (doi:10.1021/nl104269x)

64 Csaki, A. *et al.* 2010 Nanoparticle layer deposition for plasmonic tuning of microstructured optical fibers. *Small* **6**, 2584–2589. (doi:10.1002/smll.201001071)

5.3 Plasmonic nanofabrication by long-range excitation transfer via DNA nanowire [JW3]

	Autorenschaft der Publikation
Janina Wirth	Konzeptentwicklung Messungen und Evaluierung der Daten Diskussion des Konzepts und der Ergebnisse Diskussion und Korrektur des Manuskripts
Frank Garwe	Diskussion des Konzepts und der Ergebnisse Diskussion und Korrektur des Manuskripts
Gerd Hähnel	Laserbelichtung der Proben
Andrea Csáki	Diskussion und Korrektur des Manuskripts
Norbert Jahr	Diskussion und Korrektur des Manuskripts
Ondrej Stranik	Diskussion und Korrektur des Manuskripts
Wolfgang Paa	Korrektur des Manuskripts
Wolfgang Fritzsche	Diskussion des Konzepts und der Ergebnisse Diskussion und Korrektur des Manuskripts

Nano Letters, 2011. **11**(4): p. 1505-1511

NANO LETTERS

LETTER

pubs.acs.org/NanoLett

Plasmonic Nanofabrication by Long-Range Excitation Transfer via DNA Nanowire

J. Wirth, F. Garwe, G. Hähnel, A. Csáki, N. Jahr, O. Stranik, W. Paa, and W. Fritzsche*

Institute of Photonic Technology, Jena 07745, Germany

Supporting Information

ABSTRACT: Driven by the demand for ongoing integration and increased complexity of today's microelectronic circuits, smaller and smaller structures need to be fabricated with a high throughput. In contrast to serial nanofabrication techniques, based, e.g., on electron beam or scanning probe methods, optical methods allow a parallel approach and thus a high throughput. However, they rarely reach the desired resolution. One example is plasmon lithography, which is limited by the utilized plasmonic metal structures. Here we show a new approach extending plasmonic lithography with the potential for a highly parallel nanofabrication with a higher level of complexity based on nanoantenna effects combined with molecular nanowires. Thereby femtosecond laser pulse light is converted by Ag nanoparticles into a high plasmonic excitation guided along attached DNA structures. An underlying poly(methyl methacrylate) (PMMA) layer acting as an electron-sensitive resist is so structured along the former DNA position. This apparently DNA-guided effect leads to nanometer grooves reaching even micrometers away from the excited nanoparticle, representing a novel effect of long-range excitation transfer along DNA nanowires.

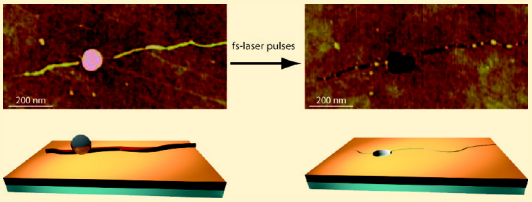

KEYWORDS: DNA, plasmonic particle, silver nanoparticle, femtosecond laser pulse

There is a growing need for technologies to produce nanostructures with high precision in a cost-efficient manner. Although serial approaches like electron beam-based methods[1] or scanning probe approaches[2] provide probably optimal precision, they are hardly applicable for large-scale production. The fabrication of structures in the nanometer scale by means of wide-field optical methods would allow for the needed high throughput due to the possible parallelization, as required for industrial applications of nanolithography. To extend the resolution limit of such methods beyond Abbe's diffraction limit techniques, two-photon excitation[3−5] and STED (stimulated emission depletion[6]) were developed. Another approach is based on collective electron excitation in metal nanostructures leading to resonances in material properties; this effect is induced by incoming light of a certain wavelength (Mie wavelength).[7] This process is termed "localized surface plasmon resonance" (LSPR) and depends on the nanostructure composition, on its geometry (size and shape), and on the permittivity of the surrounding medium.[8] Thus, the LSPR band in the extinction spectra can be tuned easily to specific wavelengths, e.g., by modifying the size of the nanostructures during their synthesis, where they efficiently absorb the energy of the light thereby acting as laser light antennas. In practice, however, small metallic nanostructures usually exhibit a size distribution.[9] Furthermore, excitation of LSPR is accompanied by a considerable enhancement of the local electric field in the vicinity of the nanoparticles.[10,11] Fast relaxation processes like electron−electron scattering, electron−surface scattering, chemical interface damping (in comparison to the slow electron−phonon scattering[12]) lead to a loss of phase coherence of the collective resonant oscillations of the electrons.[13,14] The functionality of these resonant optical nanoantennas relies on their ability to localize light on spatial scales much smaller than the wavelength.[15] In this way the LSPR excited by the resonant laser wavelength[16] can even destroy the nearest nanoparticle surrounding as demonstrated for biological systems, like the manipulation of cells,[17,18] metaphase chromosomes,[19] or protein aggregates[20] as well as technically relevant material such as PMMA.[21] The LSPR in metallic nanoparticle was already used for nanostructuring, where the particles were causing high local two photon polymerization.[22] Using continuous wave or pulsed (nanosecond, picosecond, femtosecond) lasers as excitation sources, different interaction mechanisms have to be distinguished: nanosecond and picosecond laser pulses result in an effective electron−phonon relaxation process and an increased temperature in the surrounding of the particles. In contrast, the high electrical fields of femtosecond laser pulses produce highly excited electrons in the particles, which can easily overcome the metal's work function by absorption of three to four photons.[23] These electrons and the amplified electric fields can interact with the dielectric surrounding in a high local way. In the last case, using this principle of irradiated metallic nanoantenna, the size of the original tool (laser beam) is

Received: December 7, 2010
Revised: March 15, 2011
Published: March 28, 2011

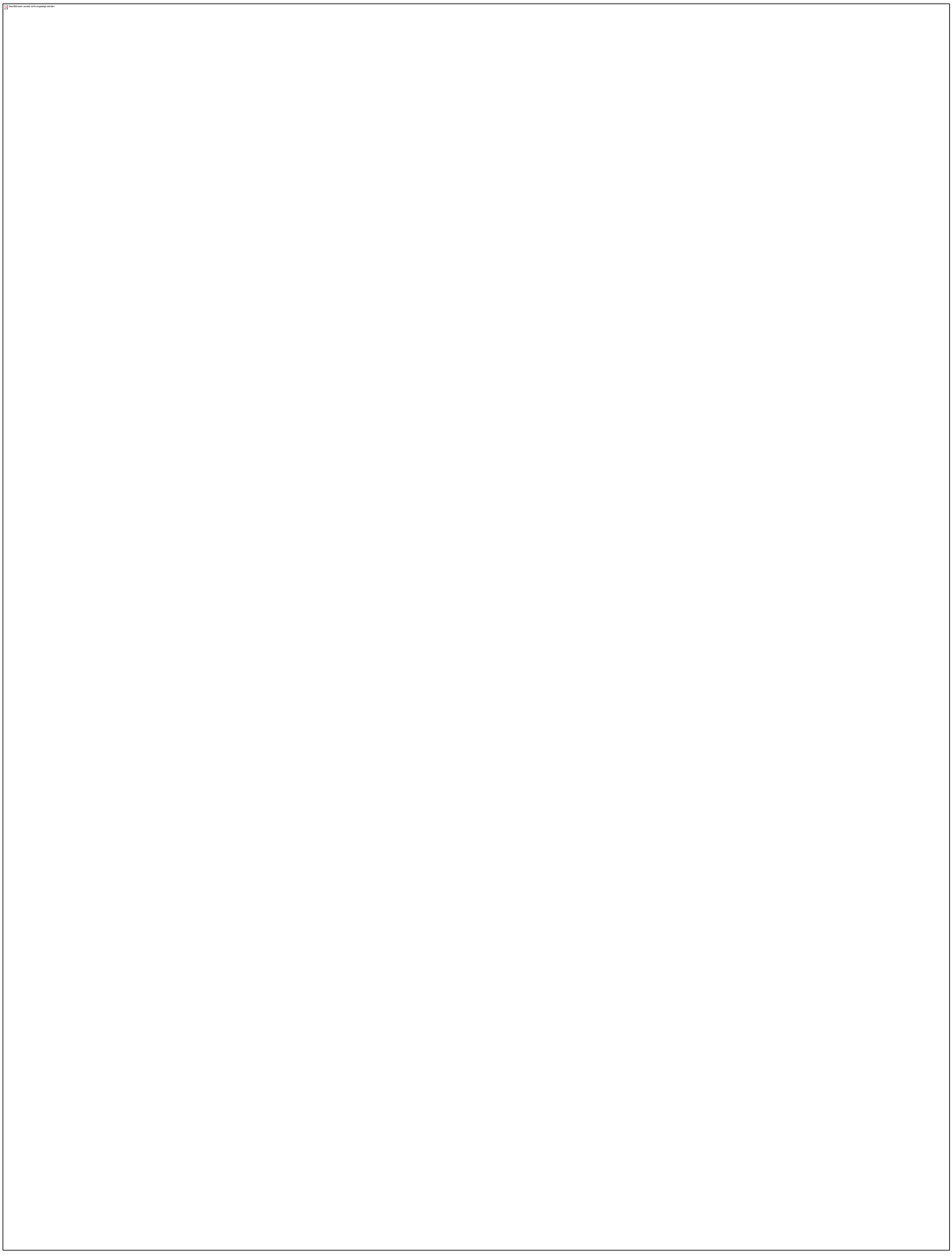

Nano Letters LETTER

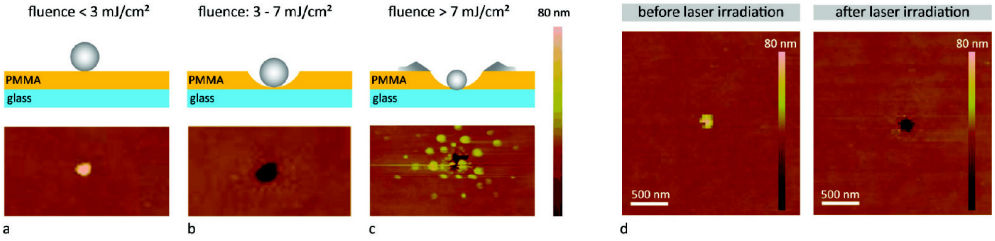

Figure 1. Effect of femtosecond laser pulses onto silver nanoparticles on PMMA substrate. (a–c) In dependence on the applied fluence, either no effect (a), a hole due to a sunken particle (b), or a destroyed particle (c) can be observed. A fluence range of about 5 mJ/cm^2 resulted in an effect as shown in (d) by AFM imaging: particles before (left) and after (right) irradiation.

on a PMMA-coated glass substrate and incubated overnight. By means of optical and atomic force microscopy, isolated nanoparticles were localized. Afterward these particles were irradiated with laser pulses of different fluences. For each tested fluence, a new sample area was chosen. The effects of the different fluences on the silver nanoparticles were characterized by atomic force microscopy again. A suitable fluence is achieved when the nanoparticles sink into the PMMA surface without ablation or fragmentation as a sign for an effective absorption of the laser light.

For the correlative characterization of the labeled DNA molecules, optical and atomic force microscopies (AFM) were used. The optical microscope (Axio Imager Z1.m, Carl Zeiss MicroImaging GmbH, Jena, Germany) was utilized in reflection and fluorescence modes with a CCD color camera (AxioCam MRc 5, Carl Zeiss MicroImaging GmbH, Jena, Germany) or a CCD black-and-white camera (Sensicam, PCO Computer Optics, Kehlheim, Germany) to detect the stretched DNA molecules and the silver nanoparticles. AFM imaging was with a NanoScope III and a Dimension 3100 detector head (Digital Instruments, Santa Barbara, CA) using tapping mode in air.

In order to characterize the structuring effects at the individual nanoparticle scale, we investigated the interaction of laser pulses with gold nanoparticles on top of a polymeric (PMMA) resist film. Continuous wave laser radiation and picosecond laser pulses with laser fluencies of about 3 m J/cm^2 did not affect the polymeric resist film nearby gold nanoparticles. Only femtosecond pulses at such a laser fluence lead to a particle-induced formation of holes in the polymer.[21] Here we confirmed these results for silver nanoparticles (Figure 1). By carefully adjusting the laser fluence, a certain parameter window (3–7 mJ/cm^2 at 800 nm wavelength and 100 fs pulse length) was established that allowed holes to be produced with the dimension of the utilized particle (Figure 1b) and thereby to nanostructure the PMMA. Lower fluences did not show any detectable effect (Figure 1a) while higher ones resulted in destruction of the particle with less defined hole formation (Figure 1c). In this parameter window, a local destruction of the PMMA surrounding (caused by conversion of laser energy in the nanoparticles resulting in destroyed structures localized only at antenna positions) was realized. Effects on the PMMA substrate material further away from the particles were not observed (Figure 1d).

In order to extend these spherical antenna-based holes into more complex structures, other elements, like wires, are required that distribute the excitation into complex patterns. Motivated by the great potential of DNA superstructures,[28,29] we chose DNA as basic material for these nanowiring experiments.

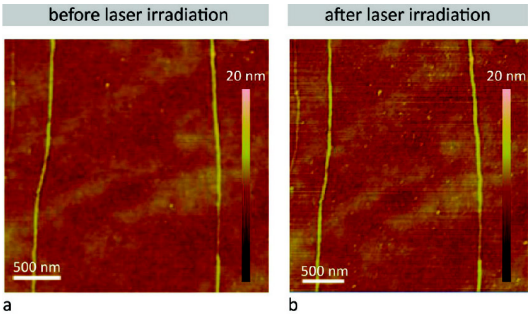

Figure 2. Control experiment regarding the effect of femtosecond laser pulses (with fluences sufficient for particle activation as shown in Figure 1d) onto DNA without metal nanoparticles. AFM images of DNA structures immobilized onto PMMA layers before (a) and after (b) laser irradiation show no light-induced changes. The DNA structures exhibit a height of up to 4–6 nm, pointing to bundles of DNA double strands (as individual double-stranded DNA exhibits a height of less than 2 nm in the AFM).

At first, we ensured that the DNA itself is not affected by femtosecond laser pulses in the selected parameter window (i.e., it shows no effect of DNA bundles topology and on the PMMA layer topology below the DNA bundles). Therefore, we visualized and compared stretched DNA bundle structures without metal nanoparticles on PMMA before and after femtosecond laser irradiation by AFM (Figure 2). No significant change could be detected.

In a second step, stretched DNA bundles with attached silver nanoparticles were studied. When irradiated with the same laser parameters as in the control experiment (cf. Figure 2), these DNA structures showed a quite impressive change: The DNA disappeared over the length of several micrometers (up to about 4 μm, limited by the length of the original DNA), and only a negative trace remained visible in the AFM as dark structures (Figure 3b,d). These grooves follow the original structure. They appeared only at particle-labeled DNA, as documented by the unlabeled DNA structures in Figures 2b and 3d which were unaffected, pointing to the nanoparticles antennas as a required condition for these structural changes.

These traces are heterogeneous in their topography: Their deepest features are 3–4 nm and the inner width (as measured by AFM at half-maximum depth) is ca. 15 nm (Figure 4). The structures appear like a dashed line, consisting of irregular

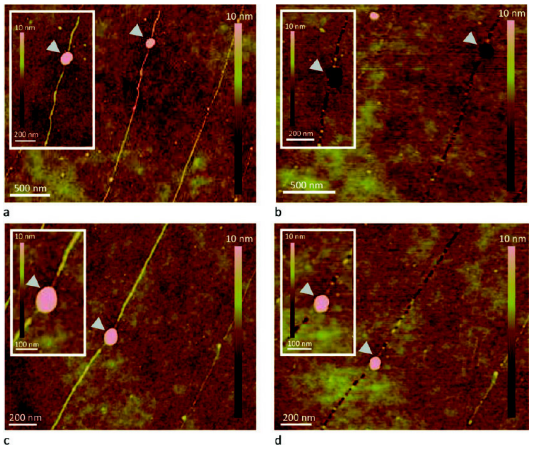

Figure 3. Plasmonically induced and DNA-mediated nanostructuring. Nanoparticle-labeled DNA bundle structures before (left: a, c) and after (right: b, d) pulsed laser irradiation. AFM imaging reveals dramatic topographic changes of particle-labeled DNA bundles: The elevated DNA structures (bright) disappear and change into a groove (dark) following the original position of the DNA. In contrast, DNA structures without a nanoparticle as the one at the lower right in (c) does not show significant changes when imaged after irradiation (d).

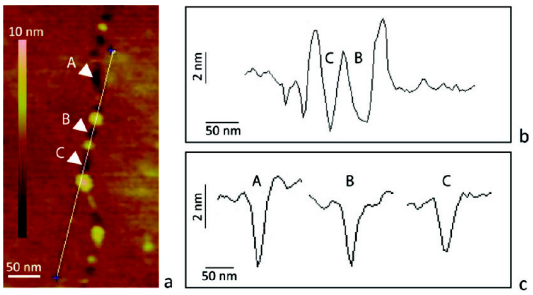

Figure 4. Topography of the induced grooves. (a) AFM image of a region showing both remaining material and grooves. (b) Section along the line in (a) revealing the height of the remains as up to 4 nm and a depth of the observed holes as 3−4 nm. (c) Cross section of the holes perpendicular to the long axis at three points marked in (a) confirm the depth measurements in (b). Moreover, a width of about 15 nm at half-maximum depth is observed.

dashlike grooves of some tens of nanometers in length, separated by shorter stretches of leveled (or even elevated) parts.

In order to characterize the apparent transfer of localized light from the particles into the DNA bundles, we investigated also the effect of silver particles located at a certain distance away from the nanowire (Figure 5). For distances below 100 nm (Figure 5a,b) no changes in DNA bundle topography could be observed. The same applies even for distances below the particle radius as shown in Figure 5c,d. Apparently, already small distances between DNA structure and particle interrupt the observed effect.

The applied femtosecond laser pulses do not affect DNA or PMMA as shown in the control experiments. However, in the

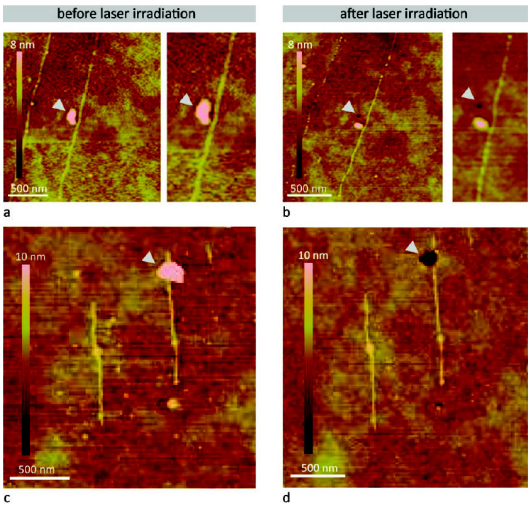

Figure 5. Efficiency variation of laser-induced particle and DNA excitation: (a, b) Only a part of the marked particle cluster in (a) leads to structure formation in PMMA (marked hole in (b)), another part remains even after irradiation. (a−d) AFM imaging of particles in the vicinity of DNA structures before (left) and after (right) laser irradiation shows that even for close distances no transfer (as documented by DNA destruction) is observed.

presence and colocalization of silver nanoparticles with DNA (Figure 3) irreversible changes are observed. These presented new experimental findings give rise to questions concerning the mechanism for guiding of the localized light from the metal nanoparticle into and along the DNA strand as well as the mechanism lying behind the observed damages in the PMMA substrate material.

First of all, photons from resonant femtosecond laser pulses are absorbed by the nanoparticles. This leads to collectively excited electrons (LSPR) and results in high electric fields, which extend into the dielectric surrounding medium.

In the following discussion temperature effects will be neglected based on these considerations: Electrons in the metal nanoparticle with high kinetic energy can principally relax due to electron−phonon coupling, which would generate phonons, i.e., heating of the particle within some 10 ps. Heat conduction into the PMMA surrounding is expected to occur on a time scale of 100 ps to 2 ns.[36] At the applied 100 fs laser pulse fluence (3−7 mJ/cm^2) however, the increase in temperature would be by far too low (45 K) to attribute significantly to the observed damage.[21] This temperature increase is far below the time-dependent glass transition temperature[37] and the time-dependent denaturation temperature.[38]

Looking at the damage mechanism, it is known that femtosecond laser irradiation at a wavelength of 800 nm causes a very high surface plasmon excitation of the electrons in 40 nm silver nanoparticles via two-photon excitation.[39] For fluences larger than 3 mJ/cm^2, the high electric field of the laser pulse excites electrons in silver nanoparticles which thus can overcome the work function by absorption of three to four photons.[23] Now Coulomb explosion, a process of cold ablation,[40] takes place. These processes begin in a range of laser fluences from 3 to 7 mJ/cm^2. To avoid irreversible changes of the particles like unwanted particle ablation, the laser fluence threshold was carefully adjusted to ensure localized surface plasmon polariton excitation.

Apart from coupling the light of the laser pulses into the particles, the question regarding the mechanism of the effects observed along the DNA structures remains. Two possible mechanisms to explain the transfer from the particle to the DNA (see Scheme 1) seem reasonable. On the one hand, electrons overcoming the work function of the nanoparticle may transfer their kinetic energy to the electrons of the PMMA or the DNA bundles. This could result in a removal of PMMA side groups (radical formation)[41] at a random position and thus in a main chain scission of PMMA bonds. In this case, momentum or electron transfer over π stacked DNA base pairs could also take place, mediated by molecular vibration of the backbone[42] in conjunction with breaks of DNA bonds. On the other hand a possibility could be that very high electric fields in the nanoparticle surrounding (10^8–10^9 V/m) accelerate electrons in PMMA or DNA. This electronic excitation can migrate along the DNA or can destroy PMMA as well as DNA bonds.

Another perspective is that nonlinear excited electrons in the metallic nanoparticles, which were created by two-photon excitation via femtosecond pulse laser irradiation (localized surface plasmon resonances (LSPR)), can be seen as light on the nanoscale far below the diffraction limit.[43] If we postulate that the DNA bundles behave as a subwavelength optical fiber (fibers smaller than 50 nm have been demonstrated[44]) a light coupling of the localized surface plasmons in the nanoparticle onto the nearest DNA bundles could occur. Alternatively, the light could propagate through the DNA bundle as quasi-particles, called phonon polaritons caused by electron polarization. They are purely electrical oscillations at optical frequencies, where every excited electron is a source for radiation. The light guiding effect of DNA bundle could also explain the dashlike groove pattern in PMMA substrate. If the propagating light is reflected at the end of the DNA, the reflected light forms standing waves. This interference pattern could then cause selective degradation of PMMA layer. A similar effect was already experimentally measured on subwavelength metal strip waveguides, where interfering plasmon modes created interference patterns of dark and bright spots.[45] The less-ideal uniformity of the interference pattern in our case is probably caused by reflections of the guided light not only at the ends of the DNA bundle but also on its defects and bends. The distance between leveled parts varies from 50 to 100 nm with an average of 70 nm. By taking into an account that standing waves exhibit lambda half patterns, the propagation constant is on the order of 90 μm^{-1}. This value indicates that higher harmonics generated by the metal nanoparticle are propagating along the DNA bundle.

Concerning the long-range momentum transfer, which is observed along the DNA, but not in the PMMA substrate, we assume that excited electrons along the DNA interact with the PMMA layer nearby the DNA and finally PMMA bonds break along the DNA. Smaller PMMA fragments would be released into the gas phase.[41] As a result a nanogroove would develop at the former DNA position. The observed final topology of the groove would be most likely attributed to an accumulation effect of the applied tens of thousands femtosecond laser pulses.

The mechanism of excitation transfer along the DNA structure is still under discussion. Because of the different structure of PMMA and DNA, different mechanisms for damage and energy transfer are assumed. Evidence for essentially distance-independent charge transfer between DNA-intercalated transition-metal complexes has been described by Barton et al. in 1993.[46] Since then, several attempts to measure the current–voltage characteristics of DNA molecules in different conformations have been carried out; for reviews see, e.g., ref 47. However, the results were controversial and a clear picture of the conduction mechanisms in DNA has not been attained so far. Indications were found to describe DNA, e.g., as an insulator,[48,49] as a wide-band gap semiconductor,[50] or as a metallic system.[51,52] From these experiments it was concluded that electrical transport is blocked in long (above tens of nanometers) single molecules that are attached to surfaces but is feasible in short DNA molecules, in networks, and in bundles,[53,54] like they were used in the experiments described here.

The results show a variety in the efficiency of the coupling between excited particles and adjacent DNA structures (cf. Figures 3b,d and 5b,d). Differences like pulse-to-pulse fluctuations, shape or diameter variations of the particles, excited electron oscillations, and DNA structure and PMMA coupling could lead to the observed differences in excitation transfer efficiency. This would explain why even a close proximity (as in Figure 5c,d) between particle and DNA is no guarantee for excitation transfer.

In conclusion, we could show that DNA bundles are able to transfer energy coupled by femtosecond pulsed laser into metal nanoparticles beyond the near-field over several micrometers and that this process leads to structures in the utilized PMMA substrate. Using, e.g., an hard mask approach, such structures could be used for nanofabrication.[55] This DNA-nanowire based plasmonic lithography presented here extends the high potential of the antenna approach of plasmonic nanolithography toward the utilization of molecular components for the transfer of excited states and the subsequent use for pattern fabrication. Molecular components allow for the combination of self-assembly approaches with established nanolithography. Especially the combination of the optically controlled nanoantenna effect with the plethora of geometries provided by DNA and their superstructures will open a whole new world for optical nanofabrication. Moreover, this first time observed long-range excitation transfer along DNA nanowires will be expanded in further work into a more detailed experimental and theoretical view on the underlying processes relevant for the observed phenomena. These new phenomena could have implications for other fields beyond lithography such as nanoplasmonics or molecular electronics.

■ ASSOCIATED CONTENT

Supporting Information. Correlative microscopy of fluorescently labeled DNA structures with attached silver nanoparticles in dark field and fluorescence contrast. This material is available free of charge via the Internet at http://pubs.acs.org.

■ AUTHOR INFORMATION

Corresponding Author
*E-mail: fritzsche@ipht-jena.de.

■ ACKNOWLEDGMENT

Funding for research initiative "MicroInter" (Beutenberg fellowship, TMWFK PE-113-1) is gratefully acknowledged. We thank A. Ihring, K. Kandera, K. Pippardt, H. Porwol, M. Sossna, D. Horn, J. Albert, G. Schmidl, and U. Hübner for assistance with sample preparation and P. Wustelt for assistance with the laser experiments.

■ REFERENCES

(1) Vieu, C.; et al. Electron beam lithography: resolution limits and applications. *Appl. Surf. Sci.* **2000**, *164*, 111–117.
(2) T'seng, A. A.; Notargiacomo, A.; Chen, T. P. Nanofabrication by scanning probe microscope lithography: A review. *J. Vac. Sci. Technol., B* **2005**, 23, 877–894.

(3) Denk, W. M.; Stickler, J. H.; Webb, W. W. Two-photon laser scanning fluorescence microscopy. *Science* **1990**, *248*, 73–76.
(4) Morikawa, J.; Orie, A.; Hashimoto, T.; Juodkazis, S. Thermal and optical properties of femtosecond-laser-structured PMMA. *Appl. Phys. A: Mater. Sci. Process.* **2010**, *101*, 27–31.
(5) Yamasaki, K.; Juodkazis, S.; Matsuo, S.; Misawa, H. Three-dimensional micro-channels in polymers: one-step fabrication. *Appl. Phys. A: Mater. Sci. Process.* **2003**, *77*, 371–373.
(6) Klar, T. A.; Hell, S. W. Subdiffraction resolution in far-field fluorescence microscopy. *Opt. Lett.* **1999**, *24*, 954–956.
(7) Mie, G. Beiträge zur Optik trüber Medien, speziell kolloidaler Metalllösungen. *Ann. Phys.* **1908**, *25*, 377–445.
(8) Kelly, K. L.; Coronado, E.; Zhao, L. L.; Schatz, G. C. The Optical Properties of Metal Nanoparticles: The Influence of Size, Shape and Dielectric Environment. *J. Phys. Chem. B* **2003**, *107*, 668–677.
(9) Vartanyan, T.; Bosbach, J.; Stietz, F.; Trager, F. Theory of spectral hole burning for the study of ultrafast electron dynamics in metal nanoparticles. *Appl. Phys. B* **2001**, *73*, 391–399.
(10) Gresillon, S.; et al. Experimental observation of localized optical excitations in random metal-dielectric films. *Phys. Rev. Lett.* **1999**, *82*, 4520–4523.
(11) Messinger, B. J.; Vonraben, K. U.; Chang, R. K.; Barber, P. W. Local-fields at the surface of noble-metal. *Phys. Rev. B* **1981**, *24*, 649–657.
(12) Link, S.; El-Sayed, M. A. Spectral properties and relaxation dynamics of surface plasmon electronic oscillations in gold and silver nanodots and nanorods. *J. Phys. Chem. B* **1999**, *103*, 8410–8426.
(13) Klar, T. A.; et al. Surface-plasmon resonance in single metallic nanoparticles. *Phys. Rev. Lett.* **1998**, *88*, 4249–4252.
(14) Sönnichsen, C.; et al. Spectroscopy of single metallic nanoparticles using total internal reflection microscopy. *Appl. Phys. Lett.* **2000**, *77*, 2949–2951.
(15) Merlein, J.; et al. Nanomechanical control of an optical antenna. *Nat. Photonics* **2008**, *2*, 230–233.
(16) Stockman, M. I. Coherent, nonlinear and active nanoplasmonics. *Antennas Propag. Int. Symp. IEEE* **2005**, *1A*, 31.
(17) Hüttmann, G.; Radt, B.; Serbin, J.; Lange, B. I.; Birngruber, R. High Precision Cell Surgery with Nanoparticles?. *Med. Laser Appl.* **2002**, *17*, 9–14.
(18) Hirsch, L. R.; et al. Nanoshell-mediated near-infared thermal therapy of tumors under magnetic guidance. *Proc. Natl. Acad. Sci. U.S.A.* **2003**, *100*, 13549–13554.
(19) Csaki, A.; Garwe, F.; Steinbrück, A.; Maubach, G.; Festag, G.; Weise, A.; Riemann, I.; König, K.; Fritzsche, W. A Parallel Approach for Subwavelength Molecular Surgery Using Gene-Specific Positioned Metal Nanoparticles as Laser Light Antennas. *Nano Lett.* **2007**, *7*, 247–253.
(20) Kogan, M. J.; Bastus, N. G.; Amigo, R.; Grillo-Bosch, D.; Ataya, E.; Turiel, A.; Labarta, A.; Giralt, E.; Puntes, V. F. Nanoparticle-mediated local and remote manipulation of protein aggregation. *Nano Lett.* **2006**, *6*, 110–115.
(21) Garwe, F.; et al. Optically controlled thermal management on the nanometer length scale. *Nanotechnology* **2008**, *19*, No. 055207.
(22) Ueno, K.; Juodkazis, S.; Shibuya, T.; Yokota, Y.; Mizeikis, V.; Sasaki, K.; Misawa, H. Nanoparticle plasmon-assisted two-photon polymerization induced by incoherent excitation source. *J. Am. Chem. Soc.* **2008**, *130*, 6928–6929.
(23) Kupersztych, J.; Raynaud, M. Anomalous multiphoton photoelectric effect in ultrashort time scales. *Phys. Rev. Lett.* **2005**, *95*, No. 147401.
(24) Kik, P. G.; Maier, S. A.; Atwater, H. A. Plasmon printing - a new approach to near-field lithography. *Mater. Res. Soc. Symp. Proc.* **2002**, *705*, Y3.6.
(25) Yang, X. F.; Zeng, B. B.; Wang, C. T.; Luo, X. G. Breaking the feature sizes down to sub-22 nm by plasmonic interference lithography using dielectric-metal multilayer. *Opt. Express* **2009**, *17*, 21560–21565.
(26) Murukeshan, V. M.; Sreekanth, K. V. Excitation of gap modes in a metal particle-surface system for sub-30 nm plasmonic lithography. *Opt. Lett.* **2009**, *34*, 845–847.
(27) Martin, O. J. F. Surface plasmon illumination scheme for contact lithography beyond the diffraction limit. *Microelectron. Eng.* **2003**, *67−8*, 24–30.
(28) Seeman, N. C. DNA nanotechnology: novel DNA constructions. *Annu. Rev. Biophys. Biomol. Struct.* **1998**, *27*, 225–248.
(29) Rothemund, P. W. Folding DNA to create nanoscale shapes and patterns. *Nature* **2006**, *440*, 297–302.
(30) Becerril, H. A.; Woolley, A. T. DNA-templated nanofabrication. *Chem. Soc. Rev.* **2009**, *38*, 329–337.
(31) Houlton, A.; Pike, A. R.; Galindo, M. A.; Horrocks, B. R. DNA-based routes to semiconducting nanomaterials. *Chem. Commun.* **2009**, 1797–1806.
(32) Hutter, E.; Fendler, J. H.; Roy, D. Surface plasmon resonance studies of gold and silver nanoparticles linked to gold and silver substrates by 2-aminoethanethiol and 1,6-hexanedithiol. *J. Phys. Chem. B* **2001**, *105*, 11159–11168.
(33) Bensimon, D.; Simon, A. J.; Croquette, V.; Bensimon, A. Stretching DNA with a Receding Meniscus: Experiments and Models. *Phys. Rev. Lett.* **1995**, *74*, 4754–4757.
(34) Maubach, G.; et al. Controlled positioning of a DNA molecule in an electrode setup based on self-assembly and microstructuring. *Nanotechnology* **2003**, *14*, 546–550.
(35) Maubach, G.; Fritzsche, W. Precise positioning of individual DNA structures in electrode gaps by self-organization onto guiding microstructures. *Nano Lett.* **2004**, *4*, 607–611.
(36) Bigot, J. Y.; Halte, V.; Merle, J. C.; Daunois, A. Electron dynamics in metallic nanoparticles. *Chem. Phys.* **2000**, *251*, 181–203.
(37) Lantz, M. A.; et al. Carbon nanotube tips for thermomechanical data storage. *Appl. Phys. Lett.* **2003**, *83*, 1266–1268.
(38) Wittwer, C. T.; Garling, D. J. Rapid cycle DNA amplification - time and temperature optimization. *Biotechniques* **1991**, *10*, 76.
(39) Scharte, M.; et al. Lifetime and dephasing of plasmons in Ag-nanoparticles. *SPIE* **2001**, *4456*, 14–21.
(40) Döppner, T.; Fennel, T.; Radcliffe, P.; Tiggesbaumker, J.; Meiwes-Broer, K. H. Ion and electron emission from silver nanoparticles in intense laser fields. *Phys. Rev. A* **2006**, 73.
(41) Hiraoka, H. Radiation Chemistry of Poly(methacrylates). *IBM J. Res. Dev.* **1977**, *21*, 121–130.
(42) Gutierrez, R.; Cuniberti, G. In *NanoBioTechnology: BioInspired Devices and Materials of the Future*; (eds. Shoseyov, O., Levy, I., Eds.; Humana Press: Totowa, NJ, 2008; pp 107−120.
(43) Stockman, M. I. Spasers explained. *Nat. Photonics* **2008**, *2*, 327–329.
(44) Tong, L. M.; et al. Subwavelength-diameter silica wires for low-loss optical wave guiding. *Nature* **2003**, *426*, 816–819.
(45) Krenn, J. R.; et al. Non diffraction-limited light transport by gold nanowires. *Europhys. Lett.* **2002**, *60*, 663–669.
(46) Murphy, C. J.; et al. Long-Range Photoinduced Electron Transfer Through a DNA Helix. *Science* **1993**, *262*, 1025–1029.
(47) Dekker, C.; Ratner, M. Electronic properties of DNA. *Phys. World* **2001**, *29*.
(48) Braun, E.; Eichen, Y.; Sivan, U.; Ben-Yoseph, G. DNA-templated assembly and electrode attachment of a conducting silver wire. *Nature* **1998**, *391*, 775–778.
(49) Storm, A. J.; van Noort, J.; de Vries, S.; Dekker, C. Insulating behavior for DNA molecules between nanoelectrodes. *Appl. Phys. Lett.* **2001**, *79*, 3881–3883.
(50) Porath, D.; Bezryadin, A.; de Vries, S.; Dekker, C. Direct measurement of electrical transport through DNA molecules. *Nature* **2000**, *403*, 635–638.
(51) Xu, B.; Zhang, P.; Li, X.; Tai, N. Direct Conductance Measurement of Single DNA Molecules in Aqueous Solution. *Nano Lett.* **2004**, *4*, 1105–1108.
(52) Yoo, K.-H.; et al. Electrical Conduction through Poly(dA)-Poly(dT) and Poly(dG)-Poly(dC) DNA Molecules. *Phys. Rev. Lett.* **2001**, *87*, No. 198102.
(53) Porath, D.; Cuniberti, G.; Di Felice, R. In *Long-Range Charge Transfer in DNA II*; Schuster, G. B., Ed.; Springer: Berlin/New York/London, 2004; pp 183−227.

(54) Cai, L.; Tabata, H.; Kawai, T. Self-assembled DNA networks and their electrical conductivity. *Appl. Phys. Lett.* **2000**, *77*, 3105–3106.
(55) Athavale, S. D.; Stojakovic, G.; Gutsche, M.; Ning, X. J. Plasma Etching Processes for Sub-Quarter Micron Devices. In *Electrochemical Society Proceedings*; Mathad, G. S., Ed.; Electrochemical Society: Pennington, NJ, 2000; pp 336−343.

5.4 Plasmonic coupling and transfer of an excitation along a DNA nanowire [JW4]

	Autorenschaft der Publikation
J. Jussi Toppari[‡]	Konzeptentwicklung Messungen und Evaluierung der Daten *LabView*-Programmierung zur optischen Ansteuerung Diskussion des Konzepts und der Ergebnisse Diskussion und Korrektur des Manuskripts
Janina Wirth[‡]	Konzeptentwicklung Messungen und Evaluierung der Daten Diskussion des Konzepts und der Ergebnisse Diskussion und Korrektur des Manuskripts
Frank Garwe[‡]	Konzeptentwicklung Messungen und Evaluierung der Daten Diskussion des Konzepts und der Ergebnisse Diskussion und Korrektur des Manuskripts
Ondrej Stranik	Diskussion des Konzepts und der Ergebnisse Diskussion und Korrektur des Manuskripts
Joachim Bergmann	Diskussion und Korrektur des Manuskripts
Wolfgang Paa	Diskussion und Korrektur des Manuskripts
Andrea Csáki	Diskussion und Korrektur des Manuskripts
Joachim Bergmann	Diskussion und Korrektur des Manuskripts
Wolfgang Paa	Diskussion und Korrektur des Manuskripts
Wolfgang Fritzsche	Diskussion und Korrektur des Manuskripts

ACS Nano, 2013. **7**(2): p. 1291-1298

Plasmonic Coupling and Long-Range Transfer of an Excitation along a DNA Nanowire

J. Jussi Toppari,[†,‡] Janina Wirth,[‡] Frank Garwe,[‡] Ondrej Stranik, Andrea Csaki, Joachim Bergmann, Wolfgang Paa, and Wolfgang Fritzsche[*]

Institute of Photonic Technology, Albert-Einstein-Strasse 9, Jena 07745, Germany. [‡]These authors contributed equally. [†]Present address: Nanoscience Center, Department of Physics, P.O. Box 35, 40014, University of Jyväskylä, Finland.

ABSTRACT We demonstrate an excitation transfer along a fluorescently labeled dsDNA nanowire over a length of several micrometers. Launching of the excitation is done by exciting a localized surface plasmon mode of a 40 nm silver nanoparticle by 800 nm femtosecond laser pulses *via* two-photon absorption. The plasmonic mode is subsequently coupled or transformed to excitation in the nanowire in contact with the particle and propagated along it, inducing bleaching of the dyes on its way. *In situ* as well as *ex situ* fluorescence microscopy is utilized to observe the phenomenon. In addition, transfer of the excitation along the nanowire to another nanoparticle over a separation of 5.7 μm was clearly observed. The nature of the excitation coupling and transfer could not be fully resolved here, but injection of an electron into the DNA from the excited nanoparticle and subsequent coupled transfer of charge (Dexter) and delocalized exciton (Frenkel) is the most probable mechanism. However, a direct plasmonic or optical coupling and energy transfer along the nanowire cannot be totally ruled out either. By further studies the observed phenomenon could be utilized in novel molecular systems, providing a long-needed communication method between molecular devices.

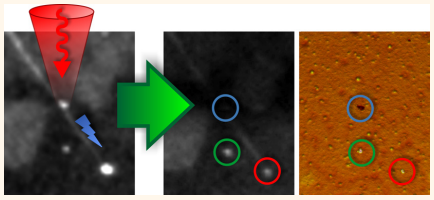

KEYWORDS: DNA · nanoparticle · surface plasmon · energy transfer · femtosecond laser pulse

The ever-growing progress of micro- and nanotechnology, which has influenced vast aspects of our lives and cultures (information and communication technology, entertainment, *etc.*) during the last decades, is crucially related to the increasing miniaturization of electronic devices. However, the development of the established *top-down* fabrication technologies is already slowing down, and substantial barriers to further progress are encountered both in the operation of devices and even more in a cost-efficiency of the fabrication. Thus, in order to ensure the continuation of Moore's law and especially to discover novel new fabrication methods for realization of the inexpensive mass production in nanoscale, many *bottom-up* technologies have been developed during the past decade. These methods are relying on totally opposite processes, such as chemical synthesis and in particularly self-assembly, for which one of the most studied and promising molecules is DNA. Its superior self-assembly properties have been proven by many different constructions, such as tile-based arrays,[1] origami structures,[2,3] and recently even 3D-origami.[4] In addition, DNA has been predicted to serve as a good conductor,[5−8] but so far the experimental results have been highly controversial and diverging.[9,10] This has been assigned mainly to the fragility of the double-stranded DNA (dsDNA) against the environment,[11−16] especially in light of recent results showing that within a well-controlled environment a real charge transfer (CT) exists in the double helix.[16,17] Due to this, a number of supposedly better DNA-based conductors have been developed, *e.g.*, M-DNA[18,19] and G4-wires,[20,21] which are also more robust. However, the long-range conductivity is still an open question.

Although an impressive variety of molecular assemblies, DNA based as well as others, is accessible already, there still exists a major obstacle: The difficulty of integration of such devices into the present technological environments. Especially, realization of a proper electrical connection to a molecule is challenging. For that, chemical affinity- and electric field-based linking, for example, have been suggested, but so far they have not proven their full potential, mostly due to the high contact resistances induced by

* Address correspondence to wolfgang.fritzsche@ipht-jena.de.

Received for review October 16, 2012 and accepted January 10, 2013.

Published online January 10, 2013 10.1021/nn304789w

mismatches between the molecular levels and the Fermi level of the metal or the band structure of a semiconductor, which are difficult to control.[22] Another widely suggested interconnection technology is based on optical coupling, *i.e.*, using light irradiation to switch the state (electrical or conformational) of an absorbing structure.[23,24] Yet, the immediate disadvantage of this approach would be the restriction of the miniaturization to the diffraction limit defined by wavelength.

However, plasmonics, based on propagating or localized surface plasmon polaritons (SPP), *i.e.*, the strongly coupled excitations of electromagnetic field and oscillation of free electrons on metal, could provide a robust optical-like connection while overcoming the diffraction limit.[25,26] By the localized SPP resonance (LSPR) appearing on metallic nanoparticles (NPs),[27,28] optical energy can be directed even down to subwavelength volumes, as demonstrated by using the high electric field of LSPR to destroy the nearest surroundings of NPs within biological systems, such as cells,[29,30] metaphase chromosomes,[31] and protein aggregates[32] or in technical materials such as PMMA.[33] These effects are mostly based on a local heating[29−32] or emission of electrons overcoming the work function of the metal *via* multiphoton absorption.[33−36] However, by combining LSPR with a nanoantenna effect[37,38] or utilizing optically active molecules[39] even a real optical access to subwavelength structures can be realized. Although this has been already demonstrated for some discrete systems, interconnections between several functional units on the surface must still be realized. So far, these interconnections have been demonstrated only by metallic strips, not providing parallel fabrication and again limited by top-down miniaturization problems as discussed before.[39−41]

More interestingly, an excited LSPR can also couple the excitation energy directly to a molecular wire, where it propagates further, as was demonstrated for the first time in our previous study of a nanometer-wide destruction of a PMMA film along a dsDNA excited *via* NPs.[42] If this effect could be thoroughly understood and utilized, a new world of optoelectronic circuitry would be accessible with the potential to address the needs of future development. In this article we use fluorescence as a more precise local tool to study this phenomenon and the nature of the propagating excitation: electrical (CT) or plasmonic/optical. We demonstrate the excitation transfer over several micrometers along a fluorescently labeled dsDNA-based molecular wire upon plasmonic excitation of a silver nanoparticle (AgNP) in contact with it. Furthermore, we demonstrate a transport of the excitation along the wire to another nanoparticle several micrometers away, thus establishing a link between the nanoparticles by combining the advantages of both the molecular assemblies and plasmonics. By utilizing this phenomenon on communication between novel molecular devices, real nanoscale integration with bottom-up fabrication capabilities could be realized. However, further studies are still needed to reveal the fundamental nature of the propagating excitation and, for example, to prevent the destruction of the AgNPs used for excitation.

RESULTS AND DISCUSSION

Molecular wires used in the experiments consisted of genomic bacteriophage λ-DNA molecules fluorescently stained with an intercalating dsDNA-specific SYBR green II dye, bundled together and elongated on a glass substrate covered with PMMA, by the receding meniscus of a drying droplet.[43−45] The number of dsDNA molecules per bundle varied from two to around 10. Plasmonic coupling was realized *via* chemically synthesized AgNPs with a diameter of ~40 nm and the resulting LSPR band around 417 nm.[46] The SYBR green II dye was chosen due to its distinct absorption and excitation maxima at 488 nm and at 266 nm, which is the third harmonic of the utilized 800 nm laser. The observed contrast in the fluorescence between the presence and the absence of dsDNA was more than a factor of 100, which is important for a reduction of the background. The fluorescent and absorption properties of the nanoparticles and the dye are presented in more detail in the Supporting Information.

The excitation transfer was initiated by illuminating the AgNP attached to a DNA wire, by 100 fs long laser pulses at a wavelength of 800 nm. Although neither the DNA, the dye, nor the AgNPs are active at this wavelength, the high electric fields of the femtosecond laser can excite plasmonic modes in the AgNPs *via* multiphoton absorption enabled by the plasmonic field enhancement.[47] Thus, this provides a real nanoscale spatial confinement for the initiation, as all the excitations of the DNA or the dye must happen *via* the localized LSPR modes of the AgNP excited by second (400 nm), third (266 nm), or higher order processes of the illumination wavelength. It should be stressed that the absorption and thus the excitation strength of the dye is very low at 400 nm but high at 266 nm (see the Supporting Information). Figure 1 represents schematics of the utilized setup. More details can be found in the Methods section.

After fabrication, the sample was characterized by atomic force microscopy (AFM) to find suitable isolated molecular wires connected with AgNPs. (Typical AFM images are presented in Figures 2 and 3.) In addition, before and after the laser excitation a fluorescence image was taken of the studied sample by illuminating it with 470 nm light and recording the fluorescence at 550 nm by a CCD camera, as shown in Figure 1. A fluorescence image of a single molecular wire with a small aggregate of nanoparticles attached in the middle is presented in Figure 2A. As seen from the image, AgNPs are highly fluorescent, which implies that

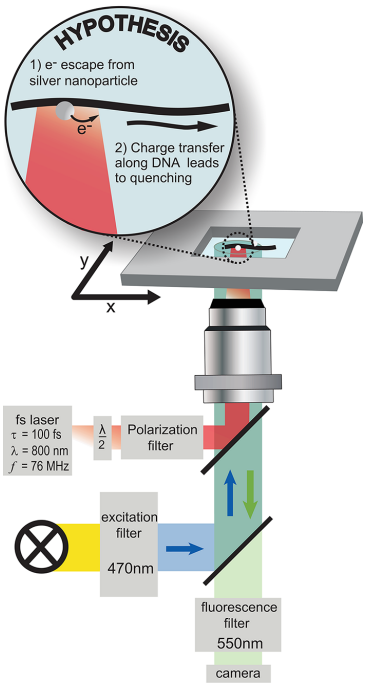

Figure 1. Schematics of the measurement setup and the observed phenomenon. The excitation of the silver nanoparticle was done by the fs laser while simultaneously imaging the fluorescence with the CCD camera. For pure fluorescence imaging, white light through the excitation filter was used for illumination. It should be noted that the laser and the white light excitation were never used simultaneously.

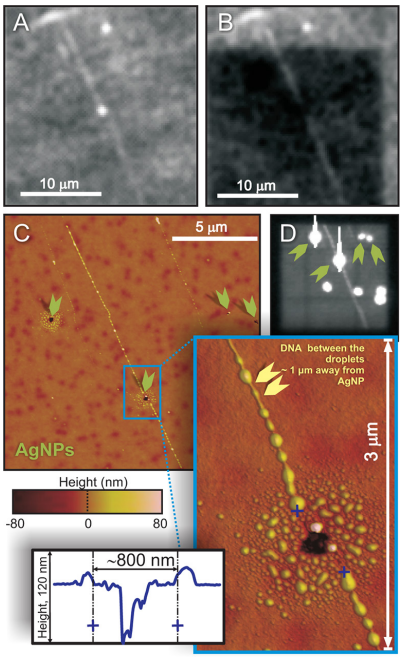

Figure 2. Experiment on a DNA nanowire with an attached AgNP. (A) Fluorescence image of a sample before the laser illumination showing a DNA nanowire with a bright AgNP in the middle. (B) Fluorescence image of the same sample after the scanning fs-laser illumination. The illuminated area is clearly visible as a darker region. The fluorescence of the excited nanoparticle has disappeared, and the dye on the DNA wire has been bleached around it. (C) AFM height image showing the DNA nanowire and the AgNP after the laser illumination. The height color scale is shown below, and the green arrows point to holes left by the destroyed nanoparticles. The zoomed area (blue rectangle) shows an enhanced view of the excited AgNP, revealing destruction of the particle and the DNA close to it, as well as the PMMA below them (visible as dark ~80 nm deep holes/wells[42]), over a 800 nm range, as shown by the cross-section taken *via* the blue crosses. However, the DNA looks intact further away. This destruction cannot be due to a simple thermal effect as explained in the text. The droplets along the DNA are probably moisture gathered from air or left from the buffer while drying. (D) Overlaid fluorescent images taken during the fs-laser illumination. The excited AgNPs are visible as bright spots. AgNPs pointed out by the green arrows were destroyed during the laser illumination, visible in the AFM image (C) as ~80 nm deep holes in the PMMA. Other particles are out of the AFM image range.

the SYBR green II attaches to them also. The reason for the observed increased fluorescence even when the dyes attached to AgNPs are not intercalated can be due to a very efficient and dense attachment or plasmonic enhancement of the dye excitation. Also some background is visible despite the high contrast of the intercalated dye compared to free dye.

After fluorescent imaging the nanoparticles were excited by scanning the femtosecond laser with a focus width of 2 μm, a pulse fluence of ~3 mJ/cm^2, and a repetition rate of 76 MHz, over the sample in 1 μm steps. The scanning was done by the sample stage within a 20 μm × 20 μm area containing the nanoparticle of interest, thus ensuring excitation at least on one of the illumination points. The laser illumination was continued for one second per position, and during the stage movements the beam was shut by an electronic shutter. On each illumination position, the whole sample was also simultaneously imaged by the CCD camera through the same 550 nm fluorescent filter, to observe the fs-laser-induced fluorescence. To ensure detection of the possible very weak signals, the camera was operated in electron multiplication mode, allowing even single photon detection. Figure 2D presents the images recorded during the laser scanning, overlaid over the whole scanned area of the same sample as in Figure 2A. Faint background visible everywhere indicates very weak direct excitation of the dye by the 800 nm laser pulses or a third-harmonic generation (THG) somewhere inside the sample. The DNA wire is clearly visible mostly due to the much higher fluorescence of the intercalated dye compared to the free dye

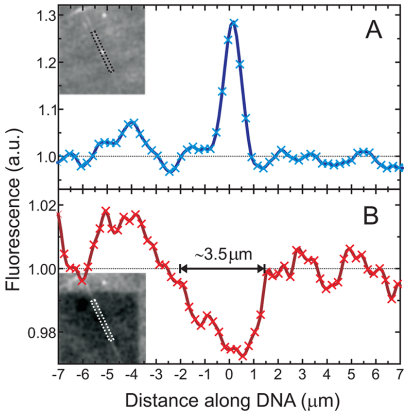

Figure 3. Bleaching along the DNA nanowire induced by the excited AgNP. Cross-section of the fluorescence profile before (A) and after (B) the laser illumination. The cross-sections have been taken along the area shown in the insets (same fluorescence images as in Figure 2A and B) by averaging the width of the area at each distance along the DNA. AgNP is situated on the origin of the graphs.

(see Supporting Information), but the excitation of the dye on the dsDNA could also be selectively enhanced by THG.[48–51]

All AgNPs within the scanned area show up as extremely bright spots, even saturating the CCD when hit by the laser pulses, as illustrated by arrows in Figure 2D. This clearly shows that the dyes attached to the AgNPs are efficiently excited *via* three-photon excitation enabled by the plasmonic modes of the particle. However, none of the individual images showed any fluorescence along the DNA nanowire during the fs-laser illumination of the AgNP, as would have been expected if the excitation travels as light or plasmonic exciton with energy similar to 266 nm light. The reason could be too weak fluorescence masked by the bright fluorescence of the AgNP or the absence of fluorescence at all.

After the fs-laser illumination, a new fluorescence image was taken as shown in Figure 2B for the same sample. The laser-illuminated area is clearly visible as a darker region due to bleaching of the dye. From the image one can see that the dye on the nanoparticle has been totally bleached, as well as the dye intercalated on the DNA wire around it. However, everywhere else the DNA wire looks intact. An AFM height image from the same sample after the laser illumination is shown in Figure 2C with the AgNP of interest zoomed on the blow-up. Due to the high excitation by the fs-laser pulses, all the laser-illuminated AgNPs (shown by green arrows) have been destroyed as well as the PMMA under them, leaving ~80 nm deep holes on the PMMA layer, as seen from the image.[42,47] Like in the previous observations, the DNA attached to the AgNP, and also the PMMA below it, was destroyed within a length of ~400 nm away from the particle.[42] This can be verified from the blow-up AFM image of Figure 2C and the attached cross-section taken from it. The observed "bumps" along the DNA are probably moisture droplets gathered from air or left from the drying of the buffer.

Further, by taking cross-sections of the fluorescence images (Figure 2A and B) along the DNA nanowire, as shown in Figure 3, one can see that the bleaching of the fluorescence has taken place over a far longer range than the destruction of the DNA, *i.e.*, at least over the range of ~1.5 μm away from the particle. This indicates the propagation of the excitation along the DNA much farther than would be expected by the destruction. To ensure that the bleaching of the dye is really attributed to the coupling of the excitation into the DNA *via* LSPR of the AgNP, the same experiment was repeated with a similar DNA nanowire, but now with a nanoparticle located 780 nm away from it. Similar high fluorescence of the nanoparticle during the laser illumination was observed, as well as destruction of it on the AFM image afterward. However, the fluorescence of the DNA was not affected, since the distance to the particle was so long that its plasmonic field on the wire is negligible. Results are shown in the Supporting Information.

This proves that the close proximity or even a direct contact between the DNA wire and AgNP is needed for the coupling, which further implies the effect being launched by the plasmonic excitation in AgNP. However, this does not yet fully rule out the simple possibility that the bleaching of the dye along the DNA would be due to a local heating of the particle during the illumination. Nevertheless, our earlier studies have shown that illumination by femtosecond pulses with similar fluencies to those here induces a maximal temperature increase of only 10 K (10 nm below the particle) and an accumulated temperature rise of about three degrees within a few nanometers from the particle,[33] which is not enough to cause the bleaching of the dye along the DNA. Also, the sinking of a nanoparticle into PMMA, as we observe in our experiments, requires nanoparticle temperatures higher than 400 °C and a large force on them over a few nanoseconds.[52] Thus, the observed phenomenon cannot be just due to a simple thermal effect.

As the simple thermal effect is ruled out, there are still a few possibilities for the nature of the excitation. The propagating excitation could be optical, assuming the DNA bundles behave as subwavelength optical fibers (fibers smaller than 50 nm have been demonstrated[53]) to where the light from the SPP modes of the nanoparticle could scatter. Also a plasmonic nature is conceivable, in which case the excitation would propagate through the DNA as quasi-particles, called excitons.[54,55] However, since the initial excitation happens *via* three-photon absorption enabled by the

LSPR of the AgNP, both of these methods should involve an optical excitation with 266 nm wavelength and thus fluorescence of the dye along the propagation, which was not observed. Anyway, we cannot totally rule out these choices, as the fluorescence could have been too weak or masked by the bright luminescence of the AgNp, as discussed before.

Most probably the observed bleaching of the dye along the DNA nanowire is due to a coupled transfer of charge (Dexter) and faster delocalized exciton (Frenkel) along the DNA.[55] Sole charge transfer has been proven for short dsDNAs, and the coupled Dexter and Frenkel transfer is feasible for a longer range within DNA bundles or similar constructions.[13,16,56] As the femtosecond laser irradiation causes a very high plasmonic excitation on the AgNPs with highly enhanced electric fields, the excited electrons in the nanoparticles can overcome the work function by absorption of multiple photons,[34,35] which leads to Coulomb explosion.[36] These processes start at a laser fluence around 3 to 7 mJ/cm^2. The escaped electrons can subsequently be injected on empty electronic states or excite other electrons on DNA. This excess charge can further propagate along the DNA, leading to a bleaching or quenching of the intercalated dye without fluorescence.[57,58] The longer propagation of the coupled charge (short-range) and Frenkel excitons (long-range) along the DNA can be sustained by the initial kinetic energy of the escaped electron, which can be as high as 50 eV.[34] Or, it can be driven by the very high electric field of the fs-laser pulses, present several micrometers away from the AgNP, possibly leading to a directional net effect *via* second-order processes; even the kinetic effect of the fundamental alternating laser field averages to zero.[48−50]

To further prove the discussed excitation transfer, we utilized a sample with two separate small aggregates of dye-labeled AgNPs attached to the same dsDNA nanowire with intercalated dye. The separation of the AgNP aggregates was ~5.7 μm, as shown by the fluorescence image of the sample in Figure 4A. The image was taken similarly to the case of one AgNP above. The fs-laser illumination area was now chosen so that from the two AgNP aggregates on the same nanowire only the upper one (blue box in Figure 4) could be excited during the scanning process. The scanning was done exactly the same way as described above except the illumination time per pixel was 500 ms this time. The fluorescence image (Figure 4B) taken after the illumination shows again bleaching of the dye on the excited AgNPs, as well as of the intercalated dye along the DNA starting from the excited nanoparticle. Also other particles within the illumination area were bleached. In addition and more interestingly, the dye on the other AgNP aggregate attached to the end of the same DNA (red box in Figure 4) was also significantly bleached, although it was not excited by the fs laser at any time. This means

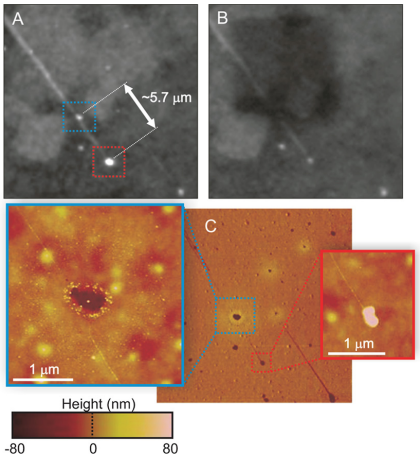

Figure 4. Experiment on a DNA nanowire with two attached AgNPs demonstrating the excitation transfer along the wire. Fluorescence images of the sample with two aggregates of nanoparticles, marked with blue (donor) and red (acceptor) boxes, before (A) and after (B) the point by point fs-laser illumination within an area including the donor but not the acceptor AgNP (visible as a darker rectangular on B). At the place of the donor only a dark region is visible in B, similarly to that for other illuminated AgNPs within the illumination area. Also the fluorescence of the acceptor outside the illumination area, is clearly bleached. Separation of the donor and acceptor particles is 5.7 μm. (C) AFM phase image of the nanoparticles and the connecting DNA wire after the fs-laser illumination. The blow-ups are zoomed height images of the donor and acceptor nanoparticles, with the height color scale shown below.

that the excitation (charge or energy on optical range) from the excited nanoparticle (donor) needed to be transferred along the DNA nanowire all the way to the other AgNP (acceptor) to induce bleaching.

From the AFM images taken after the laser illumination and shown in Figure 4C, one can see that again the excited donor nanoparticle (blue box) was destroyed by the laser illumination, as also the DNA in the vicinity of the particle and PMMA below them. Also, by comparing Figure 4B and 4C, one can see that all the AgNPs within the fs-laser illumination area have been destroyed. However, the not-excited but still bleached acceptor AgNP (red box) looks intact on the AFM image, further proving that the bleaching of the dye on it was not due to a direct plasmonic excitation by the laser focus wings.

A more quantitative analysis of this experiment is presented in Figure 5, where a fluorescence cross-section along the DNA nanowire covering both the donor (at position ~1.5 μm) and the acceptor (at position ~7.2 μm) AgNPs is plotted before (blue curve) and after (red curve) the laser illumination. The obtained result shows a clear bleaching of the dye on the excited donor AgNP, as well as of the intercalated dye along the DNA near it. However, even when the bleaching of the intercalated dye has stopped around three micrometers

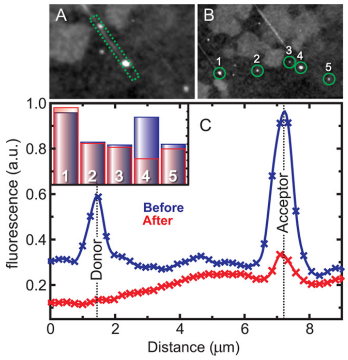

Figure 5. Measured fluorescence in the experiment on a DNA nanowire with two attached AgNPs. (C) Fluorescence along the DNA nanowire, *i.e.*, along the area shown as a green rectangle in (A) by averaging the width of the area at each point along the DNA. Both the donor and the acceptor AgNPs are clearly visible before the illumination (blue curve). After the illumination (red curve) the donor is totally bleached and the acceptor is clearly also. (C, inset) Fluorescence of the dye on several AgNPs, numbered 1–5 in (B), before (blue) and after (red) the fs-laser illumination. The fluorescence has been measured as an integral over the green circles in (B) including the particles (1–5). Particle 4 is the acceptor AgNP, and it shows a clear bleaching compared to other AgNPs. The fluorescence images (A) and (B) are the same as in Figure 4A, except showing a narrower and wider area, respectively.

from the donor particle, the dye on the acceptor still shows a significant bleaching. This proves that the charge or energy of the induced excitation has indeed traveled *via* the DNA nanowire from the donor AgNP to the acceptor 5.7 μm away and that the excitation transfer happens even further than shown by the bleaching of the intercalated dye.

In addition, to rule out possible effects by a general bleaching due to fluorescent imaging or small changes on the focus, the fluorescence of several isolated dye-labeled AgNPs (NPs 1–3 and 5 in Figure 5) as well as the acceptor AgNP at the end of the DNA wire (NP 4; red box) were compared before and after the laser illumination, as also shown in Figure 5. All the examined particles are located outside of the laser illumination area and thus were not excited by the fs laser. Their initial fluorescence varies due to different sizes and amounts of attached dye. Since the particles 1–3 and 5 are not connected to the donor by any nanowire, they act as controls. From the data (Figure 5) it is clear that dye on the acceptor AgNP (4) has been severely bleached compared to the control AgNPs. The observed bleaching is more than 10 times higher than any measurement uncertainties (see *e.g.* fluorescence of AgNPs 1 and 5) and thus clearly not due to a general bleaching induced by the imaging or differences in focusing or any other random differences during the imaging.

CONCLUSIONS

We have shown that excitation can be coupled from the LSPR modes of a silver nanoparticle excited *via* multiphoton absorption by a femtosecond laser pulse, to the attached DNA nanowire, and that the excitation can be transferred along the nanowire for distances of several micrometers. The transfer along the DNA wire was demonstrated nondestructively by bleaching of the SYBR green II dye intercalated into the DNA. Furthermore, we have demonstrated a transport of this excitation from a nanoparticle to another nanoparticle ~5.7 μm away along a DNA nanowire connecting them. The success of the excitation transport was again verified by a clear bleaching of the dyes attached to the acceptor nanoparticle. Simultaneously, bleaching of the dye intercalated into the connecting DNA nanowire was also observed near the initially excited nanoparticle, *i.e.*, the donor. All the results were verified *via* control experiments also. This study demonstrates possibilities for establishing a link between nanostructures by combining the advantages of both molecular assemblies and plasmonics. Since here the donor nanoparticle was always destroyed during the initiation of the transfer, the method is limited to single use in this form. However, by further theoretical and experimental studies this can be most probably avoided and the method could be utilized in nanoscale integration, for providing a communication method between novel molecular devices equipped with parallel bottom-up fabrication capabilities. In addition to a robust and well-localized coupling, one could easily envision altering of the coupling by molecular, electrical, or optical means, thus providing a platform for actively controlled applications.

METHODS

Sample Fabrication. The buffer used in every fabrication process was 1× TBE involving 89 mM Tris base, 89 mM boric acid, and 2 mM EDTA and precisely tuned to have a pH of 8.0 by HCl. For the fluorescent staining of the λ-DNA (Fermentas GmbH, St. Leon-Rot, Germany) the SYBR green II (Molecular Probes, Eugene, OR, USA) dye was 10 times diluted in the TBE buffer to obtain a working solution (WS). All WSs were stored at 4 °C and used on the same or next day after fabrication. The staining was carried out by further diluting the SYBR green II WS by TBE by a ratio of 1:50 000 (vol) and letting it react with 4 ng/μL genomic bacteriophage λ-DNA molecules for 30 min or more. After that, the aqueous solution of the silver nanoparticles (~10^{11} particles/mL) fabricated with the recipe from ref 42, resulting in a diameter of ~40 nm and LSPR band around 417 nm, was mixed and incubated with stained λ-DNA in a ratio of 25:1 (vol) and subsequently applied as droplets onto the surface of a cleaned glass cover slide spin-coated with an 80 nm thick PMMA layer in advance. The spinning of the PMMA was done in a clean room to ensure a smooth surface and hard baked after the spinning at

180 °C. While drying of the droplet the fluorescently stained and nanoparticle-labeled λ-DNA was immobilized and stretched by a receding meniscus.[42−44] The obtained result was verified *via* fluorescent microscopy (see below and Figure 1), as well as by atomic force microscopy (Nanoscope III with a Dimension 3100 detector head from Digital Instruments, Santa Barbara, CA, USA). All the preparations were done in ambient conditions.

Experimental Setup. The experiment used a modified Observer microscope (Zeiss Inc., Jena, Germany) (see Figure 1) in ambient conditions for taking fluorescence images of the prepared sample before and after the femtosecond pulse illumination procedure. The single-photon-sensitive IXON X3 camera (Andor Inc., Belfast, Northern Ireland) was used to take a 512 × 512 pixel image from the illuminated area using an integration time of 100 ms. During this time only very weak bleaching of the dsDNA-intercalated SYBR Green II dye was observed (Figure 5). The dye was excited by ET bandpass 470/40 (Zeiss) filtered white light, and the fluorescence was measured using an HC 550/88 fluorescence filter (Zeiss) in front of the camera.

For the excitation of AgNPs a titanium/sapphire laser (Mira Optima 900-D, Coherent Inc., Santa Clara, CA, USA) delivering 100 fs long pulses at a wavelength of 800 nm and repetition rate of 76 MHz was coupled to the same Observer microscope used in fluorescent imaging. The microscope was equipped with an oil immersion objective (magnification: 63×, numerical aperture: 1.25, Zeiss) to obtain a pulse fluence of 3 mJ/cm^2. An independent measurement of the laser fluence was carried out to ensure the optimal conditions for nanoparticle excitation.[42] For the area illumination the stage scanning method using a Nano 545 3R7 stage (PI Instruments Inc., Karlsruhe, Germany) and a PI XYZ piezo controller was utilized. The scanning was done in 1 μm steps, which guarantees the excitation of the nanoparticles within the area. Irradiation time at each position varied from 500 to 1000 ms, and the fluorescence was simultaneously recorded with the CCD camera with electron multiplication enabled, thus providing even single-photon sensitivity. During the stage movements the laser beam was closed by a shutter and the camera was reset. At the end of this procedure an area of 20 μm × 20 μm was illuminated with uniform femtosecond laser fluence and a uniform dose. LabVIEW software (National Instruments, USA) was used to realize the needed synchronization between the devices.

Conflict of Interest: The authors declare no competing financial interest.

Acknowledgment. The authors thank Rainer Heintzmann and Ivana Sumanovac for help with the CCD camera and A. Ihring, K. Kandera, K. Pippardt, H. Porwol, M. Sossna, D. Horn, J. Albert, G. Schmidl, and U. Hübner for assistance with sample preparation. Financial support from Beutenberg Fellowship (MicroInter, TMWFK PE-113-1), Academy of Finland (Project Nos. 218182 and 263262), NewIndigo ERA-NET NPP2 (AQUATEST, INDIGO-DST1-012), and COST actions MP0802 and MP0803 is greatly acknowledged.

Supporting Information Available: Detailed descriptions of the fluorescent and absorption properties of the nanoparticles and the dye. Data, results, and discussion of the control experiment. This material is available free of charge *via* the Internet at http://pubs.acs.org.

REFERENCES AND NOTES

1. Seeman, N. D. DNA in a Material World. *Nature* **2003**, *421*, 427–431.
2. Rothemund, P. W. K. Folding DNA to Create Nanoscale Shapes and Patterns. *Nature* **2006**, *440*, 297–302.
3. Andersen, E. S.; Dong, M.; Nielsen, M. M.; Jahn, K.; Subramani, R.; Mamdouh, W.; Golas, M. M.; Sander, B.; Stark, H.; Oliveira, C. L. P.; *et al.* Self-Assembly of a Nanoscale DNA Box with a Controllable Lid. *Nature* **2009**, *459*, 73–76.
4. Douglas, S. M.; Dietz, H.; Liedl, T.; Högberg, B.; Graf, F.; Shih, W. M. Self-Assembly of DNA into Nanoscale Three-Dimensional Shapes. *Nature* **2009**, *459*, 414–418.
5. Okahata, Y.; Kobayashi, T.; Tanaka, K.; Shimomura, M. Anisotropic Electric Conductivity in an Aligned DNA Cast Film. *J. Am. Chem. Soc.* **1998**, *120*, 6165–6166.
6. Kelley, S. O.; Barton, J. K. Electron Transfer Between Bases in Double Helical DNA. *Science* **1999**, *283*, 375–381.
7. Fink, H.-W.; Schönenberger, C. Electrical Conduction Through DNA Molecules. *Nature* **1999**, *398*, 407–410.
8. Porath, D.; Bezryadin, A.; De Vries, S.; Dekker, C. Direct Measurement of Electrical Transport through DNA molecules. *Nature* **2000**, *403*, 635–638.
9. Endres, R. G.; Cox, D. L.; Singh, R. R. P. *Colloquium:* The Quest for High-Conductance DNA. *Rev. Mod. Phys.* **2004**, *76*, 195–214.
10. Mallajosyula, S. S.; Pati, S. K. Toward DNA Conductivity: A Theoretical Perspective. *J. Phys. Chem. Lett.* **2010**, *1*, 1881–1894.
11. Mahapatro, A. K.; Lee, G. U.; Jeong, K. J.; B. Janes, D. B. Stable and Reproducible Electronic Conduction through DNA Molecular Junctions. *Appl. Phys. Lett.* **2009**, *95*, 083106.
12. Adessi, Ch.; Walch, S.; Anantram, M. P. Environment and Structure Influence on DNA Conduction. *Phys. Rev. B* **2003**, *67*, 081405(R).
13. Linko, V.; Paasonen, S.-T.; Kuzyk, A.; Törmä, P.; Toppari, J. J. Characterisation of the Conductance Mechanisms of the DNA Origami by AC Impedance Spectroscopy. *Small* **2009**, *5*, 2382–2386.
14. Linko, V.; Leppiniemi, J.; Paasonen, S.-T.; Hytönen, V. P.; Toppari, J. J. Defined-Sized DNA Triple Crossover Construct for Molecular Electronics: Modification, Positioning and Conductance Properties. *Nanotechnology* **2011**, *22*, 275610.
15. Xu, B.; Zhang, P.; Li, X.; Tao, N. Direct Conductance Measurement of Single DNA Molecules in Aqueous Solution. *Nano Lett.* **2004**, *4*, 1105–1108.
16. Genereux, J. C.; Barton, J. K. Mechanisms for DNA Charge Transport. *Chem. Rev.* **2010**, *110*, 1642–1662.
17. Holmlin, R. E.; Dandliker, P. J.; Barton, J. K. Charge Transfer through the DNA Base Stack. *Angew. Chem., Int. Ed.* **2004**, *36*, 2714–2730.
18. Rakitin, A.; Aich, P.; Papadopoulos, C.; Kobzar, Y.; Vedeneev, A. S.; Lee, J. S.; Xu, J. M. Metallic Conduction through Engineered DNA: DNA Nanoelectronic Building Blocks. *Phys. Rev. Lett.* **2001**, *86*, 3670–3673.
19. Aich, P.; Labiuk, S. L.; Tari, L. W.; Delbaere, L. J. T.; Roesler, W. J.; Falk, K. J.; Steer, R. P.; Lee, J. S. M-DNA: A Complex Between Divalent Metal Ions and DNA which Behaves as a Molecular Wire. *J. Mol. Biol.* **1999**, *294*, 477–485.
20. Calzolari, A.; Di Felice, R.; Molinari, E.; Garbesi, A. G-Quartet Biomolecular Nanowires. *Appl. Phys. Lett.* **2002**, *80*, 3331–3333.
21. Phillips, K.; Dauter, Z.; Morchie, A. I. H.; Lilley, D. M. J.; Luisi, B. The Crystal Structure of a Parallel-Stranded Guanine Tetraplex at 0.95 Å Resolution. *J. Mol. Biol.* **1997**, *273*, 171–182.
22. Moth-Poulsen, K.; Bjørnholm, T. Molecular Electronics with Single Molecules in Solid-State Devices. *Nat. Nanotechnol.* **2009**, *4*, 551–556.
23. Debreczeny, M. P.; Svec, W. A.; Wasielewski, M. R. Optical Control of Photogenerated Ion Pair Lifetimes: An Approach to a Molecular Switch. *Science* **1996**, *274*, 584–587.
24. Battacharyya, S.; Kibel, A.; Kodis, G.; Liddell, P. A.; Gervaldo, M.; Gust, D.; Lindsay, S. Optical Modulation of Molecular Conductance. *Nano Lett.* **2011**, *11*, 2709–2714.
25. Zayats, A. V.; Smolyaninov, I. I.; Maradudin, A. A. Nano-Optics of Surface Plasmon Polaritons. *Phys. Rep.* **2005**, *408*, 131–314.
26. Raether, H. *Surface Plasmons on Smooth and Rough Surfaces and Grattings*; Springer-Verlag: New York, 1988.
27. Grésillon, S.; Algouy, L.; Boccara, A. C.; Rivoal, J. C.; Quelin, X.; Desmarest, C.; Gadenne, P.; Shubin, V. A.; Sarychev, A. K.; Shalaev, V. M. Experimental Observation of Localized Optical Excitations in Random Metal-Dielectric Films. *Phys. Rev. Lett.* **1999**, *82*, 4520–4523.
28. Messinger, B. J.; Vonraben, K. U.; Chang, R. K.; Barber, P. W. Local-Fields at the Surface of Noble-Metal. *Phys. Rev. B* **1981**, *24*, 649–657.

29. Hüttmann, G.; Radt, B.; Serbin, J.; Lange, B. I.; Birngruber, R. High Precision Cell Surgery with Nanoparticles? *Med. Laser Appl.* **2002**, *17*, 9–14.
30. Hirsch, L. R.; Stafford, R. J.; Bankson, J. A.; Sershen, S. R.; Rivera, B.; Price, R. E.; Hazle, J. D.; Halas, N. J.; West, J. L. Nanoshell-Mediated Near-Infared Thermal Therapy of Tumors Under Magnetic Guidance. *Proc. Natl. Acad. Sci. U. S. A.* **2003**, *100*, 13549–13554.
31. Csaki, A.; Garwe, F.; Steinbrück, A.; Maubach, G.; Festag, G.; Weise, A.; Riemann, I.; König, K.; Fritzsche, W. A Parallel Approach for Subwavelength Molecular Surgery Using Gene-Specific Positioned Metal Nanoparticles as Laser Light Antennas. *Nano Lett.* **2007**, *7*, 247–253.
32. Kogan, M. J.; Bastus, N. G.; Amigo, R.; Grillo-Bosch, D.; Ataya, E.; Turiel, A.; Labarta, A.; Giralt, E.; Puntes, V. F. Nanoparticle-Mediated Local and Remote Manipulation of Protein Aggregation. *Nano Lett.* **2006**, *6*, 110–115.
33. Garwe, F.; Bauerschäfer, U.; Csaki, A.; Steinbrück, A.; Ritter, K.; Bochmann, A.; Bergmann, J.; Weise, A.; Akimov, D.; Maubach, G. Optically Controlled Thermal Management on the Nanometer Length Scale. *Nanotechnology* **2008**, *19*, 055207.
34. Kupersztych, J.; Monchicourt, P.; Raynaud, M. Ponderomotive Acceleration of Photoelectrons in Surface-Plasmon-Assisted Multiphoton Photoelectric Emission. *Phys. Rev. Lett.* **2001**, *86*, 5180–5183.
35. Kupersztych, J.; Raynaud, M. Anomalous Multiphoton Photoelectric Effect in Ultrashort Time Scales. *Phys. Rev. Lett.* **2005**, *95*, 147401.
36. Döppner, T.; Fennel, T.; Radcliffe, P.; Tiggesbaumker, J.; Meiwes-Broer, K. H. Ion and Electron Emission from Silver Nanoparticles in Intense Laser Fields. *Phys. Rev. A* **2006**, *73*, 031202(R).
37. Bharadwaj, P.; Deutsch, B.; Novotny, L. Optical Antennas. *Adv. Opt. Photonics* **2009**, *1*, 438–483.
38. Merlein, J.; Kahl, M.; Zuschlag, A.; Sell, A.; Halm, A.; Boneberg, J.; Leiderer, P.; Leitenstorfer, A.; Bratschitsch, R. Nanomechanical Control of an Optical Antenna. *Nat. Photonics* **2008**, *2*, 230–233.
39. Kuzyk, A.; Pettersson, M.; Toppari, J. J.; Hakala, T. K.; Tikkanen, H.; Kunttu, H.; Törmä, P. Molecular Coupling of Light with Plasmonic Waveguides. *Opt. Express* **2007**, *15*, 9908–9917.
40. Giannini, V.; Fernández-Domínguez, A. I.; Heck, S. C.; Maier, S. A. Plasmonic Nanoantennas: Fundamentals and Their Use in Controlling the Radiative Properties of Nanoemitters. *Chem. Rev.* **2011**, *111*, 3888–3912.
41. Stockman, M. I. Nanoplasmonics: Past, Present, and Glimpse into Future. *Opt. Express* **2011**, *19*, 22029–22106.
42. Wirth, J.; Garwe, F.; Hähnel, G.; Csáki, A.; Jahr, N.; Stranik, O.; Paa, W.; Fritzsche, W. Plasmonic Nanofabrication by Long-Range Excitation Transfer *via* DNA Nanowire. *Nano Lett.* **2011**, *11*, 1505–1511.
43. Bensimon, D.; Simon, A. J.; Croquette, V.; Bensimon, A. Stretching DNA with a Receding Meniscus: Experiments and Models. *Phys. Rev. Lett.* **1995**, *74*, 4754–4757.
44. Maubach, G.; Csáki, A.; Born, D.; Fritzsche, W. Controlled Positioning of a DNA Molecule in an Electrode Setup Based on Self-Assembly and Microstructuring. *Nanotechnology* **2003**, *14*, 546–550.
45. Maubach, G.; Fritzsche, W. Precise Positioning of Individual DNA Structures in Electrode Gaps by Self-Organization onto Guiding Microstructures. *Nano Lett.* **2004**, *4*, 607–611.
46. Hutter, E.; Fendler, J. H.; Roy, D. Surface Plasmon Resonance Studies of Gold and Silver Nanoparticles Linked to Gold and Silver Substrates by 2-Aminoethanethiol and 1,6-Hexanedithiol. *J. Phys. Chem. B* **2001**, *105*, 11159–11168.
47. Scharte, M.; Porath, R.; Ohms, T.; Aeschlimann, M.; Lamprecht, B.; Ditlbacher, H.; Aussenegg, F. R. Lifetime and Dephasing of Plasmons in Ag-Nanoparticles. *SPIE* **2001**, *4456*, 14–21.
48. Boman, F. C.; Musorrafiti, M. J.; Gibbs, J. M.; Stepp, B. R.; Salazar, A. M.; Nguyen SonBinh, T.; Geiger, F. M. DNA Single Strands Tethered to Fused Quartz/Water Interfaces Studied by Second Harmonic Generation. *J. Am. Chem. Soc.* **2005**, *127*, 15368–15369.
49. Stokes, G. Y.; Gibbs-Davis, J. M.; Boman, F. C.; Stepp, B. R.; Condie, A. G.; Nguyen, S. T.; Geiger, F. M. Making "Sense" of DNA. *J. Am. Chem. Soc.* **2007**, *129*, 7492–7493.
50. Boman, F. C.; Gibbs-Davis, J. M.; Heckman, L M.; Stepp, B. R.; Nguyen, S. T.; Geiger, F. M. DNA at Aqueous/Solid Interfaces: Chirality-Based Detection *via* Second Harmonic Generation Activity. *J. Am. Chem. Soc.* **2009**, *131*, 844–848.
51. Szabó, A.; Wang, Y.; Lee, S. A.; Simon, H. J.; Rupprecht, A. Optical Third Harmonic Generation Study of the Hydration of DNA Films. *Biophys. J.* **1993**, *65*, 2656–2660.
52. Eleftherion, E.; Antonakopoulos, T.; Binning, G. K.; Cherubini, G.; Despont, M.; Dholakia, A.; Dürig, U.; Lantz, M. A.; Potidis, H.; Rothuizen, H. E.; Vettiger, P. Millipede—A MEMS-Based Scanning-Probe Data Storage System. *IEEE Trans. Magn.* **2003**, *39*, 938–945.
53. Tong, L.; Gattass, R. R.; Ashcom, J. B.; He, S.; Lou, J.; Shen, M.; Maxwell, I.; Mazur, E. Subwavelength-Diameter Silica Wires for Lowloss Optical Wave Guiding. *Nature* **2003**, *426*, 816–819.
54. Trifonov, A.; Raytchev, M.; Buchvarov, I.; Rist, M.; Barbaric, J.; Wagenknecht, H.-A.; Fiebig, T. Ultrafast Energy Transfer and Structural Dynamics in DNA. *J. Phys. Chem. B* **2005**, *109*, 19490–19495.
55. May, V.; Kühn, O. *Charge and Energy Transfer Dynamics in Molecular Systems*; Wiley-VCH: Weinheim, 2011; pp 467—558.
56. Porath, D.; Cuniberti, G.; Di Felice, R. In *Long-Range Charge Transfer in DNA II*; Schuster, G. B., Ed.; Springer: Berlin, 2004; pp 183—227.
57. Takada, T.; Fujitsuka, M.; Majima, T. Single-Molecule Observation of DNA Charge Transfer. *Proc. Natl. Acad. Sci.* **2007**, *104*, 11179–11183.
58. Kawai, K.; Matsutani, E.; Maruyama, A.; Majima, T. Probing the Charge-Transfer Dynamics in DNA at the Single-Molecule Level. *J. Am. Chem. Soc.* **2011**, *133*, 15568–15577.

5.5 Plasmonically-enhanced electron escape from gold nanoparticles and their polarization-dependent excitation transfer along DNA nanowires [JW5]

	Autorenschaft der Publikation
Janina Wirth[‡]	Konzeptentwicklung Messungen und Evaluierung der Daten Diskussion des Konzepts und der Ergebnisse Diskussion und Korrektur des Manuskripts
Frank Garwe[‡]	Konzeptentwicklung Diskussion des Konzepts und der Ergebnisse Diskussion und Korrektur des Manuskripts
Robert Meyer	Laserbelichtung der Proben
Andrea Csáki	Diskussion und Korrektur des Manuskripts
Ondrej Stranik	Diskussion des Konzepts und der Ergebnisse Diskussion und Korrektur des Manuskripts
Wolfgang Fritzsche	Diskussion und Korrektur des Manuskripts

Nano Letters, 2014. **14**(7): p. 3809-3816

NANO LETTERS

Letter

pubs.acs.org/NanoLett

Plasmonically Enhanced Electron Escape from Gold Nanoparticles and Their Polarization-Dependent Excitation Transfer along DNA Nanowires

J. Wirth,† F. Garwe,† R. Meyer, A. Csáki, O. Stranik, and W. Fritzsche*

Leibniz Institute of Photonic Technology, Jena 07745, Germany

Supporting Information

ABSTRACT: Here we show plasmon mediated excitation transfer along DNA nanowires over up to one micrometer. Apparently, an electron excitation is initiated by a femtosecond laser pulse that illuminates gold nanoparticles (AuNP) on double stranded DNA (dsDNA). The dependency of this excitation on laser wavelength and polarization are investigated. Excitation of the plasmon resonance of the AuNPs via one- and two-photon absorption at 520 and 1030 nm, respectively, was explored. We demonstrate an excitation transfer along dsDNA molecules at plasmon supported four-photon excitation of AuNP cluster or at laser field driven nanoparticle electron tunneling for an alignment of the attached dsDNA to the polarization of the electric field of the laser light. These results extend the previously observed plasmonically induced three-photon excitation transfer along DNA nanowires to another nanoparticle material (gold) and the adapted irradiation wavelengths.

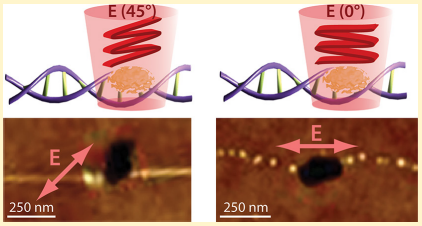

KEYWORDS: *DNA, nanoparticle, femtosecond laser pulse, plasmonic excitation, polarization, energy transfer*

The conduction electrons of metal nanoparticles (NP) can be resonantly excited at their plasmonic frequencies at the visible (VIS) and near-infrared (NIR) wavelengths. This localized surface plasmon polariton resonances, depend on the nanostructure composition, on its geometry (size and shape), as well as on the permittivity of the surrounding medium.[1] It results in intense scattering and absorption of light, leading to large enhancements of the electromagnetic field near the particles,[2] and provides for the ability to localize light on spatial scales even down to subwavelength volumes. Knight et al.[3] built up metallic nanostructures with Schottky barriers of 0.5 eV, determined by ultrathin titanium layers of 1 nm thickness. Here electrons, resonantly excited by single IR photons, could override the metal−semiconductor Schottky barrier and induced a detectable photocurrent. The excitation of the LSPR with a resonant laser wavelength at lower fluences can result in an irreversible transformation (damage) of the nearest surroundings of NPs within biological systems, such as cells,[4] metaphase chromosomes,[5] and protein aggregates[6] or other organic materials, like poly(methyl methacrylate) (PMMA).[7] The character of these damaging effects strongly depend on the given laser pulse duration. While nano- and picosecond laser pulses result in an effective electron−phonon relaxation process and an increased temperature in the surrounding area of the particles, femtosecond (fs) laser pulses produce highly excited electrons in the particles, which may result in their escape via multiphoton absorption. Thereby, the excitation of the LSPR supports the electron escape resulting in electron-based damages of the dielectric surrounding area around the particles. This effect occurs at much lower laser fluences compared to a destruction by plasma generation due to nonresonant absorption of dielectric material upon laser pulses.[8] Furthermore, fs laser pulse excited electrons of the nanoparticle, which are supported by LSPR, can also couple into attached aligned molecular wires, as recently discovered.[9] These studies of fs laser irradiated silver nanoparticles (AgNP) attached on double-stranded DNA (dsDNA) molecules have shown that such a plasmonic excitation of the particle can couple to dsDNA and cause a long-range excitation transfer along these molecules. This was demonstrated by a micrometer long (~5 μm) destruction of an underlying PMMA film along dsDNA molecules.[9] This phenomenon was then studied more thoroughly by fluorescence experiments, where a fs pulse plasmonic excitation of an acceptor AgNP induced bleaching of fluorophores at a donor AgNP by excitation transport along the DNA molecules, which connected both nanoparticles over a distance of ~5.7 μm.[10] Further studies of this phenomenon are still needed to reveal the fundamental nature of the propagating excitation, but they are hampered by the aging effect that changes AgNPs under ambient conditions due to oxidation of silver. When stored in air, these aging processes result in a continuous change of the resonance wavelength over time, rendering these particles as useless for a defined resonant excitation by a given laser wavelength.[1] Thus, experiments with more stable nanoparticles such as AuNPs would be helpful to

Received: March 11, 2014
Revised: May 30, 2014
Published: June 2, 2014

Table 1. Overview of Experiments of Metal Nanoparticles (Ag versus Au of a Diameter ⌀) Attached to dsDNA and Excited with 100 fs Laser Pulses, Divided in 3 Excitation Steps: (1) Plasmon Resonance Excitation, (2) Electron Escape, and (3) Excitation Transfer[a]

	steps of excitation	Ag NP[9,10] (⌀ ~ 40 nm) (λ_{LSPR} ~ 415 nm)	Au NP (⌀ ~ 45 nm) (λ_{LSPR} ~ 530 nm)	Au NP multimer (⌀ ~ 2 × 45 nm) (λ_{LSPR} ~ 530/680/1000 nm)
1.	plasmonic excitation	800 nm via 2 photon excitation	520 nm via 1 photon excitation	1030 nm via 1 photon excitation
2.	necessary energy for electron escape	4.1–4.6 eV (306–270 nm)	4.8–5.4 eV (258–230 nm)	4.8–5.4 eV (258–230 nm)
	number of photons for electron escape	3 photons	2 photons	4 photons
	laser fluence needed for electron escape and hole formation	3 mJ/cm^2 (single NPs)	0.3 mJ/cm^2 (single NPs)	≥20 mJ/cm^2 (only NP aggregates)
3.	excitation transfer along dsDNA (E-field aligned with DNA)	Yes	No	Yes only at 0° (parallel)

[a]The parameters for AgNP are taken from our previous work.[9,10] The plasmonic excitation (1) was studied using UV/VIS microspectroscopy and the energy required for electron escape (2) was determined upon observation of destruction of PMMA substrate below irradiated NPs. The fluence necessary for transfer along the nanowire (3) was determined by observing possible DNA destruction under irradiation.

overcome the stability problems, and therefore to allow for further study of the excitation transfer via DNA nanowire. In this paper, we examine the behavior of commonly used AuNPs (instead of AgNP) on DNA molecules while irradiated with fs laser pulses. In particular, we focus on the question whether the plasmonic excitation of AuNPs by fs laser pulses can also induce an excitation transfer along attached DNA molecules, and if so, what are the key experimental parameters. An overview of the experiments carried out with AuNPs in comparison to former experiments with AgNPs is given in Table 1 and depicted in Scheme 1. The experimental approach is illustrated in Scheme 2.

Scheme 1. Steps of Excitation during fs Laser Irradiation of Metallic Nanoparticles with the Phenomena on the Particle Surface and Their Effects in the Surrounding

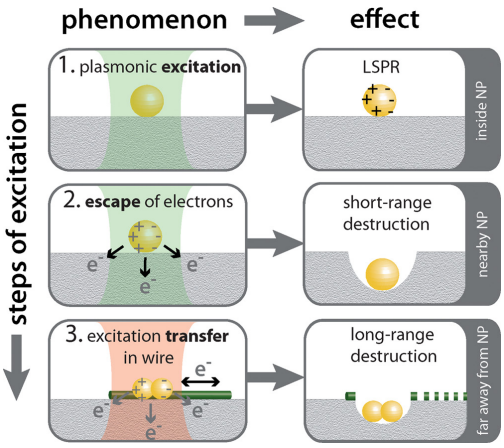

The plasmonic excitation of AuNPs attached to dsDNA molecules was done with fs laser pulses, whose high electromagnetic fields can excite electrons and even induce their escape from the AuNPs enabled by the plasmonic field enhancement.[11] Two different laser wavelengths were tested to provide the excitation of AuNPs within their plasmon band. First, lower-intensity fs laser fields with wavelength in the visible (VIS) range of 520 nm were used to excite the AuNPs directly in their plasmon band via one-photon absorption to efficiently overcome the electron work function by simultaneous absorption of only two photons. Therefore, one additional photon is needed. A second laser wavelength in the near-infrared (NIR) range of 1030 nm was utilized for an indirect plasmonic excitation of single AuNPs via two-photon absorption or of AuNP dimers via one-photon absorption. To enable an electron escape from the AuNPs at a laser wavelength of 1030 nm, a simultaneous absorption of four photons is needed. Therefore, much higher laser fluences and thus higher laser fields are necessary before effects can be observed. After this investigation of the influence of the strength of the laser excitation of the particles, the alignment between the direction of the (polarized) laser field and the DNA-nanowire was studied.

For the preparation of gold nanoparticle labeled DNA molecules, chemically synthesized gold nanoparticles[12,13] with a diameter of about 45 nm and genomic DNA-molecules of bacteriophage λ (MBI Fermentas, St. Leon-Rot, Germany) fluorescently labeled with 0.5 M YOYO-1 iodide (Invitrogen, Karlsruhe, Germany) were utilized. Both solutions were mixed, containing a final DNA concentration of 40 pg/μL with about 3 × 10^8 particles. A preferred adsorption of gold nanoparticles to DNA structures was used (see Figure S1 in Supporting Information). For the immobilization, the labeled DNA molecules were stretched by the receding meniscus method[14] by incubation of 50 μL of the prepared solution overnight on a glass chip with chromium microstructures (IPHT, Jena, Germany) spin-coated with a 80 nm thick poly(methyl methacrylate) (PMMA) layer. Thereby, the smooth PMMA surface allows the topographic characterization of DNA molecules down to the single molecule level by atomic force microscopy (AFM) and additionally serves as an electron sensitive substrate.

After sample fabrication, the immobilized AuNP labeled dsDNA molecules were characterized by optical microscopy (Axio Imager Z1.m, Carl Zeiss MicroImaging GmbH, Jena, Germany) to detect suitable arrays with isolated dsDNA molecules (using fluorescence contrast) and AuNPs (using dark-field illumination) in its proximity. Furthermore, these selected positions were characterized before irradiation by AFM with a NanoScope III and a Dimension 3100 detector head (Digital Instruments, Santa Barbara, CA) using tapping mode in air. AFM imaging suggests a variation of 5 to about 10 dsDNA molecules per bundle with attached aggregates of up to

Scheme 2. Setup for the fs Laser Irradiation Experiments for a Wavelength of 520 nm (Left) or 1030 nm (Right)

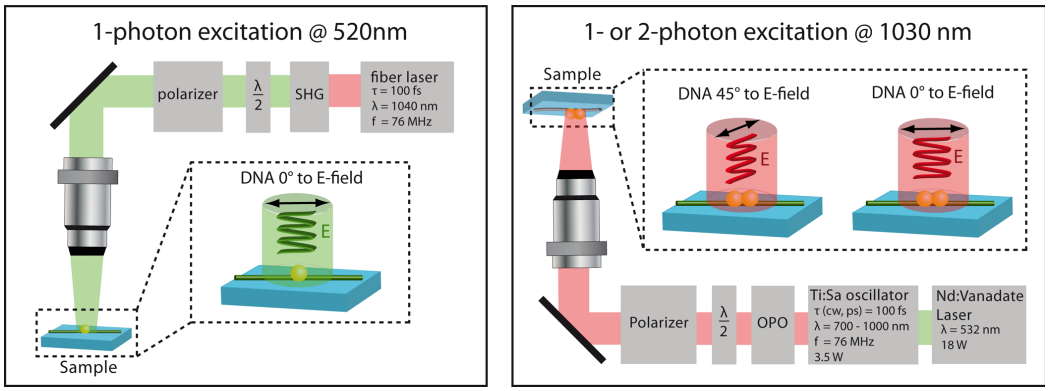

three AuNPs. Afterward the scattering UV/vis spectra of the immobilized single or aggregated AuNP were determined with an Acton Research SpectraPro 2300i microspectrometer (Princeton Instruments, Trenton, NJ, U.S.A.). Thereby, only the reflected light within a region of interest is selected by a pinhole with a diameter of 75 μm, before it is guided through an optical fiber to the spectrometer. The scattering spectra were normalized for source spectrum and detector response.

To provide the excitation of the AuNPs via one-photon or two-photon absorption, we used two different fs laser systems with a wavelength of 520 and 1030 nm, respectively, but with the same pulse duration of 100 fs and a repetition rate of 76 MHz for each laser system. For the one-photon excitation at 520 nm, a fiber laser system (Fraunhofer IOF, Jena, Germany) was applied. Thereby a fiber-coupled seed laser (OneFive, Zurich, Switzerland) with a wavelength of 1040 nm was focused into a nonlinear lithium triborate (LBO) crystal generating the second harmonic (wavelength: 520 nm) of the output beam, which was coupled into a Zeiss Axiotech 100 HD microscope (Jena, Germany) equipped with an objective (magnification 20×; numerical aperture 0.4) to obtain high laser fluences on the sample. For the two-photon excitation at a wavelength of 1030 nm, a titanium/sapphire fs oscillator (Mira-HP, Coherent, Santa Clara, CA) was pumped by a DPSS laser with a wavelength of 532 nm (Verdi, Coherent, Santa Clara, CA), which was coupled into the OPO (APE/Coherent, Dieburg, Germany) to obtain various wavelengths. The output beam passed a power regulation consisting of half-wave plate and polarizer before directly being coupled into an inverse microscope (Zeiss Axiotech 135, Jena, Germany) with an oil immersion objective (magnification, 40×; numerical aperture, 1.3). For a homogeneous irradiation of the samples in each laser system, a piezo-controlled Nano 545 3R7 stage (PI instruments Inc., Karlsruhe, Germany) was utilized with a scanning velocity of 1 μm/s and an irradiation time of 50 ms per step. About 3.8 million pulses are thereby applied per scanned surface area.

Before NP-labeled DNA molecules were treated with laser pulses, the required laser fluence was established using AuNPs on PMMA. Thus, AuNPs only were initially immobilized by incubation of the nanoparticle solution overnight on a PMMA-coated glass substrate. For each tested fluence, an area of 10 × 10 μm was characterized by AFM, containing up to 70 AuNPs, before and after treating with a certain laser fluence, respectively. Therefore, a certain parameter window was established for both laser wavelengths (520 and 1030 nm), where the excited AuNPs destroyed the underlying PMMA as confirmed by the formation of holes with the dimension of the utilized particles.

At fs laser pulses with a wavelength of 520 nm, such hole formation is observed for a fluence range between 0.3 and 0.4 mJ/cm^2 (pulse peak intensity range between 3 and 4 GW/cm^2) (Figure 1b), while lower fluences did not show any detectable

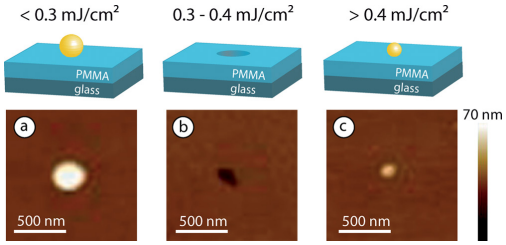

Figure 1. Effects of 520 nm fs laser pulses onto single gold nanoparticles located on PMMA substrate (a–c). Low laser fluences below 0.3 mJ/cm^2 affect neither the particle nor the PMMA (a), whereas high laser fluences above 0.4 mJ/cm^2 result in particle ablation without substrate damages (c). Only between 0.3 and 0.4 mJ/cm^2 (intensity range between 3 and 4 GW/cm^2) the excited particle affects the PMMA significantly by the formation of a hole in the dimension of the utilized particle (b).

effect (Figure 1a). A further increase to more than 0.4 mJ/cm^2 resulted in ablation of the particle without affecting the underlying PMMA (Figure 1c). Therefore, only in a parameter window from 0.3 to 0.4 mJ/cm^2, a local destruction of the PMMA surrounding area at AuNPs positions occurred. This effect is based on the LSPR supported escape of electrons by overcoming the work function of the metal (for Au ~ 5 eV) via two-photon absorption.[7]

In a second step, stretched DNA bundles (parallel aligned to the electric laser field) with attached single AuNPs were irradiated with a fluence of ~0.4 mJ/cm^2. Thereby, the plasmonic excitation of the attached AuNP resulted in a sinking of the particle into the substrate, destroying the PMMA

dx.doi.org/10.1021/nl5009184 | Nano Lett. 2014, 14, 3809–3816

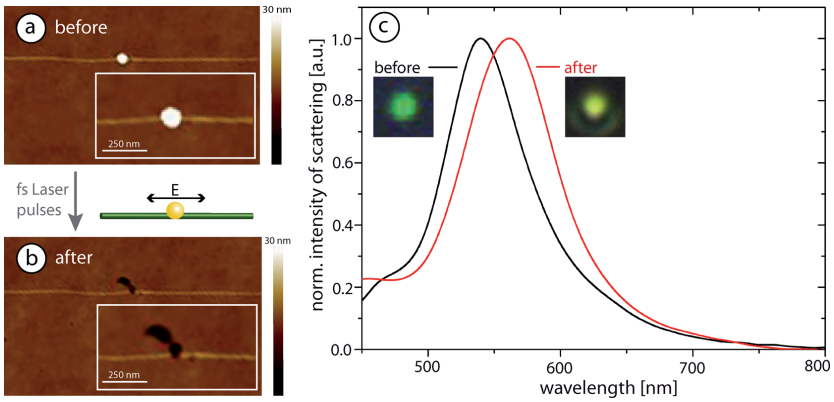

Figure 2. Plasmonically induced destruction of DNA. The same nanoparticle-labeled DNA bundle structures before (a) and after (b) pulsed laser irradiation. AFM imaging reveals a local destruction of the PMMA as well as DNA, resulting in a hole. Dark-field imaging reveals that the particle is still present in the hole (inset in c), however the color and so the spectrum is changed by this process. The observed shift to longer wavelength can be explained by refractive index changes that occur when the particles move from air to PMMA.

as well as the DNA located below the nanoparticle by escaped (hot) electrons (Figure 2a,b). The dark-field contrast still shows the particle (inset in Figure 2c), so apparently it is now buried into the PMMA. The LSPR spectrum of the AuNP shifted typically from 540 nm (before) to 560 nm (after laser irradiation) (Figure 2c). The spectral red shift is probably caused by changing the refractive index of the nanoparticle surrounding area from lower ($n_{air} = 1$) to a higher value ($n_{PMMA} = 1.5$).

However, in contrast to previous experiments of fs laser excited silver nanoparticles attached to DNA structures that showed an excitation transfer along the DNA over micrometers,[9] no transfer effects along the DNA were observed in the described experiments using gold nanoparticles. What is the difference between the two experiments? In the reported case, silver nanoparticles with a resonance around 400 nm were irradiated by 800 nm laser light and excited plasmonically via two-photon exciation. To enable the escape of these plasmonically excited electrons out of the AgNP surface, the absorption of an additional photon is required. Therefore, a fluence of 3 mJ/cm^2 (intensity of 30 GW/cm^2) is needed. Femtosecond laser illumination with this fluence below the ablation threshold causes a temperature increase of 40 K in maximum.[7] This is too low for a thermally induced sinking of the metal nanoparticle into the PMMA layer, as confirmed by experimental determination of the required temperature of at least 300 °C.[15] An accumulated temperature raise during irradiation by femtosecond laser pulses with 76 MHz repetition rate can be excluded as shown by FEM calculations of heat conduction that result in an accumulated temperature increase of just 3.5 K.[7]

In our experiments, gold particles with a resonance near 520 nm were irradiated with a 520 nm wavelength laser, resulting in an plasmonic excitation via one-photon absorption. In this case, the absorption of one more photon by the plasmonically excited electron is needed for electron escape, too. But here much lower fluences are sufficient (0.4 mJ/cm^2) due to a finally needed absorption of just two photons compared to AgNP where three photons are required. Also the temperature effect is much weaker as before. The high fluences in the case of silver particles cause highly enhanced electric fields (10^8–10^9 V/m) in the particle surrounding area, which seems to be necessary for the transfer of the escaped electrons excitation into attached DNA nanowire. One way to prove the importance of an enhanced electric laser field would be to increase the laser fluence, but this will lead to the ablation of the AuNPs by Coulomb explosion (see Figure 1c) as well as to an unspecific plasma generation in PMMA and therefore to the unspecific destruction of PMMA over the whole irradiated area by two-photon absorption (see Figure S2 in Supporting Information). Because of these reasons, the experiments were repeated, but now using a two-photon excitation of the AuNPs LSPR using a wavelengths in the NIR range (1030 nm). Here, higher fluences and higher electric fields could be utilized while avoiding the destruction of the PMMA by unspecific plasma generation.

Again, the fluence range for efficient excitation by 1030 nm wavelength was determined. Fluences below 3 mJ/cm^2 did not show any effects. An increase of the fluence lead to the hole formation in the PMMA only in the case of AuNP aggregates, while single AuNPs remain unaffected. Even a further enhancement to maximal possible OPO output laser fluence of 20 mJ/cm^2 (intensity of 200 GW/cm^2) could not affect single AuNPs (Figure 3a, b).

For a destruction of PMMA at a wavelength of 1030 nm, a multiphoton absorption of at least four photons is needed for AuNPs electrons to overcome the work function (see Table 1). This process has a low probability and the plasmonic excitation at 515 nm (needing two photons) for the supported electron escape is quite weak (see Figure 3c monomer), therefore none of the single particles sinks into the PMMA. Only AuNP aggregates lead to hole formation in the PMMA. We explain this phenomenon by the strong coupling of bonding dipole–dipole modes of two adjacent nanoparticles. The strong coupling induces a redshift of the long wavelength mode around 1000 nm[16,17] (not shown in Figure 3c due to the limited spectral range of the spectrometer). In this case where both particles have the same size, both dipole–dipole modes (520 nm, 1000 nm) overlap less and the Fano-resonance weakens.[17] Also the bounding dipole–quadrupole mode at 780 nm does not play a significant role, it shows a dip. So we conclude that the strong dipole mode in the 1030 nm range

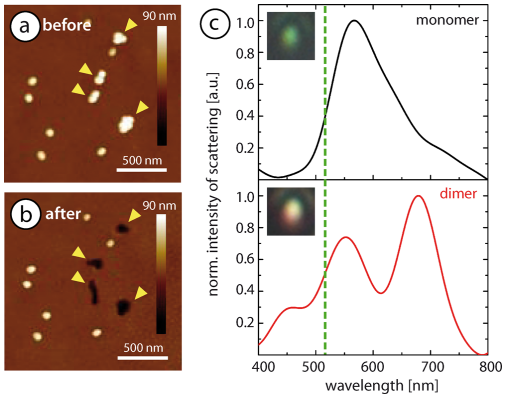

Figure 3. Left (a,b) NIR fs laser treatment (wavelength: 1030 nm) of AuNPs (single and nanoparticle aggregates) at a fluence of 20 mJ/cm^2 (intensity of 200 GW/cm^2). Only the marked particle aggregates (yellow arrowheads) induce hole formation in PMMA when irradiated, while the single particles remain unaffected. Right (c) Typical dark-field scattering spectra of a AuNP monomer and a dimer. The dimer shows the typical dipole mode for external fields oriented along the particle axis in the NIR range. A third resonance peak in range of 1030 nm[16] is not recorded due to the limited spectral range of the spectrometer. The green dashed line at 515 nm marks the second harmonic of the used laser wavelength. Insets show the corresponding dark-field images.

supports a quite efficient single photon plasmonic excitation of nanoparticle dimer electrons. Another important fact could be a significant charge localization in gaps between individual NPs. This charge pileup is compensated on the opposite side of the particles, resulting in an enhanced magnitude of the smooth charge distribution on the AuNP aggregate surfaces.[16] On the other hand, quantum mechanical studies have shown that incident electromagnetic fields generate a field enhancement in the gap of separated AuNP homodimer (d_{gap} = 0.2–1 nm), which causes an increased electron tunneling current through the junction.[18] This could neutralize the induced charges at the AuNP aggregate surface. However, at fs laser field exciation, the higher amount of free tunneling electrons and the concentration of the optical energy in the junction induces probably more escaped electrons.[19] Here a damage of underlying PMMA layer is less probable, because these electrons tunnel nearby the contact point of the two ~45 nm spheres, which is more than 20 nm above the PMMA surface. Another explanation could be a laser-field driven Schottky barrier passing of nanoparticle electrons due to the utilized high intensities of 200 GW/cm^2.

In these experiments, the larger dipole strength and the proper resonance wavelength is applied at a parallel orientation of the longitudinal AuNP dimer axis to the incident electric field. In order to confirm these arguments, the dependency of the laser light polarization angle on AuNP dimers during NIR laser irradiation was verified in further experiments. For this, several areas on the chip with a total number of 41 immobilized AuNP dimers with orientations between 0 and 90° to the long particle dimer axis were selected from AFM images, and the angles of the AuNP dimers were determined. Afterward, each area containing several oriented AuNP dimers were irradiated

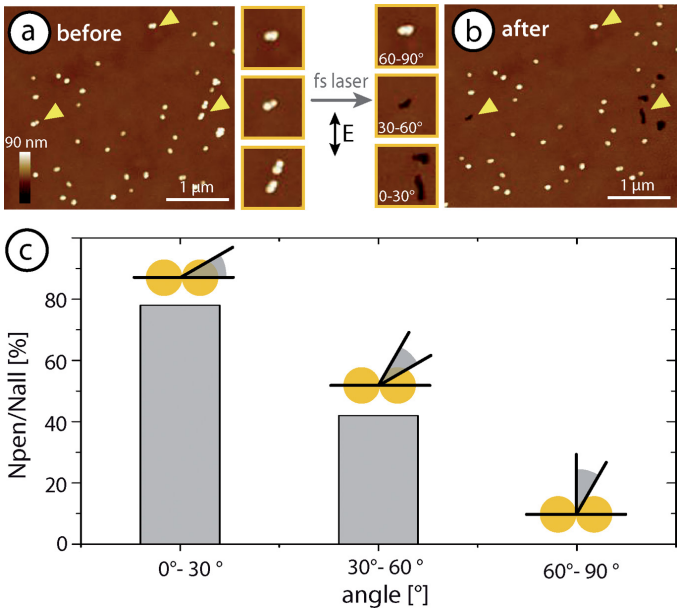

Figure 4. Effect of field alignment with repect to the long AuNP dimer axis. (a,b) AFM images before and after irradiation (height scale: 90 nm). No effect is observed for a field alignment of 60–90°, while the most significant result is observed for a nearly parallel (0–30°) alignment (insets). (c) Relative amount of affected AuNPs (Npen) in dependency of the polarization angle of the incident laser pulses longitudinal to the AuNP dimer axis.

dx.doi.org/10.1021/nl5009184 | Nano Lett. 2014, 14, 3809–3816

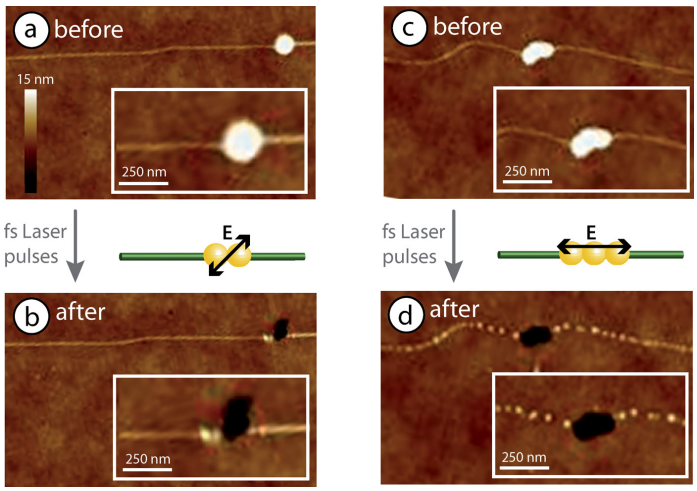

Figure 5. Effects of electric field alignment (with respect to the long axis of nanoparticle multimers) on excitation transfer along DNA (height scale: 15 nm). (Left) For 45°, only local damages along the DNA are observed (~200 nm fragmentation), only the particle present before irradiation (a) disappears in the substrate (b). (Right) When the field is aligned (0°) (c), irradiation results also in long-range damages (~2 μm fragmentation) along the DNA (d).

with fs laser pulses (starting with light polarized between 0 and 30° to the AuNP dimer axis) with a wavelength of 1030 nm at fluences between 10 and 20 mJ/cm^2 (intensities between 100 and 200 GW/cm^2). At polarization angles between 60 and 90°, where the electric field is almost perpendicular to the long AuNP dimer axis, no sinking of the dimer into PMMA occurs, while angles between 0 and 30° lead to hole formation due to sinking of the AuNP dimer (Figure 4). Polarization angles from 30 to 60° lead to a less significant number of observed penetration of AuNP dimers into the PMMA substrate.

This results are confirmed by a study where theoretical FDTD simulations have shown the highest field enhancement at a parallel polarization of incident radiation to the longitudinal mode of an AuNP dimer, which was additionally supported experimentally by the generation of deeper holes in the substrate during parallel polarized fs laser irradiation of an AuNP dimer.[20] These field enhancements are given for incident wavelengths corresponding to the intense plasmon band in the NIR range[21] of AuNP aggregates, as described above.

To further study this effect for a one-photon excitation at 1030 nm, the experiments were continued with AuNP aggregates situated in an angle of 45° as well as parallel to the electric laser field. After laser irradiation, only the parallel alignment revealed in the AFM a clear fragmentations which follow the original dsDNA position up to one micrometer on each side of the sunken AuNP trimer (Figure 5b). Such DNA fragmentation was only observed around nanoparticles. In the case of nonparallel alignment, only the particle exhibited changes, but not the DNA.

These results show that a parallel orientation of the incident laser light is necessary for a transfer of the highly excited Au aggregate electrons energy along the attached dsDNA molecules. Laser pulses with polarization angles of 0 and 45° longitudinal to the AuNP aggregates axis lead to an efficient manipulation in the local proximity by overcoming the metals work function or by field-driven barrier tunneling of electrons (demonstrated by the local destruction of the underlying PMMA visible in both cases in Figure 5). Only a parallel orientation of the electric laser field to the attached dsDNA seems to provide sufficient energy coupling (ejection of highly excited electrons from nanoparticle induce a charge avalanche in DNA) for an excitation transfer by charge transfer (electron hopping) processes or nearly elastic electron impact from the donor- to the acceptor electrons along the stretched DNA molecules. One possible explanation of this strong polarization dependency is that the excited DNA electrons aquire a higher initial kinetic energy due to the higher electric laser field at a parallel orientation of the AuNP trimer and DNA.[10] Subsequently, these electrons could excite more strongly other DNA electrons by overlapping π-bonds of the base pair stacks, leading to a propagation of this excitation along the DNA molecules before the electron−phonon relaxation process is starting. After many fs pulses, this could result finally in the fragmentation of these bonds following the original DNA position. In contrast to our early work with silver particles,[9] where a PMMA layer situated below the DNA was destroyed too, here the excitation transfer along DNA seems to be more local. Although the experimental results are not sufficient to fully clarify the mechanism of this propagation, a coupled transfer of charge (Dexter) and delocalized exciton (Frenkel) process appears to be most likely for a long-range excitation transfer through DNA.[22]

These findings are in contrast to several former experiments, where the current voltage characteristics of DNA molecules in different conformations was measured.[23−26] Here the results were controversal and a clear picture of conduction mechanism in DNA has not been attained so far. Other experiments show photoinduced charge transfer after light excitation of an donor dye molecule to an acceptor dye molecule, both attached on DNA only some nanometer away from each other.[27,28] On the basis of these experiments, hopping mechanism and super exchange were discussed as relevant transfer mechanism of

charge. It was concluded that electron transport is blocked in long molecules (above tens of nanometers) that are attached to the surface but is feasible for much shorter distances. Here, we presented experiments where excitation transfer over micrometers is observed without DNA intercalation of transition metal complexes.[29]

In conclusion, we showed sinking of single gold nanoparticles into the PMMA layer by plasmonic one photon excitation via low fluence fs laser pulses at wavelength of 520 nm. No incoupling of energy into DNA could be observed under these conditions. Nevertheless, we extended successfully the plasmonically induced incoupling of energy into DNA to gold nanoparticles, using particle multimers. Thereby we were able to realize a DNA destruction far beyond distances typical for electron-hopping processes.[23,30] The behavior of gold nanoparticles was quite different to the silver case studied previously. Irradiation of single gold particles (monomers) using two photon excitation did not support electron escape, visible as a sinking into the PMMA substrate. Only multimers (dimers, trimers) showed this behavior for an aligned exciting laser pulse field. When attached to DNA structures, AuNP multimers coupled the energy from the fs laser pulses via four-photon excitation/laser field driven barrier tunneling of electrons only under a certain alignment of electric laser field to the long multimers axis. The much more weaker excitation of gold particles compared to silver is explained by a smaller photon energy of laser excitation wavelength and by the requirement of more than three-photon excitation for overriding the electron workfunction.

The results extend the usable particle material significantly (now to a material stable under ambient conditions) and reveal novel parameters for influencing of the recently discovered coupling of energy into the DNA nanowires, allowing thereby extended control of this new optoelectronic functionality at the molecular scale.

■ ASSOCIATED CONTENT

Supporting Information

Correlative microscopy of fluorescently labeled DNA structures with attached gold nanoparticles in dark-field and fluorescence contrast. SEM and dark-field images showing the destruction of PMMA by VIS fs laser pulses in dependence of the laser fluence This material is available free of charge via the Internet at http://pubs.acs.org.

■ AUTHOR INFORMATION

Corresponding Author

*E-mail: wolfgang.fritzsche@ipht-jena.de.

Author Contributions

†J.W. and F.G. contributed equally.

Notes

The authors declare no competing financial interest.

■ ACKNOWLEDGMENTS

Funding for research initiative "MicroInter" (Beutenberg fellowship, TMWFK PE-113-1) is gratefully acknowledged. We thank K. Kandera, K. Pippardt, H. Porwol, M. Sossna, D. Horn, J. Albert, G. Schmidl, and U. Hübner for assistance with sample preparation and S. Heuke, D. Akimov, N. Vogler, B. Dietzek, J. Toussaint, and T. May for assistance with the laser experiments.

■ REFERENCES

(1) Kelly, K. L.; Coronado, E.; Zhao, L. L.; Schatz, G. C. *J. Phys. Chem. B* **2003**, *107*, 668−677.
(2) Xu, H. X.; Aizpurua, J.; Kall, M.; Apell, P. *Phys. Rev. E* **2000**, *62*, 4318−4324.
(3) Knight, M. W.; Sobhani, H.; Nordlander, P.; Halas, N. J. *Science* **2011**, *332*, 702−704.
(4) Hirsch, L. R.; Stafford, R.; Bankson, J.; Sershen, S.; Rivera, B.; Price, R.; Hazle, J.; Halas, N.; West, J. *Proc. Natl. Acad. Sci. U.S.A.* **2003**, *100*, 13549−13554.
(5) Csaki, A.; Garwe, F.; Steinbrück, A.; Maubach, G.; Festag, G.; Weise, A.; Riemann, I.; König, K.; Fritzsche, W. *Nano Lett.* **2007**, *7*, 247−253.
(6) Yao, C. P.; Rahmanzadeh, R.; Endl, E.; Zhang, Z. X.; Gerdes, J.; Huttmann, G. *J. Biomed. Opt.* **2005**, *10*, 064012.
(7) Garwe, F.; Bauerschäfer, U.; Csaki, A.; Steinbrück, A.; Ritter, K.; Bochmann, A.; Bergmann, J.; Weise, A.; Akimov, D.; Maubach, G. *Nanotechnology* **2008**, *19*, 055207.
(8) König, K.; Riemann, I.; Fritzsche, W. *Opt. Lett.* **2001**, *26*, 819−821.
(9) Wirth, J.; Garwe, F.; Hahnel, G.; Csaki, A.; Jahr, N.; Stranik, O.; Paa, W.; Fritzsche, W. *Nano Lett.* **2011**, *11*, 1505−1511.
(10) Toppari, J. J.; Wirth, J.; Garwe, F.; Stranik, O.; Csaki, A.; Bergmann, J.; Paa, W.; Fritzsche, W. *ACS Nano* **2013**, *7*, 1291−1298.
(11) Scharte, M.; Porath, R.; Ohms, T.; Aeschlimann, M.; Lamprecht, B.; Ditlbacher, H.; Aussenegg, F. R. In *Lifetime and Dephasing of Plasmons in Ag Nanoparticles*; International Symposium on Optical Science and Technology; International Society for Optics and Photonics: San Diego, CA, USA, 2001; pp 14−21.
(12) Turkevich, J.; Stevenson, P. C.; Hillier, J. *Discuss. Faraday Soc.* **1951**, 55−75.
(13) Turkevich, J.; Stevenson, P. C.; Hillier, J. *J. Phys. Chem.* **1953**, *57*, 670−673.
(14) Bensimon, D.; Simon, A.; Croquette, V.; Bensimon, A. *Phys. Rev. Lett.* **1995**, *74*, 4754.
(15) Lantz, M. A.; Gotsmann, B.; Durig, U. T.; Vettiger, P.; Nakayama, Y.; Shimizu, T.; Tokumoto, H. *Appl. Phys. Lett.* **2003**, *83*, 1266−1268.
(16) Romero, I.; Aizpurua, J.; Bryant, G. W.; de Abajo, F. J. G. *Opt. Express* **2006**, *14*, 9988−9999.
(17) Brown, L. V.; Sobhani, H.; Lassiter, J. B.; Nordlander, P.; Halas, N. J. *ACS Nano* **2010**, *4*, 819−832.
(18) Marinica, D.; Kazansky, A.; Nordlander, P.; Aizpurua, J.; Borisov, A. G. *Nano Lett.* **2012**, *12*, 1333−1339.
(19) Atay, T.; Song, J. H.; Nurmikko, A. V. *Nano Lett.* **2004**, *4*, 1627−1631.
(20) Nedyalkov, N.; Takada, H.; Obara, M. *Appl. Phys. A: Mater. Sci. Process.* **2006**, *85*, 163−168.
(21) Wustholz, K. L.; Henry, A.-I.; McMahon, J. M.; Freeman, R. G.; Valley, N.; Piotti, M. E.; Natan, M. J.; Schatz, G. C.; Duyne, R. P. V. *J. Am. Chem. Soc.* **2010**, *132*, 10903−10910.
(22) May, V.; Kühn, O. *Charge and energy transfer dynamics in molecular systems*; John Wiley & Sons: New York, 2008.
(23) Porath, D.; Bezryadin, A.; de Vries, S.; Dekker, C. *Nature* **2000**, *403*, 635−638.
(24) Porath, D.; Cuniberti, G.; Di Felice, R. Charge transport in DNA-based devices. In *Topics in Current Chemistry*; Springer: New York, 2004; pp 183−228.
(25) Xu, B.; Zhang, P.; Li, X.; Tao, N. *Nano Lett.* **2004**, *4*, 1105−1108.
(26) Yoo, K.-H.; Ha, D.; Lee, J.-O.; Park, J.; Kim, J.; Kim, J.; Lee, H.-Y.; Kawai, T.; Choi, H. Y. *Phys. Rev. Lett.* **2001**, *87*, 198102.
(27) Varghese, R.; Wagenknecht, H. A. *Chem.—Eur. J.* **2009**, *15*, 9307−9310.
(28) Ehrenschwender, T.; Varga, B.; Kele, P.; Wagenknecht, H.-A. *Chem. - Asian J.* **2010**, *5*, 1761−1764.
(29) Murphy, C.; Arkin, M.; Jenkins, Y.; Ghatlia, N.; Bossmann, S.; Turro, N.; Barton, J. *Science* **1993**, *262*, 1025−1029.

(30) Cohen, H.; Nogues, C.; Naaman, R.; Porath, D. *Proc. Natl. Acad. Sci. U.S.A.* **2005**, *102*, 11589−11593.

6 Liste der Publikationen

6.1 Peer-reviewed Publikationen

Plasmonic nanofabrication by long-range excitation transfer via DNA nanowire
J. Wirth, F. Garwe, G. Hähnel, A. Csáki, N. Jahr, O. Stranik, W. Paa, W. Fritzsche. Nano Letters, 2011. 11(4): p. 1505-1511

Molecular plasmonics: light meets molecules at the nanoscale

A. Csáki, T. Schneider, J. Wirth, N. Jahr, A. Steinbrück, O. Stranik, F. Garwe, R. Müller, W. Fritzsche. Philosophical Transactions of the Royal Society A: Mathematical, Physical and Engineering Sciences, 2011. **369** (1950): p. 3483-3496

Plasmonic coupling and transfer of an excitation along a DNA nanowire

J. J. Toppari[‡], J. Wirth[‡], F. Garwe[‡], O. Stranik, A. Csáki, J. Bergmann, W. Paa, W. Fritzsche. ACS Nano, 2013. 7(2): p. 1291-1298

Tuning of spectral and angular distribution of scattering from single gold nanoparticles by sub-wavelength interference layers

J. Wirth[‡], F. Garwe[‡], J. Bergmann, W. Paa, A. Csáki, O. Stranik, W. Fritzsche. Nano Letters, 2014. 14 (2): p. 570–577

Plasmonically-enhanced electron escape from gold nanoparticles and their polarization-dependent excitation transfer along DNA nanowires
J. Wirth[‡], F. Garwe[‡], R. Meyer, A. Csáki, O. Stranik, W. Fritzsche. Nano Letters, 2014. **14**(7): p. 3809-3816

PMMA nanostructuring by polarization dependent fs laser irradiation of single-walled carbon nanotubes
J. Wirth, F. Garwe, O. Stranik, A. Csáki, W. Fritzsche. **in preparation**

6.2 Konferenzbeiträge

6.2.1 Vorträge

DNA manipulation by laser pulses using nanoantennas,
Janina Wirth, Andrea Csáki, Frank Garwe, Norbert Jahr, Gerd Hähnel, Philipp Wustelt, Wolfgang Fritzsche

International Symposia "DNA-based Micro-Nanointegration",
Jena (Germany), 27.05. - 29.05.2010

Plasmonic manipulation of DNA and its potential for nanofabrication
Janina Wirth, Frank Garwe, Gerd Hähnel, Andrea Csáki, Norbert Jahr, Ondrej Stranik, Wolfgang Paa, Wolfgang Fritzsche

Doctoral student´s conference for the discuccion of optical concepts "DoKDoK ",
Naumburg (Germany), 21.03. - 25.03.2011

fs laser pulse excitation of noble nanoparticles attached on DNA-molecules and cancer cells
Janina Wirth, Frank Garwe, Gerd Hähnel, Andrea Csáki, Norbert Jahr, Ondrej Stranik, Wolfgang Paa, Wolfgang Fritzsche

Student Conference on Microbial Communication "MiCom",
Jena (Germany), 13.09. - 16.09.2011

Long-range excitation transfer via DNA molecules by fs laser pulse excitation of silver nanoparticles
Janina Wirth, Frank Garwe , Andrea Csáki, Norbert Jahr, Ondrej Stranik, Wolfgang Paa, Wolfgang Fritzsche

Summer School on Plasmonics "SSOPII",
Porquerolles (France), 03.10. - 07.10.2011

6.2.2 Poster

Noble metal nanostructures as optical biosensor for biomolecular interactions
Janina Wirth, Thomas Schneider, Andrea Csáki, Wolfgang Fritzsche

International Student Conference on Microbial Communication "MiCom",
Jena (Germany), 28.09. - 01.10.2010

Long-range excitation transfer via DNA nanowire by fs laser pulse excitation of
silver nanoparticles
Janina Wirth, Frank Garwe, Andrea Csáki, Norbert Jahr, Ondrej Stranik, Wolfgang Paa, Wolfgang Fritzsche

"Photonics4Life" Annual Meeting, Heraklion (Crete), 27.04. - 29.04.2011

Long-range excitation transfer via DNA nanowire using noble nanoparticles as
laser antennas
Janina Wirth, Frank Garwe, Gerd Hähnel, Andrea Csáki, Norbert Jahr, Ondrej Stranik, Wolfgang Paa, Wolfgang Fritzsche

"Nano Bio Europe"International Conference, Cork (Ireland), 21.06. - 23.06.2011

Interaction between metal nanoparticles and short laser pulses and their application in the manipulation of biological matrices
Janina Wirth, Frank Garwe, Robert Meyer, Jussi Toppari, Andrea Csáki, Wolfgang Paa, Wolfgang Fritzsche

"DNA Nanosensors" International Symposium, Jena (Germany),
10.05. - 12.05.2012

Coupling of plasmonic energy into DNA nanowire
Janina Wirth, Robert Meyer, Frank Garwe, Andrea Csáki, Wolfgang Fritzsche

International Student Conference on Microbial Communication "MiCom",
Jena (Germany), 05.11. - 08.11.2012

Literaturverzeichnis

1 Tschachotin, S. Die mikroskopische strahlenstichmethode, eine zelloperationsmethode. *Biol. Zentralbl* **32**, 30 (1912).

2 Bessis, M., Gires, F., Mayer, G. & Nomarski, G. IRRADIATION OF CELLULAR ORGANELLES WITH THE AID OF A RUBY LASER. (Laboratoire CSF, Corbeville, France, 1962).

3 Jonáš, A. & Zemanek, P. Light at work: The use of optical forces for particle manipulation, sorting, and analysis. *Electrophoresis* **29**, 4813-4851 (2008).

4 Chen, Y.-T., Naessens, K., Baets, R., Liao, Y.-S. & Tseng, A. A. Ablation of transparent materials using excimer lasers for photonic applications. *Optical review* **12**, 427-441 (2005).

5 Gattass, R. R. & Mazur, E. Femtosecond laser micromachining in transparent materials. *Nat Photonics* **2**, 219-225 (2008).

6 Hüttmann, G., Radt, B., Serbin, J., Lange, B. I. & Birngruber, R. High precision cell surgery with nanoparticles? *Medical Laser Application* **17**, 9-14 (2002).

7 Hirsch, L. R. *et al.* Nanoshell-mediated near-infrared thermal therapy of tumors under magnetic resonance guidance. *Proceedings of the National Academy of Sciences* **100**, 13549-13554 (2003).

8 Csaki, A. *et al.* A parallel approach for subwavelength molecular surgery using gene-specific positioned metal nanoparticles as laser light antennas. *Nano Letters* **7**, 247-253, doi:Doi 10.1021/Nl061966x (2007).

9 Kogan, M. J. *et al.* Nanoparticle-mediated local and remote manipulation of protein aggregation. *Nano Letters* **6**, 110-115 (2006).

10 Mie, G. Beiträge zur Optik trüber Medien, speziell kolloidaler Metallösungen. *Annalen der physik* **330**, 377-445 (1908).

11 Cheng, C.-S., Chen, Y.-Q. & Lu, C.-J. Organic vapour sensing using localized surface plasmon resonance spectrum of metallic nanoparticles self assemble monolayer. *Talanta* **73**, 358-365 (2007).

12 Chen, K.-J. & Lu, C.-J. A vapor sensor array using multiple localized surface plasmon resonance bands in a single UV–vis spectrum. *Talanta* **81**, 1670-1675 (2010).

13 Karakouz, T., Vaskevich, A. & Rubinstein, I. Polymer-Coated Gold Island Films as Localized Plasmon Transducers for Gas Sensing†. *The Journal of Physical Chemistry B* **112**, 14530-14538 (2008).

14 Nuopponen, M. & Tenhu, H. Gold nanoparticles protected with pH and temperature-sensitive diblock copolymers. *Langmuir* **23**, 5352-5357 (2007).

15 Lee, S., Mayer, K. M. & Hafner, J. H. Improved localized surface plasmon resonance immunoassay with gold bipyramid substrates. *Analytical chemistry* **81**, 4450-4455 (2009).
16 Li, C. *et al.* LSPR sensing of molecular biothiols based on noncoupled gold nanorods. *Langmuir* **26**, 9130-9135 (2010).
17 Lin, T.-J., Huang, K.-T. & Liu, C.-Y. Determination of organophosphorous pesticides by a novel biosensor based on localized surface plasmon resonance. *Biosensors and Bioelectronics* **22**, 513-518 (2006).
18 Marinakos, S. M., Chen, S. & Chilkoti, A. Plasmonic detection of a model analyte in serum by a gold nanorod sensor. *Analytical chemistry* **79**, 5278-5283 (2007).
19 Wang, Y., Qian, W., Tan, Y. & Ding, S. A label-free biosensor based on gold nanoshell monolayers for monitoring biomolecular interactions in diluted whole blood. *Biosensors and Bioelectronics* **23**, 1166-1170 (2008).
20 Nath, N. & Chilkoti, A. A colorimetric gold nanoparticle sensor to interrogate biomolecular interactions in real time on a surface. *Analytical Chemistry* **74**, 504-509 (2002).
21 Mayer, K. M., Hao, F., Lee, S., Nordlander, P. & Hafner, J. H. A single molecule immunoassay by localized surface plasmon resonance. *Nanotechnology* **21**, 255503 (2010).
22 Mayer, K. M. *et al.* A label-free immunoassay based upon localized surface plasmon resonance of gold nanorods. *Acs Nano* **2**, 687-692 (2008).
23 Schneider, T. *et al.* Localized surface plasmon resonance (LSPR) study of DNA hybridization at single nanoparticle transducers. *J Nanopart Res* **15**, doi:Unsp 1531Doi 10.1007/S11051-013-1531-7 (2013).
24 Yoo, S. Y. *et al.* Detection of the most common corneal dystrophies caused by BIGH3 gene point mutations using a multispot gold-capped nanoparticle array chip. *Analytical chemistry* **82**, 1349-1357 (2010).
25 Haes, A. J. & Van Duyne, R. P. A nanoscale optical biosensor: sensitivity and selectivity of an approach based on the localized surface plasmon resonance spectroscopy of triangular silver nanoparticles. *Journal of the American Chemical Society* **124**, 10596-10604 (2002).
26 Haes, A. J., Chang, L., Klein, W. L. & Van Duyne, R. P. Detection of a biomarker for Alzheimer's disease from synthetic and clinical samples using a nanoscale optical biosensor. *Journal of the American Chemical Society* **127**, 2264-2271 (2005).
27 Lévêque, G. & Martin, O. J. F. Optical interactions in a plasmonic particle coupled to a metallic film. *Opt. Express* **14**, 9971-9981, doi:10.1364/oe.14.009971 (2006).
28 Lévêque, G. & Martin, O. J. F. Tunable composite nanoparticle for plasmonics. *Opt. Lett.* **31**, 2750-2752, doi:10.1364/ol.31.002750 (2006).

29 Mock, J. J. *et al.* Distance-dependent plasmon resonant coupling between a gold nanoparticle and gold film. *Nano Letters* **8**, 2245-2252, doi:Doi 10.1021/Nl080872f (2008).
30 Schmidt, M. A., Lei, D. Y., Wondraczek, L., Nazabal, V. & Maier, S. A. Hybrid nanoparticle–microcavity-based plasmonic nanosensors with improved detection resolution and extended remote-sensing ability. *Nature communications* **3**, 1108 (2012).
31 Schalkhammer, T. *et al.* The use of metal-island-coated pH-sensitive swelling polymers for biosensor applications. *Sensors and Actuators B: Chemical* **24**, 166-172 (1995).
32 Burda, C., Chen, X., Narayanan, R. & El-Sayed, M. A. Chemistry and properties of nanocrystals of different shapes. *Chemical reviews* **105**, 1025-1102 (2005).
33 Hodak, J. H., Henglein, A. & Hartland, G. V. Photophysics of nanometer sized metal particles: electron-phonon coupling and coherent excitation of breathing vibrational modes. *The Journal of Physical Chemistry B* **104**, 9954-9965 (2000).
34 Link, S. & El-Sayed, M. A. Shape and size dependence of radiative, non-radiative and photothermal properties of gold nanocrystals. *International Reviews in Physical Chemistry* **19**, 409-453 (2000).
35 Govorov, A. O. *et al.* Gold nanoparticle ensembles as heaters and actuators: melting and collective plasmon resonances. *Nanoscale Research Letters* **1**, 84-90 (2006).
36 Richardson, H. H. *et al.* Thermooptical properties of gold nanoparticles embedded in ice: characterization of heat generation and melting. *Nano letters* **6**, 783-788 (2006).
37 Zharov, V., Letfullin, R. & Galitovskaya, E. Microbubbles-overlapping mode for laser killing of cancer cells with absorbing nanoparticle clusters. *Journal of Physics D: Applied Physics* **38**, 2571 (2005).
38 Hüttmann, G., Radt, B., Serbin, J. & Birngruber, R. in *European Conference on Biomedical Optics 2003.* 88-95 (International Society for Optics and Photonics).
39 Pitsillides, C. M., Joe, E. K., Wei, X., Anderson, R. & Lin, C. P. Selective cell targeting with light-absorbing microparticles and nanoparticles. *Biophysical journal* **84**, 4023-4032 (2003).
40 Stehr, J. *et al.* Gold nanostoves for microsecond DNA melting analysis. *Nano letters* **8**, 619-623 (2008).
41 Brigger, I., Dubernet, C. & Couvreur, P. Nanoparticles in cancer therapy and diagnosis. *Advanced Drug Delivery Reviews* **54**, 631-651 (2002).
42 Huang, X., Jain, P., El-Sayed, I. & El-Sayed, M. Plasmonic photothermal therapy (PPTT) using gold nanoparticles. *Lasers in Medical Science* **23**, 217-228 (2008).

43 Lapotko, D. Plasmonic nanoparticle-generated photothermal bubbles and their biomedical applications. *Nanomedicine* **4**, 813-845, doi:10.2217/Nnm.09.59 (2009).
44 Lapotko, D. Therapy with gold nanoparticles and lasers: what really kills the cells? *Nanomedicine* **4**, 253-256, doi:10.2217/NNM.09.2 (2009).
45 Lapotko, D. Optical excitation and detection of vapor bubbles around plasmonic nanoparticles. *Opt. Express* **17**, 2538-2556 (2009).
46 Lapotko, D. & Lukianova, E. Laser-induced micro-bubbles in cells. *International Journal of Heat and Mass Transfer* **48**, 227-234, doi:10.1016/j.ijheatmasstransfer.2004.08.012 (2005).
47 Lapotko, D. O. Laser-induced bubbles in living cells. *Lasers in Surgery and Medicine* **38**, 240-248, doi:10.1002/lsm.20284 (2006).
48 Lapotko, D. O., Lukianova, E. & Oraevsky, A. A. Selective laser nano-thermolysis of human leukemia cells with microbubbles generated around clusters of gold nanoparticles. *Laser Surg Med* **38**, 631-642, doi:Doi 10.1002/Lsm.20359 (2006).
49 Lee, S. E., Liu, G. L., Kim, F. & Lee, L. P. Remote optical switch for localized and selective control of gene interference. *Nano letters* **9**, 562-570 (2009).
50 Yao, C., Qu, X., Zhang, Z., Hüttmann, G. & Rahmanzadeh, R. Influence of laser parameters on nanoparticle-induced membrane permeabilization. *Journal of biomedical optics* **14**, 054034-054034-054037 (2009).
51 Chakravarty, P., Qian, W., El-Sayed, M. A. & Prausnitz, M. R. Delivery of molecules into cells using carbon nanoparticles activated by femtosecond laser pulses. *Nature Nanotechnology* **5**, 607-611, doi:Doi 10.1038/Nnano.2010.126 (2010).
52 Schomaker, M. *et al.* Delivery of molecules into living cells by fs- laser pulses using gold nanoparticles and nanostructures. *Human Gene Therapy* **20**, 1517-1517 (2009).
53 Lapotko, D. O., Anderson, L. J. E., Hansen, E., Lukianova-Hleb, E. Y. & Hafner, J. H. Optically guided controlled release from liposomes with tunable plasmonic nanobubbles. *Journal of Controlled Release* **144**, 151-158, doi:10.1016/j.jconrel.2010.02.012 (2010).
54 Bouhelier, A., Beversluis, M., Hartschuh, A. & Novotny, L. Near-field second-harmonic generation induced by local field enhancement. *Physical review letters* **90**, 013903 (2003).
55 Danckwerts, M. & Novotny, L. Optical frequency mixing at coupled gold nanoparticles. *Physical review letters* **98**, 026104 (2007).
56 Palomba, S., Danckwerts, M. & Novotny, L. Nonlinear plasmonics with gold nanoparticle antennas. *Journal of Optics A: Pure and Applied Optics* **11**, 114030 (2009).

57 Nedyalkov, N., Takada, H. & Obara, M. Nanostructuring of silicon surface by femtosecond laser pulse mediated with enhanced near-field of gold nanoparticles. *Applied Physics A* **85**, 163-168 (2006).
58 Nedyalkov, N. N., Atanasov, P. A. & Obara, M. Near-field properties of a gold nanoparticle array on different substrates excited by a femtosecond laser. *Nanotechnology* **18**, 305703 (2007).
59 Nedyalkov, N., Sakai, T., Miyanishi, T. & Obara, M. Near field properties in the vicinity of gold nanoparticles placed on various substrates for precise nanostructuring. *Journal of Physics D: Applied Physics* **39**, 5037 (2006).
60 Leiderer, P., Bartels, C., Koenig-Birk, J., Mosbacher, M. & Boneberg, J. Imaging optical near-fields of nanostructures. *Applied physics letters* **85**, 5370-5372 (2004).
61 Kolloch, A. *et al.* Femtosecond and picosecond near-field ablation of gold nanotriangles: nanostructuring and nanomelting. *Applied Physics A* **104**, 793-799 (2011).
62 Garwe, F. *et al.* Optically controlled thermal management on the nanometer length scale. *Nanotechnology* **19**, 055207 (2008).
63 Kamat, P. V., Flumiani, M. & Hartland, G. V. Picosecond dynamics of silver nanoclusters. Photoejection of electrons and fragmentation. *The Journal of Physical Chemistry B* **102**, 3123-3128 (1998).
64 Letfullin, R. R., Joenathan, C., George, T. F. & Zharov, V. P. Laser-induced explosion of gold nanoparticles: potential role for nanophotothermolysis of cancer. (2006).
65 Yamada, K., Tokumoto, Y., Nagata, T. & Mafuné, F. Mechanism of laser-induced size-reduction of gold nanoparticles as studied by nanosecond transient absorption spectroscopy. *The Journal of Physical Chemistry B* **110**, 11751-11756 (2006).
66 Yamada, K., Miyajima, K. & Mafuné, F. Thermionic emission of electrons from gold nanoparticles by nanosecond pulse-laser excitation of interband. *The Journal of Physical Chemistry C* **111**, 11246-11251 (2007).
67 Shoji, T. *et al.* Permanent fixing or reversible trapping and release of DNA micropatterns on a gold nanostructure using continuous-wave or femtosecond-pulsed near-infrared laser light. *J Am Chem Soc* **135**, 6643-6648 (2013).
68 Jain, P. K., Qian, W. & El-Sayed, M. A. Ultrafast cooling of photoexcited electrons in gold nanoparticle-thiolated DNA conjugates involves the dissociation of the gold-thiol bond. *Journal of the American Chemical Society* **128**, 2426-2433 (2006).
69 König, K., Riemann, I. & Fritzsche, W. Nanodissection of human chromosomes with near-infrared femtosecond laser pulses. *Opt. Lett.* **26**, 819-821 (2001).

70 Eleftheriou, E. *et al.* Millipede-a MEMS-based scanning-probe data-storage system. *Magnetics, IEEE Transactions on* **39**, 938-945 (2003).
71 Lantz, M. A. *et al.* Carbon nanotube tips for thermomechanical data storage. *Applied physics letters* **83**, 1266-1268 (2003).
72 Kupersztych, J., Monchicourt, P. & Raynaud, M. Ponderomotive acceleration of photoelectrons in surface-plasmon-assisted multiphoton photoelectric emission. *Physical review letters* **86**, 5180 (2001).
73 Kupersztych, J. & Raynaud, M. Anomalous multiphoton photoelectric effect in ultrashort time scales. *Physical review letters* **95**, 147401 (2005).
74 Hiraoka, H. Radiation chemistry of poly (methacrylates). *IBM Journal of Research and Development* **21**, 121-130 (1977).
75 Döppner, T., Fennel, T., Radcliffe, P., Tiggesbäumker, J. & Meiwes-Broer, K.-H. Ion and electron emission from silver nanoparticles in intense laser fields. *Physical Review A* **73**, 031202 (2006).
76 Bensimon, D., Simon, A., Croquette, V. & Bensimon, A. Stretching DNA with a receding meniscus: experiments and models. *Physical Review Letters* **74**, 4754 (1995).
77 Sontz, P. A., Muren, N. B. & Barton, J. K. DNA Charge Transport for Sensing and Signaling. *Accounts of Chemical Research* **45**, 1792-1800, doi:10.1021/ar3001298 (2012).
78 Seeman, N. C. DNA nanotechnology: novel DNA constructions. *Annual Review of Biophysics and Biomolecular Structure* **27**, 225-248 (1998).
79 Seeman, N. C. DNA engineering and its application to nanotechnology. *Trends in biotechnology* **17**, 437-443 (1999).
80 Rothemund, P. W. Folding DNA to create nanoscale shapes and patterns. *Nature* **440**, 297-302 (2006).
81 Pinheiro, A. V., Han, D., Shih, W. M. & Yan, H. Challenges and opportunities for structural DNA nanotechnology. *Nat Nanotechnol* **6**, 763-772 (2011).
82 Cai, L., Tabata, H. & Kawai, T. Self-assembled DNA networks and their electrical conductivity. *Applied Physics Letters* **77**, 3105-3106 (2000).
83 Braun, E., Eichen, Y., Sivan, U. & Ben-Yoseph, G. DNA-templated assembly and electrode attachment of a conducting silver wire. *Nature* **391**, 775-778 (1998).
84 Becerril, H. A. & Woolley, A. T. DNA-templated nanofabrication. *Chemical Society Reviews* **38**, 329-337 (2009).
85 Lok, C.-N. *et al.* Silver nanoparticles: partial oxidation and antibacterial activities. *J Biol Inorg Chem* **12**, 527-534, doi:10.1007/s00775-007-0208-z (2007).
86 Bi, H. *et al.* Optical study of redox process of Ag nanoparticles at high temperature. *Journal of Applied Physics* **92**, 7491-7497, doi:doi:http://dx.doi.org/10.1063/1.1518147 (2002).

Abkürzungsverzeichnis

AFM	Rasterkraftmikroskop
Ag	Silber
Au	Gold
AgNP	Silber-Nanopartikel
AuNP	Gold-Nanopartikel
CCD	charge-coupled device
DFM	Dunkelfeldmikroskop
DNA	Desoxyribonukleinsäure
E-Feld	elektrisches Feld
Laser	Light Amplification by Stimulated Emission of Radiation
LSPR	lokalisierte Oberflächenplasmonenresonanz
PMMA	Polymethylmethacrylat
λ-DNA	Lambda Deoxyribonucleic acid

Verwendete Formelzeichen und Einheiten

Formelzeichen

A	Fläche
C_{abs}	Absorptionsquerschnitt
C_{sca}	Streuquerschnitt
ε	dielektrische Konstante
F	Fluenz
f	Repetitionsrate
k	Wellenzahl
P	Leistung
V	Volumen
t_p	Pulslänge
ω	Kreisfrequenz
Δd	Schichtdicke, Abstand
λ	Wellenlänge

Einheiten

cm	Zentimeter
eV	Elektronenvolt
fs	Femtosekunden
MHz	Megahertz
mJ	Millijoule
nm	Nanometer
ns	Nanosekunden
pM	Pikomolar
ps	Pikosekunden
°	Grad
°C	Grad Celsius
µm	Mikrometer

Danksagung

An dieser Stelle möchte ich mich bei allen Personen bedanken, die mich im Zusammenhang mit meiner Arbeit unterstützt haben.

Ein besonderer Dank gilt meiner Mutter für die Unterstützung auf meinem gesamten Lebensweg.

Ich danke Dr. Wolfgang Fritzsche für die Betreuung meiner Arbeit, für sein Vertrauen mir verantwortungsvolle Aufgaben zu übertragen sowie mir die Möglichkeit gegeben zu haben Erfahrungen in einem kreativen wissenschaftlichen Umfeld zu sammeln.

Prof. Volker Deckert danke ich für sein Interesse an meiner Arbeit und für die Übernahme des Gutachtens.

Des Weiteren danke ich Prof. Dr. Jürgen Popp für die Betreuung meiner Arbeit seitens der Universität und für die Möglichkeit zur Chemisch-Geowissenschaftlichen Fakultät wechseln zu können.

Mein besonderer Dank gilt Dr. Frank Garwe für seine stetige Hilfsbereitschaft und Geduld. Mit seinem zielsicheren Blick für die Physik hat er die Arbeit stark bereichert.

Ebenso gilt mein besonderer Dank Dr. Andrea Csáki für die Hilfsbereitschaft und Motivation während meiner gesamten Zeit am IPHT.

Der *Jena School for Microbial Communication (JSMC)* danke ich für die finanzielle Unterstützung sowie auch Ulrike Schleier und Dr. Carsten Thoms für die Organisation seitens der Graduiertenschule.

Des Weiteren bedanke ich mich bei Dr. Frank Garwe, Robert Meyer, Dr. Jussi Toppari (University of Jyväskylä), Gerd Hähnel, Norbert Jahr, Dr. Ondrej Stranik, Dr. Christian Leiterer, Dr. Andrea Steinbrück, Dr. Joachim Bergmann, David Zopf, Matthias Thiele, André Dathe, Dr. Robert Müller, Franka Jahn, Dr. Uwe Hübner und Dr. Annett Eitner (Universitätsklinikum Jena) und den gesamten

Mitarbeitern des Reinraums und der Abteilung Nanobiophotonik des IPHTs für die tatkräftige Unterstützung und Zusammenarbeit während meiner Promotion.

Weiterhin danke ich Dr. Wolfgang Paa, Prof. Benjamin Dietzek, Thorsten May und Prof. Rainer Heinzmann für die Bereitstellung der Lasersysteme und technischen Ausrüstung sowie Sandro Heuke, Dr. Denis Akimov, Dr. Nadine Vogler und Ivana Šumanovac für die dabei geleistete Hilfestellung.

Ebenso danke ich Dr. Antti-Pekka Eskelinen und Prof. Päivi Törmä von der Aalto University Helsinki sowie Robert Woolley und Prof. Colette McDonagh von der Dublin City University. Unter ihrer Anleitung hatte ich die Möglichkeit, die Arbeit aus einem anderen Blickwinkel zu betrachten.

Ich danke Florian Talkenberg für seine Unterstützung bei den Konvertierungen.

Ein herzliches Dankeschön gilt meinen Kollegen und Freunden Peter Horbert, Dr. Barbara Seise, Dr. Norbert Jahr, Dr. Nils Gleichmann, Andreas Kopielski, Dr. Christian Leiterer, David Zopf, Jaqueline Jatschka, Matthias Thiele, André Dathe und Dr. Daniéll Malsch, sowie den ehemaligen Studenten und Gastwissenschaftlern Leonor Soares, Steffen Berg, Nicole Franke und Dr. Pedro Quaresma für die schöne gemeinsame Zeit, die mir noch lange in Erinnerung bleiben wird.

Curriculum Vitae

Personal Information

Name:	Janina Wirth
Date of Birth:	20th June 1984
Place of Birth:	Soemmerda (Germany)
Nationality:	German
Gender:	Female

Contact Information

Place of Residence:	Talstraße 68, 07743 Jena (Germany)
Telephone Number:	+49-176-81695401
E-mail address:	janina.wirth@gmail.com

School Education

08/2004 – 06/2005	Walter Gropius Schule (Erfurt) Professional education (Certificated Design-Assistant)
08/2001 – 06/2004	Walter Gropius Schule (Erfurt) Degree: Abitur
08/1995 – 06/2001	Johann Gottlieb Fichte Schule (Soemmerda) Degree: Realschulabschluss
08/1991 – 06/1995	Johann Heinrich Pestalozzi Schule (Soemmerda) Primary school

Academic Education

10/2005 – 03/2010	*Studies in Biomedical Engineering* *University of Applied Sciences (Jena)* Grade: Diploma Degree: Dipl. Ing.
09/2007 – 02/2008	*Practical Semester* *Center for Molecular Biomedicine (Jena)* "Inhibition of the CXCR4-gene in HEK-293 cells by RNA interference"
03/2008 – 02/2009	*Project Thesis* *University of Applied Sciences (Jena)* "Fluorescence microscopy of cellular structures of the epithelial cell line HT-29/B6 by indirect immunofluorescence"
03/2009 – 02/2010	*Diploma Thesis* *Leibniz Institute of Photonic Technology (Jena)* "fs laser manipulation of DNA molecules and human cells with metal nanoparticle antennas"
Since 03/2010	*PhD Thesis* *Leibniz Institute of Photonic Technology (Jena)* Guest researcher at Aalto University Helsinki, Finland (DAAD scholarship) Guest researcher at Dublin City University, Ireland (ESF short visit grant) Supervising of Bachelor and Master Thesis Supervising of pupils ("Jugend forscht") Teaching activities within practical course for physical chemistry Workshop in Inter- and transdisciplinary research

Janina Wirth, Jena, 04th April 2014

Selbstständigkeitserklärung

Ich erkläre, dass ich die vorliegende Arbeit selbstständig und unter Verwendung der angegebenen Hilfsmittel, persönlichen Mitteilungen und Quellen angefertigt habe.

Ort, Datum .....

Unterschrift .....